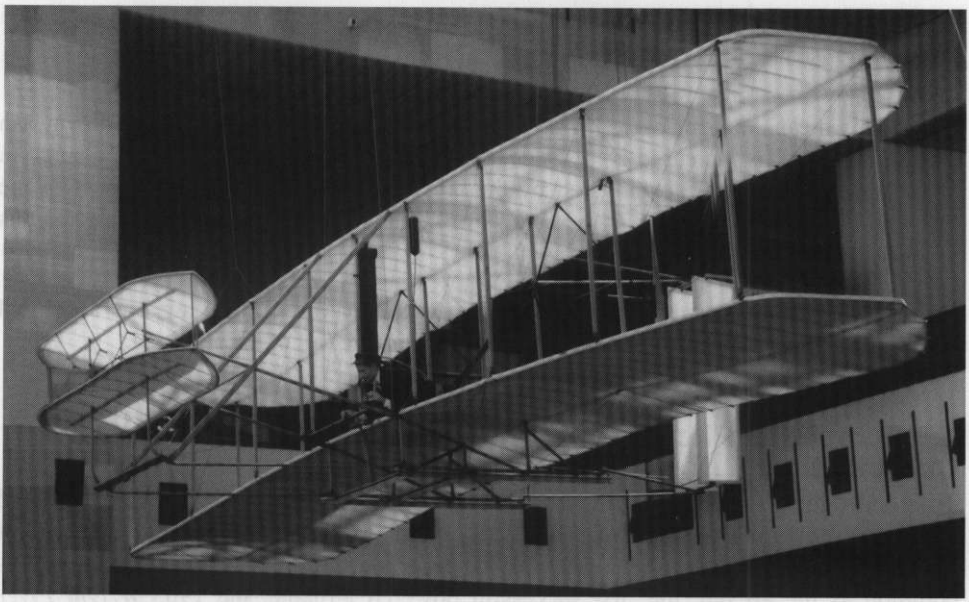


Figure 4.6.2. The 1903 Wright flyer in the Smithsonian National Air and Space Museum.

Here we shall proceed with our analysis of the wing-canard configuration just as we did with the wing-tail configuration. First we consider the requirements for trim and then proceed to an examination of the pitch stability requirement. For the analysis presented in this section, we use the simplified configuration shown in Fig. 4.6.3. We again take the fuselage reference line to pass through the center of gravity parallel to the freestream velocity at trim. Following the simplified analysis for the aft tail, we assume that the aerodynamic centers of the wing and canard, as well as the center of thrust, all fall on this fuselage reference line. Again, we also assume the thrust vector to be aligned with the direction of motion.

The position of the CG shown in Fig. 4.6.3 may at first be confusing to the student who is already familiar with the canard configuration. Here, for consistency, the CG is shown as being forward of both the canard and the wing. In this textbook, the length, l, for any lifting surface is always defined to be the distance that the aerodynamic center of the surface is aft of the center of gravity. If this notation is consistently used, we need not be concerned beforehand as to the location of any surface relative to the CG. If our analysis shows that a negative value of l is required for any surface, this simply means that this particular surface must be forward of the CG.

As was the case with the simplified analysis for the aft tail, the force balance in the direction of flight simply allows us to determine the thrust required to maintain constant airspeed. The trim requirements for pitch are the same as they were for the simplified aft tail configuration. Simply restated, the total lift must balance the normal component of weight, and the total pitching moment about the CG must be zero. Using the small-angle approximations for the upwash angle ε_u, this gives

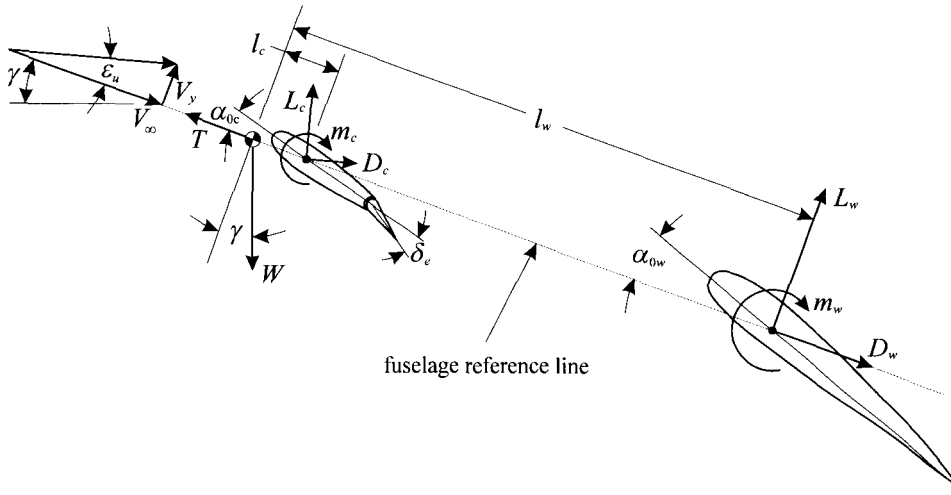


Figure 4.6.3. Forces and moments acting on a wing combined with a forward canard.

$$C_{L_w} + \frac{S_c}{S_w} C_{L_c} = \frac{W \cos\gamma}{\frac{1}{2}\rho V_\infty^2 S_w} \tag{4.6.1}$$

and

$$C_m = C_{m_w} + \frac{S_c \bar{c}_c}{S_w \bar{c}_w} C_{m_c} - \frac{l_w}{\bar{c}_w} C_{L_w} - \frac{S_c l_c}{S_w \bar{c}_w} C_{L_c} = 0 \tag{4.6.2}$$

where a dynamic pressure ratio of 1.0 has been assumed for both the forward canard and the main wing.

As was the case with the wing-tail analysis, the requirements that are specified by Eqs. (4.6.1) and (4.6.2) relate the lift forces developed by the wing and the canard to the weight of the aircraft and the position of the center of gravity. Equation (4.6.1) requires that at trim, the combined lift developed by the wing and the canard must support the normal component of the weight of the aircraft. Equation (4.6.2) specifies how the total lift must be divided between the wing and the canard in order to maintain the attitude required for trim. These two equations can be solved for the lift on the wing and the canard to give

$$C_{L_w} = \frac{\bar{c}_w}{l_w - l_c} C_{m_w} + \frac{S_c \bar{c}_c}{S_w (l_w - l_c)} C_{m_c} - \frac{l_c}{l_w - l_c} \frac{W \cos\gamma}{\frac{1}{2}\rho V_\infty^2 S_w} \tag{4.6.3}$$

$$C_{L_c} = \frac{S_w l_w}{S_c (l_w - l_c)} \frac{W \cos\gamma}{\frac{1}{2}\rho V_\infty^2 S_w} - \frac{S_w \bar{c}_w}{S_c (l_w - l_c)} C_{m_w} - \frac{\bar{c}_c}{l_w - l_c} C_{m_c} \tag{4.6.4}$$

By definition, the canard is forward of the main wing and $(l_w - l_c)$ is positive. Furthermore, the area and chord length for both the wing and the canard are always positive. Thus, if neither the wing nor the canard have negative camber, both moment coefficients and the first two terms on the right-hand side of Eq. (4.6.3) must be less than or equal to zero. Since the lift on the main wing must be positive to support a major portion of the weight, we see that the last term on right-hand side of Eq. (4.6.3) must make a positive contribution to the lift. This requires $l_c < 0$. In other words, **the canard must always be mounted forward of the CG to maintain trim.**

For pitch stability, we require that the change in the total pitching moment coefficient with respect to angle of attack is negative. Since C_{m_w} and C_{m_c} are the moment coefficients relative to the aerodynamic centers of the wing and the canard, the moment terms in Eq. (4.6.2) are independent of angle of attack, and differentiating Eq. (4.6.2), the stability condition for this wing-canard combination requires that

$$\frac{\partial C_m}{\partial \alpha} = -\frac{l_w}{\bar{c}_w}\frac{\partial C_{L_w}}{\partial \alpha} - \frac{S_c l_c}{S_w \bar{c}_w}\frac{\partial C_{L_c}}{\partial \alpha} < 0 \tag{4.6.5}$$

The aerodynamic interactions between the wing and the canard are very complex. Because the canard is forward of the lifting wing, the wing induces upwash on the canard. Any lift that is generated on the canard will also produce wingtip vorticity that interacts with the main wing. Because the span of the canard is typically less than that of the wing, these wingtip vortices can even pass directly over the wing. As one might imagine, this produces a very complex flow about the wing. This interaction can only be evaluated from detailed computer simulations or wind tunnel tests. For preliminary calculations, we have no choice but to neglect the effects of the canard's vorticity on the performance of the main wing. The effect of the upwash induced on the canard by the main wing is typically small but is easily accounted for by using the method presented in Sec. 4.5. With these approximations, the lift coefficients for the wing and the canard can be expressed in terms of angle of attack. For small angles of attack, the lift coefficient for the main wing is a linear function of angle of attack,

$$C_{L_w} = C_{L_w,\alpha}(\alpha + \alpha_{0w} - \alpha_{L0w}) \tag{4.6.6}$$

where $C_{L_w,\alpha}$ is the lift slope for the wing, α is the angle of attack for the airplane as measured relative to the fuselage reference line, α_{0w} is the angle that the wing chord makes with the fuselage reference line, and α_{L0w} is the zero-lift angle of attack for the wing. Assuming small angles of attack and control surface deflections, the lift coefficient for the canard varies linearly with angle of attack and control surface deflection,

$$C_{L_c} = C_{L_c,\alpha}(\alpha + \alpha_{0c} - \alpha_{L0c} + \varepsilon_u + \varepsilon_e \delta_e) \tag{4.6.7}$$

where $C_{L_c,\alpha}$ is the lift slope for the isolated canard, α_{0c} is the angle that the canard chord makes with the fuselage reference line, α_{L0c} is the zero-lift angle of attack for the canard with no control surface deflection, ε_u is the upwash angle, ε_e is the control

surface effectiveness, and δ_e is the control surface deflection. For small angles of attack, the upwash angle is also a linear function of angle of attack,

$$\varepsilon_u = \varepsilon_{u0} + \varepsilon_{u,\alpha}\,\alpha \tag{4.6.8}$$

Using Eqs. (4.6.6) through (4.6.8) in Eq. (4.6.5), the stability criterion for this wing-canard combination is

$$\frac{\partial C_m}{\partial \alpha} = -\frac{l_w}{\bar{c}_w} C_{L_w,\alpha} - \frac{S_c l_c}{S_w \bar{c}_w} C_{L_c,\alpha}(1+\varepsilon_{u,\alpha}) < 0 \tag{4.6.9}$$

The first term to the right of the equal sign in Eq. (4.6.9) is the wing contribution to the airplane stability and the second term is the canard contribution. We have already seen that trim requires $l_c < 0$. Thus, since the lift slope is positive for angles of attack below stall, Eq. (4.6.9) shows that **a canard always has a destabilizing effect on the airplane**. At this point the student may ask: How is it possible to replace an aft stabilizer with a destabilizing canard? The answer is also found in Eq. (4.6.9).

Since the second term to the right of the equal sign in Eq. (4.6.9) always makes a positive contribution to the pitch stability derivative, the first term must make a negative contribution if the airplane is to be stable in pitch. For angles of attack less than stall, the lift slope is positive and this requires $l_w > 0$, which means that **the aerodynamic center of the main wing must always be aft of the CG for a stable wing-canard configuration**. Furthermore, it must be far enough aft of the CG to counter the destabilizing effects of the cambered wing, the fuselage, and the canard. Thus, **it is the main wing and not the canard that provides stability for the wing-canard configuration**. Even though the canard is destabilizing, it provides the essential function of generating a positive pitching moment about the CG, which is necessary to trim the airplane against the negative pitching moment caused by having the CG ahead of the main wing. From Eq. (4.6.4) we see that since both moment coefficients are typically less than or equal to zero and l_w must be positive, **the lift on the canard must be positive** as well.

In summary, **to maintain both trim and static stability, the center of gravity for any wing-canard airplane must be located between the wing and the canard**. Additionally, in trimmed flight, **both the wing and the canard will always carry positive lift**. This is one of the intrinsic advantages of the canard design. With a conventional aft tail, the lift on the tail is negative over at least some portion of the airplane's operating range. This requires additional lift on the main wing and produces additional induced drag on both the wing and the tail. With the canard configuration, the positive lift that is always generated by the canard reduces the lift required on the main wing and thus results in less induced drag than would be generated by a similar conventional airplane carrying negative lift on the aft tail.

Notice that in both Eqs. (4.6.2) and (4.6.9), a dimensionless ratio appears that looks like the volume ratio, which was defined for the horizontal aft tail. Since the length, l_c, is always negative, we shall define the *canard volume ratio* as

$$\mathcal{V}_c \equiv \frac{S_c(-l_c)}{S_w \bar{c}_w} \tag{4.6.10}$$

Using this definition in Eq. (4.6.2) and rearranging gives

$$\mathcal{V}_c = \frac{l_w}{\bar{c}_w}\frac{C_{L_w}}{C_{L_c}} - \frac{C_{m_w}}{C_{L_c}} - \frac{S_c \bar{c}_c}{S_w \bar{c}_w}\frac{C_{m_c}}{C_{L_c}} \tag{4.6.11}$$

Using this same definition, for angles of attack less than stall, Eq. (4.6.9) can be rearranged to yield

$$\mathcal{V}_c < \frac{l_w}{\bar{c}_w}\frac{C_{L_w,\alpha}}{C_{L_c,\alpha}(1+\varepsilon_{u,\alpha})} \tag{4.6.12}$$

From Eq. (4.6.11), we see that trim requires a canard volume ratio large enough to counter the negative pitching moments generated by the lift of the main wing and any camber in the wing and/or canard. On the other hand, from Eq. (4.6.12), stability requires a canard volume ratio small enough so as not to overpower the stability provided by the main wing. Thus, the trim and stability analysis for the design of a canard configuration is more critical than it is for the design of an aft tail. With the aft tail, pitch control and pitch stability are both improved by increasing the volume ratio of the horizontal tail. However, sizing the volume ratio for a canard requires a trade-off between pitch control and pitch stability, which makes sizing a canard more critical than sizing an aft tail.

Using the volume ratio requirement for trim, as given by Eq. (4.6.11), we can eliminate the volume ratio from Eq. (4.6.12), and after some rearranging, we obtain

$$\frac{C_{L_w}}{C_{L_c}} < \frac{C_{L_w,\alpha}}{C_{L_c,\alpha}(1+\varepsilon_{u,\alpha})} + \frac{\bar{c}_w}{l_w}\frac{C_{m_w}}{C_{L_c}} + \frac{S_c \bar{c}_c}{S_w l_w}\frac{C_{m_c}}{C_{L_c}} \tag{4.6.13}$$

Because the canard must always support a portion of the aircraft weight, for best aerodynamic efficiency, the canard should be designed with an aspect ratio as high as possible, just like the wing. As a result, the lift slope for the canard should be about the same as that for the wing. Since the upwash gradient, $\varepsilon_{u,\alpha}$, is positive ahead of the main wing, the first term on the right of Eq. (4.6.13) is typically slightly less than 1.0. Furthermore, if both the wing and the canard have positive camber, the last two terms in Eq. (4.6.13) have small negative values. Thus, **to maintain both trim and static stability with a typical wing-canard combination, the lift coefficient for the canard must be greater than that for the wing**. This underscores the importance of designing the canard with a fairly high aspect ratio.

The fact that the canard must support a higher lift coefficient than the wing points out what is sometimes considered to be another advantage of the canard configuration. As the trim speed is reduced, the lift coefficients for both the wing and the canard must be increased. However, since the lift coefficient for the canard must be greater than that for the wing, the maximum lift coefficient is typically reached for the canard before the

main wing stalls. Once the canard has stalled, it is not possible to generate the additional positive pitching moment necessary to further increase the angle of attack and stall the main wing. Thus, with a wing-canard combination so designed, it is almost impossible to stall the main wing in a gradual maneuver. The wing can still be stalled in a rapidly accelerating pitch-up maneuver known as a *whip stall.*

The higher lift coefficient carried by the canard also results in what can sometimes be a disadvantage of the wing-canard design. If a very high maximum lift coefficient is required for short takeoff and landing, it does no good to fit the main wing with complex high-lift devices, unless the canard is similarly fitted. The maximum lift coefficient for the complete airplane is controlled primarily by the maximum lift coefficient for the canard. Furthermore, when high-lift devices are deployed, the magnitude of the negative pitching moment coefficient for both the main wing and the canard is increased significantly. From Eq. (4.6.13), we see that this decreases even further the ratio of the allowable lift coefficient for the wing to that for the canard. Thus, even though the main wing must carry the largest portion of the airplane's weight, the canard must produce a significantly larger lift coefficient to provide the positive pitching moment necessary to rotate the airplane to liftoff. For this reason, the canard design is not particularly well suited for short takeoff and landing applications.

EXAMPLE 4.6.1. Consider a general aviation airplane of a size and weight similar to the one described in Example 4.3.1. This airplane is a wing-canard configuration and weighs 2,700 lbf. The wing and the canard are geometrically similar, having the same aspect ratio and airfoil section with no sweep. The following properties are known:

$$S_w = 180\ \text{ft}^2, \quad b_w = 33\ \text{ft}, \quad R_{T_w} = 0.40, \quad C_{L_w,\alpha} = 4.44,$$
$$\alpha_{L0w} = -2.20°, \quad C_{m_w} = -0.053,$$
$$S_c = 36\ \text{ft}^2, \quad \varepsilon_e = 0.60, \quad C_{m_c,\delta_e} = -0.55, \quad l_w - l_c = 15\ \text{ft}$$

The aerodynamic centers of the wing and the canard both fall on the fuselage reference line, which is the minimum drag axis of the fuselage. The wing and the canard are mounted so that when the airplane is in level flight with an airspeed of 120 mph at standard sea level, trim is attained with no control surface deflection and a zero angle of attack for the fuselage reference line. In the range of linear lift, the static margin for this wing-canard combination is 5 percent. Neglecting any moments associated with the thrust deck and the fuselage, determine the location of the center of gravity and the mounting angles for the wing and the canard. Plot the control surface deflection and the angle of attack at trim as a function of airspeed from 80 to 160 mph. Also plot the lift coefficient on the wing and canard at trim for the same range of airspeed.

Solution. From Figs. 4.5.2 and 4.5.3 (or using a computer program based on the series solution to Prandtl's lifting-line equation), for a wing aspect ratio of 6.05 and a wing taper ratio of 0.40, the following results are obtained:

$$\kappa_v = 1.035$$

$$\kappa_b = 0.759$$

From Eqs. (4.5.6) and (4.5.12), the position factor and the sweep factor for the position $\bar{x} = -0.909$ and $\bar{y} = 0.0$ are found to be

$$\kappa_p = -0.061$$

$$\kappa_s = 1.0$$

From Eq. (4.5.11), the upwash at the position of the canard is

$$\varepsilon_u = -\varepsilon_d = -\frac{\kappa_v \kappa_p \kappa_s}{\kappa_b} \frac{C_{L_w}}{R_{A_w}} = -\frac{1.035(-0.061)1.0}{0.759} \frac{C_{L_w}}{R_{A_w}} = 0.083 \frac{C_{L_w}}{R_{A_w}}$$

The upwash gradient is then

$$\varepsilon_{u,\alpha} = \frac{\partial \varepsilon_u}{\partial \alpha} = 0.083 \frac{1}{R_{A_w}} \frac{\partial C_{L_w}}{\partial \alpha} = 0.083 \frac{C_{L_w,\alpha}}{R_{A_w}} = 0.083 \frac{4.44}{6.05} = 0.0609$$

Since the canard and the wing have the same aspect ratio,

$$\frac{b_c^2}{S_c} = \frac{b_w^2}{S_w}$$

$$b_c = b_w \sqrt{\frac{S_c}{S_w}} = 33 \text{ ft} \sqrt{\frac{36}{180}} = 14.758 \text{ ft}$$

and

$$\bar{c}_w = \frac{S_w}{b_w} = \frac{180 \text{ ft}^2}{33 \text{ ft}} = 5.455 \text{ ft}$$

$$\bar{c}_c = \frac{S_c}{b_c} = \frac{36 \text{ ft}^2}{14.758 \text{ ft}} = 2.439 \text{ ft}$$

By definition, the moment slope relative to the neutral point is zero. Thus,

$$\frac{\partial C_{m_{np}}}{\partial \alpha} = -\frac{l_w - l_{np}}{\bar{c}_w} C_{L_w,\alpha} - \frac{S_c(l_c - l_{np})}{S_w \bar{c}_w} C_{L_c,\alpha}(1 + \varepsilon_{u,\alpha}) = 0$$

Because the wing and the canard are geometrically similar, the lift slope is the same for both surfaces. Thus, solving for the wing position,

$$\frac{l_w - l_{np}}{\bar{c}_w} C_{L_w,\alpha} + \frac{S_c(l_c - l_w + l_w - l_{np})}{S_w \bar{c}_w} C_{L_c,\alpha}(1+\varepsilon_{u,\alpha}) = 0$$

$$\frac{l_w - l_{np}}{\bar{c}_w} + \frac{S_c(l_w - l_{np})}{S_w \bar{c}_w}(1+\varepsilon_{u,\alpha}) = \frac{S_c(l_w - l_c)}{S_w \bar{c}_w}(1+\varepsilon_{u,\alpha})$$

$$\frac{l_w}{\bar{c}_w} = \frac{\dfrac{S_c(l_w - l_c)}{S_w \bar{c}_w}(1+\varepsilon_{u,\alpha})}{1 + \dfrac{S_c}{S_w}(1+\varepsilon_{u,\alpha})} + \frac{l_{np}}{\bar{c}_w}$$

$$= \frac{\dfrac{36(15)}{180(5.455)}(1+0.0609)}{1 + \dfrac{36}{180}(1+0.0609)} + 0.05 = \underline{0.53}$$

Thus, the CG is nearly 35 inches forward of the wing quarter-chord. The canard volume ratio is then

$$\frac{S_c(-l_c)}{S_w \bar{c}_w} = \frac{S_c}{S_w}\left(\frac{l_w - l_c}{\bar{c}_w} - \frac{l_w}{\bar{c}_w}\right) = \frac{36}{180}\left(\frac{15}{180/33} - 0.5314\right) = 0.4437$$

For this configuration, trim requires that the total lift must equal the weight and the total pitching moment about the CG must be zero,

$$C_{L_w} + \frac{S_c}{S_w} C_{L_c} = \frac{W}{\frac{1}{2}\rho V_\infty^2 S_w}$$

$$C_{m_w} + \frac{S_c \bar{c}_c}{S_w \bar{c}_w} C_{m_c} - \frac{l_w}{\bar{c}_w} C_{L_w} - \frac{S_c l_c}{S_w \bar{c}_w} C_{L_c} = 0$$

At the design airspeed of 120 mph, the airplane is trimmed with no control surface deflection at zero angle of attack. Since the wing and the canard are geometrically similar, they both have the same moment coefficient and lift slope, with no control surface deflection. Thus, with zero fuselage angle of attack and zero control surface deflection,

$$C_{L_w 0} + \frac{36}{180} C_{L_c 0} = \frac{2{,}700}{\frac{1}{2} 0.0023769 (120 \times 5{,}280/3{,}600)^2 180}$$

$$-0.053 - \frac{36(2.439)}{180(5.455)} 0.053 - 0.5314 C_{L_w 0} + 0.4437 C_{L_c 0} = 0$$

or

$$\begin{bmatrix} 1 & 0.2 \\ -0.53136 & 0.44373 \end{bmatrix} \begin{Bmatrix} C_{L_w 0} \\ C_{L_c 0} \end{Bmatrix} = \begin{Bmatrix} 0.40746 \\ 0.05774 \end{Bmatrix}$$

The lift coefficients for the wing and the canard, with the fuselage reference line at zero angle of attack and no control surface deflection, are then

$$\begin{Bmatrix} C_{L_w 0} \\ C_{L_c 0} \end{Bmatrix} = \begin{Bmatrix} 0.30773 \\ 0.49864 \end{Bmatrix}$$

With this lift coefficient on the wing, the upwash angle on the canard is

$$\varepsilon_{u0} = 0.083 \frac{C_{L_w 0}}{R_{A_w}} = 0.083 \frac{0.30772}{6.05} = 0.00422 \text{ rad}$$

For the range of linear lift, the lift coefficients are

$$C_{L_w} = C_{L_w,\alpha} (\alpha + \alpha_{0w} - \alpha_{L0w})$$

$$C_{L_c} = C_{L_c,\alpha} [(1 + \varepsilon_{u,\alpha})\alpha + \alpha_{0c} - \alpha_{L0c} + \varepsilon_{u0} + \varepsilon_e \delta_e]$$

For zero angle of attack and control surface deflection, this gives

$$C_{L_w 0} = C_{L_w,\alpha} (\alpha_{0w} - \alpha_{L0w}) = 0.30772$$

$$C_{L_c 0} = C_{L_c,\alpha} (\alpha_{0c} - \alpha_{L0c} + \varepsilon_{u0}) = 0.49868$$

The mounting angles for the wing and the canard are then found to be

$$\alpha_{0w} = \frac{C_{L_w 0}}{C_{L_w,\alpha}} + \alpha_{L0w} = \frac{0.30772}{4.44} + (-2.20)\frac{\pi}{180} = 0.0309 \text{ rad} = \underline{1.8°}$$

$$\alpha_{0c} = \frac{C_{L_c 0}}{C_{L_c,\alpha}} + \alpha_{L0c} - \varepsilon_{u0} = \frac{0.49868}{4.44} + (-2.20)\frac{\pi}{180} - 0.00422$$

$$= 0.0697 \text{ rad} = \underline{4.0°}$$

For the range of linear lift, the canard moment coefficient about the aerodynamic center is

$$C_{m_c} = C_{m_c 0} + C_{m_c,\delta_e} \delta_e$$

where $C_{m_c 0}$ is the moment coefficient with no control surface deflection. The trim requirements for pitch are then written in terms of angle of attack and control surface deflection,

$$C_{L_w,\alpha}(\alpha+\alpha_{0w}-\alpha_{L0w})+\frac{S_c}{S_w}C_{L_c,\alpha}[(1+\varepsilon_{u,\alpha})\alpha+\alpha_{0c}-\alpha_{L0c}+\varepsilon_{u0}+\varepsilon_e\delta_e] = \frac{W}{\frac{1}{2}\rho V_\infty^2 S_w}$$

$$C_{m_w}+\frac{S_c\bar{c}_c}{S_w\bar{c}_w}(C_{m_c 0}+C_{m_c,\delta_e}\delta_e)-\frac{l_w}{\bar{c}_w}C_{L_w,\alpha}(\alpha+\alpha_{0w}-\alpha_{L0w}) - \frac{S_c l_c}{S_w\bar{c}_w}C_{L_c,\alpha}[(1+\varepsilon_{u,\alpha})\alpha+\alpha_{0c}-\alpha_{L0c}+\varepsilon_{u0}+\varepsilon_e\delta_e] = 0$$

These two equations can be written as

$$\begin{bmatrix} C_{L,\alpha} & C_{L,\delta_e} \\ C_{m,\alpha} & C_{m,\delta_e} \end{bmatrix} \begin{Bmatrix} \alpha \\ \delta_e \end{Bmatrix} = \begin{Bmatrix} C_L - C_{L0} \\ -C_{m0} \end{Bmatrix}$$

where

$$C_{L,\alpha} = C_{L_w,\alpha}+\frac{S_c}{S_w}C_{L_c,\alpha}(1+\varepsilon_{u,\alpha}) = 5.38209$$

$$C_{L,\delta_e} = \frac{S_c}{S_w}C_{L_c,\alpha}\varepsilon_e = 0.53280$$

$$C_L = \frac{W}{\frac{1}{2}\rho V_\infty^2 S_w}$$

$$C_{L0} = C_{L_w,\alpha}(\alpha_{0w}-\alpha_{L0w})+\frac{S_c}{S_w}C_{L_c,\alpha}(\alpha_{0c}-\alpha_{L0c}+\varepsilon_{u0}) = 0.40746$$

$$C_{m,\alpha} = -\frac{l_w}{\bar{c}_w}C_{L_w,\alpha}-\frac{S_c l_c}{S_w\bar{c}_w}C_{L_c,\alpha}(1+\varepsilon_{u,\alpha}) = -0.26910$$

$$C_{m,\delta_e} = \frac{S_c\bar{c}_c}{S_w\bar{c}_w}C_{m_c,\delta_e}-\frac{S_c l_c}{S_w\bar{c}_w}C_{L_c,\alpha}\varepsilon_e = 1.13289$$

and

$$C_{m0} = C_{m_w}+\frac{S_c\bar{c}_c}{S_w\bar{c}_w}C_{m_c 0}-\frac{l_w}{\bar{c}_w}C_{L_w,\alpha}(\alpha_{0w}-\alpha_{L0w}) - \frac{S_c l_c}{S_w\bar{c}_w}C_{L_c,\alpha}(\alpha_{0c}-\alpha_{L0c}+\varepsilon_{u0}) = 0.0$$

After substituting the values for this particular airplane, we obtain a linear system of equations that can be solved for the angle of attack and elevator deflection, which are needed to support a given total lift coefficient:

$$\begin{bmatrix} 5.38209 & 0.53280 \\ -0.26910 & 1.13289 \end{bmatrix} \begin{Bmatrix} \alpha \\ \delta_e \end{Bmatrix} = \begin{Bmatrix} C_L - 0.40746 \\ 0 \end{Bmatrix}$$

At 80 mph, the total lift coefficient is

$$C_L = \frac{W}{\frac{1}{2}\rho V_\infty^2 S_w} = \frac{2{,}700}{\frac{1}{2}0.0023769(80\times 5{,}280/3{,}600)^2 180} = 0.916785$$

and

$$\begin{bmatrix} 5.38209 & 0.53280 \\ -0.26910 & 1.13289 \end{bmatrix} \begin{Bmatrix} \alpha \\ \delta_e \end{Bmatrix} = \begin{Bmatrix} 0.916785 - 0.40746 \\ 0 \end{Bmatrix}$$

$$\begin{Bmatrix} \alpha \\ \delta_e \end{Bmatrix} = \begin{Bmatrix} 0.09246 \\ 0.02196 \end{Bmatrix} = \underline{\begin{Bmatrix} 5.3^\circ \\ 1.3^\circ \end{Bmatrix}}$$

With these values of angle of attack and control surface deflection, the lift coefficients for the wing and the canard are

$$C_{L_w} = C_{L_w,\alpha}(\alpha + \alpha_{0w} - \alpha_{L0w}) = \underline{0.72}$$

and

$$C_{L_c} = C_{L_c,\alpha}[(1+\varepsilon_{u,\alpha})\alpha + \alpha_{0c} - \alpha_{L0c} + \varepsilon_{u0} + \varepsilon_e \delta_e] = \underline{0.99}$$

Repeating these calculations at different airspeeds, the data plotted in Fig. 4.6.4 are obtained. Notice that the lift coefficient for both the wing and the canard are always positive and the lift coefficient for the canard is always greater than that for the wing. These two characteristics are common to all canard configurations and it is these characteristics that provide both the advantage and the disadvantage of the canard design.

Figure 4.6.5 shows how the trim conditions change when the CG is moved forward to give a static margin of 10 percent. Notice that while this CG location provides greater stability, more control surface deflection is needed to trim the airplane. This increases the lift on the canard, and the ratio of the lift coefficient for the canard to that of the wing becomes even greater. Because moving the CG forward increases the lift coefficient for the canard at any given airspeed, it increases the stall speed for the airplane.

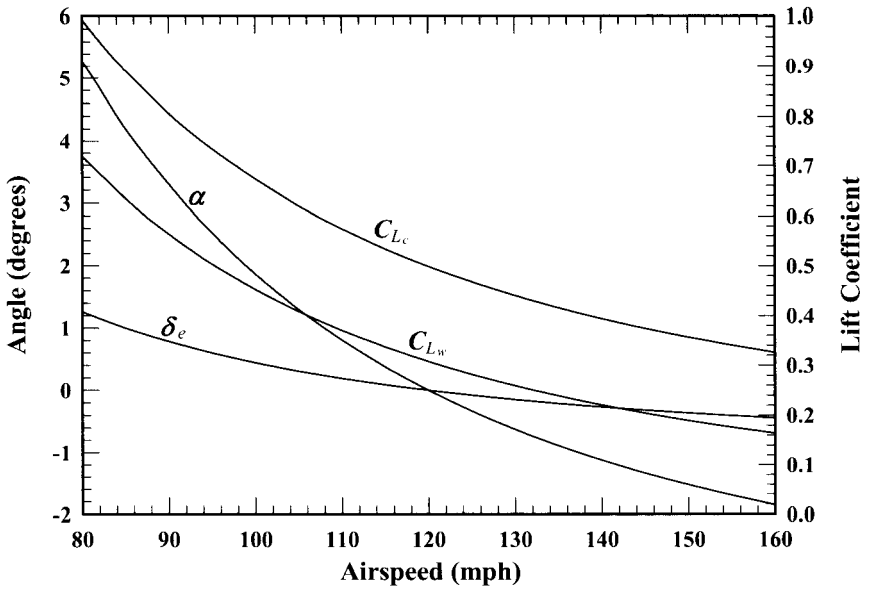


Figure 4.6.4. Conditions at level trim for the canard airplane in Example 4.6.1, with a static margin of 5 percent.

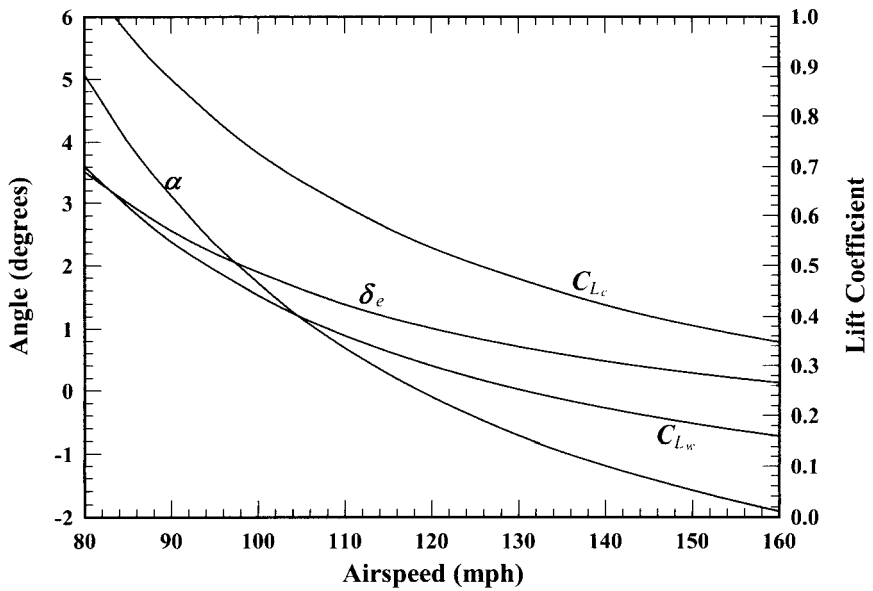


Figure 4.6.5. Conditions at level trim for the canard airplane in Example 4.6.1, with a static margin of 10 percent.

EXAMPLE 4.6.2. Estimate the maximum total lift coefficient and the stall speed for the wing-canard combination described in Example 4.6.1. Assume that the CG is located to give a static margin of 5 percent. The maximum lift coefficient for the main wing is 1.40. Because of control surface deflection, the maximum lift coefficient for the canard is increased slightly to 1.50. However, this control surface deflection also increases the magnitude of the negative pitching moment coefficient for the canard to –0.077.

Solution. The maximum lift coefficient for the wing-canard combination is reached when either the wing or the canard stalls. Since the lift coefficient for the canard is higher than that for the wing, we will start by assuming that the canard stalls first. Thus, for this airplane and operating condition, we have

$$S_w = 180\ \text{ft}^2, \quad \bar{c}_w = 5.455\ \text{ft}, \quad l_w = 2.899\ \text{ft}, \quad C_{L_w \max} = 1.40, \quad C_{m_w} = -0.053,$$
$$S_c = 36\ \text{ft}^2, \quad \bar{c}_c = 2.439\ \text{ft}, \quad l_c = -12.101\ \text{ft}, \quad C_{L_c \max} = 1.50, \quad C_{m_c} = -0.077$$

At trim, the total moment about the CG must be zero,

$$C_{m_w} + \frac{S_c \bar{c}_c}{S_w \bar{c}_w} C_{m_c} - \frac{l_w}{\bar{c}_w} C_{L_w} - \frac{S_c l_c}{S_w \bar{c}_w} C_{L_c} = 0$$

When the canard is at maximum lift coefficient, this gives

$$\begin{aligned} C_{L_w} &= \frac{\bar{c}_w}{l_w} C_{m_w} + \frac{S_c \bar{c}_c}{S_w l_w} C_{m_c} - \frac{S_c l_c}{S_w l_w} C_{L_c \max} \\ &= \frac{5.455}{2.899}(-0.053) + \frac{36(2.439)}{180(2.899)}(-0.077) - \frac{36(-12.101)}{180(2.899)}1.50 = 1.14 \end{aligned}$$

This is less than the maximum lift coefficient for the wing, so our assumption that the canard stalls first was correct. At trim the total lift must also equal the weight,

$$C_L = C_{L_w} + \frac{S_c}{S_w} C_{L_c} = \frac{W}{\frac{1}{2}\rho V_\infty^2 S_w}$$

When the canard is at the maximum lift coefficient, this gives

$$C_{L\max} = C_{L_w} + \frac{S_c}{S_w} C_{L_c \max} = 1.14 + \frac{36}{180}1.50 = \underline{1.44}$$

The stall speed is then

$$V_{\text{stall}} = \sqrt{\frac{W}{\frac{1}{2}\rho S_w C_{L\max}}} = \sqrt{\frac{2{,}700}{\frac{1}{2}0.0023769(180)1.44}} = 93.6\ \text{ft/sec} = \underline{63.8\ \text{mph}}$$

EXAMPLE 4.6.3. The main wing of the wing-canard combination described in Example 4.6.2 is fitted with high lift flaps. When these flaps are deflected by 10 degrees, the maximum lift coefficient for the main wing is increased to 1.7 and the negative pitching moment coefficient for the wing is increased to –0.149. Determine the maximum total lift coefficient and the stall speed for the wing-canard combination with these flaps so engaged.

Solution. Again, we will start by assuming that the canard stalls first. Thus, for this airplane and operating condition, we have

$$S_w = 180\ \text{ft}^2, \quad \bar{c}_w = 5.455\ \text{ft}, \quad l_w = 2.899\ \text{ft}, \quad C_{L_w \max} = 1.70, \quad C_{m_w} = -0.149,$$
$$S_c = 36\ \text{ft}^2, \quad \bar{c}_c = 2.439\ \text{ft}, \quad l_c = -12.101\ \text{ft}, \quad C_{L_c \max} = 1.50, \quad C_{m_c} = -0.077$$

When the canard is at maximum lift coefficient, trim requires that

$$C_{L_w} = \frac{\bar{c}_w}{l_w} C_{m_w} + \frac{S_c \bar{c}_c}{S_w l_w} C_{m_c} - \frac{S_c l_c}{S_w l_w} C_{L_c \max}$$
$$= \frac{5.455}{2.899}(-0.149) + \frac{36(2.439)}{180(2.899)}(-0.077) - \frac{36(-12.101)}{180(2.899)}1.50 = 0.96$$

This is again less than the maximum lift coefficient for the wing, which means that our original assumption was correct. With the canard at maximum lift coefficient, the second trim requirement gives

$$C_{L\max} = C_{L_w} + \frac{S_c}{S_w} C_{L_c \max} = 0.96 + \frac{36}{180}1.50 = \underline{1.26}$$

and the stall speed is

$$V_{\text{stall}} = \sqrt{\frac{W}{\frac{1}{2}\rho S_w C_{L\max}}} = \sqrt{\frac{2{,}700}{\frac{1}{2}0.0023769(180)1.26}} = 100.1\ \text{ft/sec} = \underline{68.2\ \text{mph}}$$

Thus, we see that deploying flaps on the main wing will actually reduce the maximum lift coefficient and increase the stall speed for this wing-canard combination.

In summary, the canard configuration provides an alternative to the aft tail for maintaining trim and static pitch stability in an airplane. To maintain both trim and static stability with the canard configuration, the center of gravity must be located between the wing and the canard, and the lift coefficient for the canard must be greater than that for the main wing. A canard always has a destabilizing effect on an airplane and it is only the main wing that provides pitch stability for the wing-canard design. One advantage of the canard over the aft tail is that both the wing and the canard will always

carry positive lift. In addition, the stall characteristics for the wing-canard configuration are usually quite forgiving. This is because the canard typically stalls before the wing, making it almost impossible to stall the main wing in a gradual maneuver. The major disadvantage of the canard design is the difficulty in achieving the high overall lift coefficient needed for short takeoff and landing applications.

4.7. Effects of Drag and Vertical Offset

In the stability analyses that we have considered to this point, we have assumed that the aerodynamic center of both the wing and the tail or canard, as well as the center of thrust and the center of gravity, all fall on the fuselage reference line. Additionally, the fuselage reference line was assumed parallel to the freestream velocity at trim. These simplifying assumptions allowed us to examine the major contributions to aircraft stability, without unduly complicating the formulation. However, in reality, these conditions are almost never exactly satisfied. In this section we examine some of the secondary effects that result from relaxing these assumptions.

In general, the wing and the horizontal control surface, as well as the center of thrust, can each be offset from the center of gravity in both the horizontal and vertical directions. A general schematic of the forces and moments acting on such a system is shown in Fig. 4.7.1. In this figure, the horizontal control surface has been drawn in the configuration of an aft tail. However, all values associated with this surface are labeled using the subscript, h. This has been done because the results of the following analysis

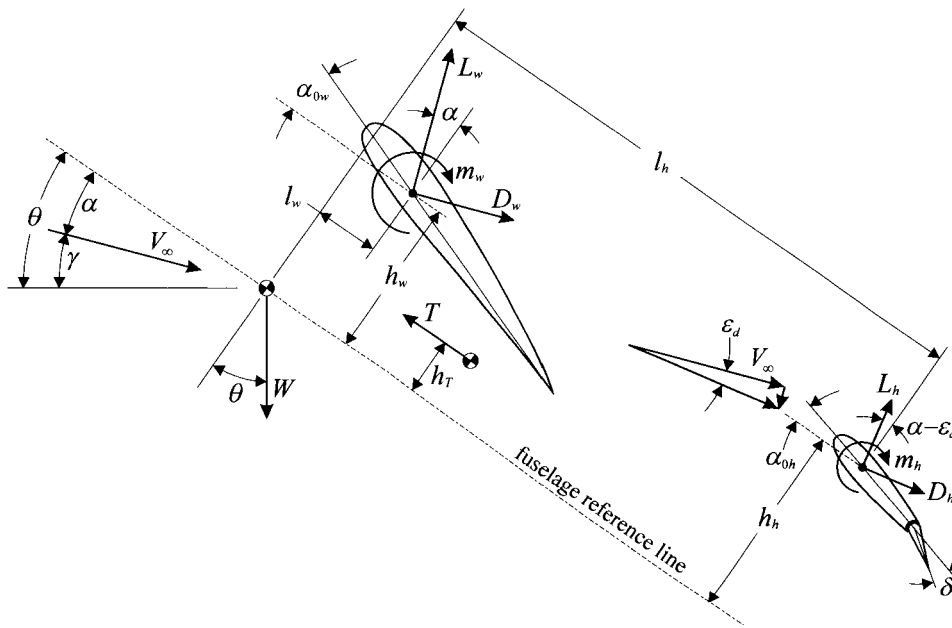


Figure 4.7.1. Forces and moments acting on a wing combined with a horizontal control surface.

can be applied to either an aft tail or a canard. The canard is distinguished from the aft tail only by the signs of l_h and ε_d. For an aft tail, both l_h and ε_d are positive, whereas for the canard, both l_h and ε_d are negative. As has been our usual practice, the variable l is used to denote a distance aft of the CG in a direction parallel to the fuselage reference line. Similarly, the variable h is used to indicate a distance measured above the CG in a direction normal to the fuselage reference line. If this sign convention is adhered to rigorously, we need not make any distinction between the wing-tail configuration and the wing-canard configuration. The signs will take care of the difference.

In the previous stability analyses, we assumed steady flight, with the thrust vector and the fuselage reference line parallel to the direction of motion. For the present analysis, we consider the more general case where the airplane is in a steady climb at some climb angle, γ, and has an angle of attack, α, relative to the fuselage reference line. For this case, the fuselage reference line makes an angle, θ, with the horizontal, where $\theta = \gamma + \alpha$. The angle, θ, is commonly referred to as the *elevation angle*. Since the orientation of the fuselage reference line is arbitrary, for this analysis, we have chosen it to be parallel to the thrust vector.

From Fig. 4.7.1, a force balance along the fuselage reference line requires that

$$T = W\sin\theta + D_w\cos\alpha - L_w\sin\alpha + D_h\cos(\alpha-\varepsilon_d) - L_h\sin(\alpha-\varepsilon_d) \tag{4.7.1}$$

Similarly, a balance of forces in the direction normal to the fuselage reference line gives

$$L_w\cos\alpha + D_w\sin\alpha + L_h\cos(\alpha-\varepsilon_d) + D_h\sin(\alpha-\varepsilon_d) = W\cos\theta \tag{4.7.2}$$

A net moment balance in pitch about the center of gravity requires that the sum of the aerodynamic moment, m, and the thrust moment, $-h_T T$, is zero. Thus, we have

$$\begin{aligned} m = {} & m_w - l_w L_w\cos\alpha - h_w L_w\sin\alpha + h_w D_w\cos\alpha - l_w D_w\sin\alpha \\ & + m_h - l_h L_h\cos(\alpha-\varepsilon_d) - h_h L_h\sin(\alpha-\varepsilon_d) \\ & + h_h D_h\cos(\alpha-\varepsilon_d) - l_h D_h\sin(\alpha-\varepsilon_d) = h_T T \end{aligned} \tag{4.7.3}$$

Notice that when the thrust vector does not pass through the center of gravity, the aerodynamic moment, m, is not zero at trim but must balance the moment produced by the thrust of the engine. Since the thrust must balance the drag, it is a nonlinear function of angle of attack, and significant nonlinearity is introduced into the trim equations. Equation (4.7.1) specifies the thrust required for steady flight, while Eqs. (4.7.2) and (4.7.3) provide the trim requirements.

Nondimensionalizing Eqs. (4.7.1) through (4.7.3) in the usual manner, we have

$$\begin{aligned} \frac{T}{\frac{1}{2}\rho V_\infty^2 S_w} &= \frac{W}{\frac{1}{2}\rho V_\infty^2 S_w}\sin\theta \\ &+ C_{D_w}\cos\alpha - C_{L_w}\sin\alpha + \frac{S_h}{S_w}\eta_h\left[C_{D_h}\cos(\alpha-\varepsilon_d) - C_{L_h}\sin(\alpha-\varepsilon_d)\right] \end{aligned} \tag{4.7.4}$$

$$C_{L_w}\cos\alpha + C_{D_w}\sin\alpha + \frac{S_h}{S_w}\eta_h\left[C_{L_h}\cos(\alpha-\varepsilon_d) + C_{D_h}\sin(\alpha-\varepsilon_d)\right] = \frac{W}{\frac{1}{2}\rho V_\infty^2 S_w}\cos\theta \tag{4.7.5}$$

$$\begin{aligned} C_m = {} & C_{m_w} - \left(\frac{l_w}{\bar{c}_w}\cos\alpha + \frac{h_w}{\bar{c}_w}\sin\alpha\right)C_{L_w} + \left(\frac{h_w}{\bar{c}_w}\cos\alpha - \frac{l_w}{\bar{c}_w}\sin\alpha\right)C_{D_w} \\ & + \frac{S_h\bar{c}_h}{S_w\bar{c}_w}\eta_h C_{m_h} - \left[\frac{S_h l_h}{S_w\bar{c}_w}\cos(\alpha-\varepsilon_d) + \frac{S_h h_h}{S_w\bar{c}_w}\sin(\alpha-\varepsilon_d)\right]\eta_h C_{L_h} \\ & + \left[\frac{S_h h_h}{S_w\bar{c}_w}\cos(\alpha-\varepsilon_d) - \frac{S_h l_h}{S_w\bar{c}_w}\sin(\alpha-\varepsilon_d)\right]\eta_h C_{D_h} = \frac{h_T}{\bar{c}_w}\frac{T}{\frac{1}{2}\rho V_\infty^2 S_w} \end{aligned} \tag{4.7.6}$$

In the absence of stall, the lift coefficients for the main wing and the horizontal surface can be written as

$$C_{L_w} = C_{L_{w,\alpha}}(\alpha + \alpha_{0w} - \alpha_{L0w}) \tag{4.7.7}$$

$$C_{L_h} = C_{L_{h,\alpha}}(\alpha + \alpha_{0h} - \alpha_{L0h} - \varepsilon_d + \varepsilon_e\delta_e) \tag{4.7.8}$$

Similarly, the drag coefficients for the main wing and the horizontal surface can be written as

$$C_{D_w} = C_{D0w} + C_{D_0,L_w}C_{L_w} + \frac{C_{L_w}^2}{\pi e_w R_{A_w}} \tag{4.7.9}$$

$$C_{D_h} = C_{D0h} + C_{D_0,L_h}C_{L_h} + \frac{C_{L_h}^2}{\pi e_h R_{A_h}} \tag{4.7.10}$$

The moment coefficient for the wing, about its aerodynamic center, is constant and that for the horizontal surface depends only on the elevator deflection. In the range of linear lift, we can write

$$C_{m_h} = C_{m_h 0} + C_{m_h,\delta_e}\delta_e \tag{4.7.11}$$

We can use Eq. (4.7.4) and Eqs. (4.7.7) through (4.7.11) in the trim requirements given by Eqs. (4.7.5) and (4.7.6) to determine the required angle of attack and elevator deflection. If the geometry of the airplane is completely known, this gives two equations containing only two unknowns, the angle of attack, α, and the elevator deflection, δ_e. However, this pair of equations is nonlinear, so in general, it must be solved numerically. From such a solution, we can determine the angle of attack and elevator deflection required for trim.

Notice from Eqs. (4.7.5) and (4.7.6) that even for the special case when h_w, h_h, and h_T are all zero, the equations that specify the trim requirements are still nonlinear. The simplified linear analysis presented in Sec. 4.3 and 4.6 was based on the assumption that the fuselage reference line was parallel to the direction of flight. Since the aircraft angle of attack depends on airspeed, this condition can be exactly satisfied only at one particular airspeed. However, since the angle of attack is usually small, this condition is nearly satisfied at all airspeeds and the approximate linear analysis gives good results when the wing, the horizontal surface, and the thrust vector are all in close vertical alignment with the center of gravity. This is demonstrated in the following example.

EXAMPLE 4.7.1. Consider the general aviation airplane with an aft tail that was described in Example 4.3.1. Neglecting any moments associated with the thrust deck and the fuselage but accounting for the nonlinear trim requirements, plot the elevator deflection and the angle of attack for trimmed level flight as a function of airspeed from 80 to 160 mph. Also plot the lift on the horizontal tail at level trim for the same range of airspeed. Compare the results with those obtained in Example 4.3.1. For this airplane, the wing and the horizontal tail have the following properties:

$$S_w = 180\ \text{ft}^2,\quad \bar{c}_w = 5.4545\ \text{ft},\quad R_{A_w} = 6.05,\quad e_w = 0.95,\quad l_w = -0.7094\ \text{ft},$$
$$h_w = 0.0\ \text{ft},\quad W = 2{,}700\ \text{lbf},\quad C_{L_w,\alpha} = 4.44,\quad \alpha_{0w} = 0.05338,$$
$$\alpha_{L0w} = -0.03840,\quad C_{m_w} = -0.053,\quad C_{D_{0w}} = 0.01,\quad C_{D_0,L_w} = 0.00,$$
$$S_h = 36\ \text{ft}^2,\quad \bar{c}_h = 3.0\ \text{ft},\quad R_{A_h} = 4.0,\quad e_h = 0.97,\quad l_h = 14.2906\ \text{ft},$$
$$h_h = 0.0\ \text{ft},\quad \eta_h = 1.0,\quad C_{L_h,\alpha} = 3.97,\quad \alpha_{0h} = 0.04041,$$
$$\alpha_{L0h} = 0.0,\quad \varepsilon_e = 0.60,\quad C_{m_{h0}} = 0.0,\quad C_{m_h,\delta_e} = -0.55,\quad C_{D_{0h}} = 0.015,$$
$$C_{D_0,L_h} = 0.00,\quad \varepsilon_{d0} = 0.04041,\quad \varepsilon_{d,\alpha} = 0.44033,\quad h_T = 0.0\ \text{ft}$$

Solution. For level flight, $\gamma = 0.0$ and thus $\theta = \alpha$. A free-body diagram of this wing-tail combination is shown in Fig. 4.7.2. A balance of forces normal to the fuselage reference line requires that

$$C_{L_w}\cos\alpha + C_{D_w}\sin\alpha + \frac{S_h}{S_w}\left[C_{L_h}\cos(\alpha-\varepsilon_d) + C_{D_h}\sin(\alpha-\varepsilon_d)\right] = \frac{W}{\frac{1}{2}\rho V_\infty^2 S_w}\cos\alpha$$

and a moment balance in pitch about the center of gravity gives

$$C_{m_w} - \frac{l_w}{\bar{c}_w}\left(C_{L_w}\cos\alpha + C_{D_w}\sin\alpha\right) + \frac{S_h\bar{c}_h}{S_w\bar{c}_w}C_{m_h} - \frac{S_h l_h}{S_w\bar{c}_w}\left[C_{L_h}\cos(\alpha-\varepsilon_d) + C_{D_h}\sin(\alpha-\varepsilon_d)\right] = 0$$

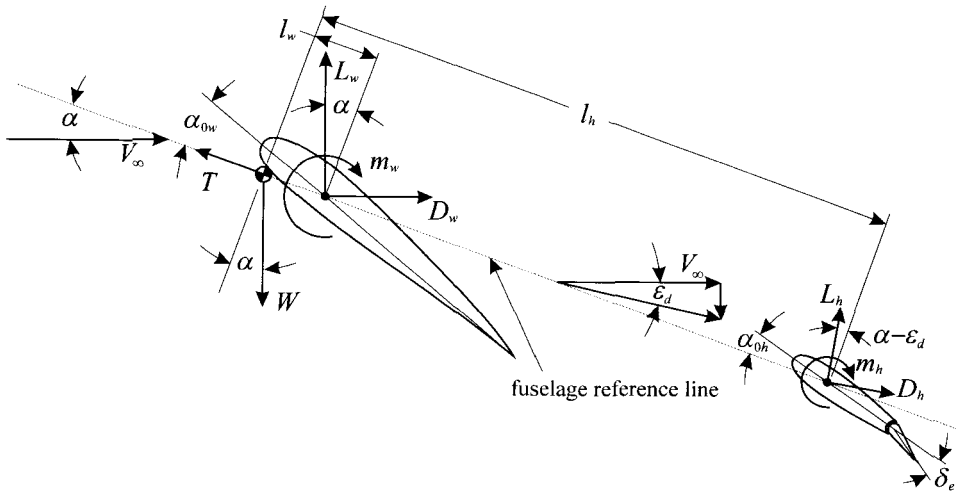


Figure 4.7.2. Free-body diagram of the wing-tail combination in Example 4.7.1.

where

$$\varepsilon_d = \varepsilon_{d0} + \varepsilon_{d,\alpha}\alpha$$

$$C_{L_w} = C_{L_w,\alpha}(\alpha + \alpha_{0w} - \alpha_{L0w})$$

$$C_{L_h} = C_{L_h,\alpha}(\alpha + \alpha_{0h} - \alpha_{L0h} - \varepsilon_d + \varepsilon_e\delta_e)$$

$$C_{D_w} = C_{D_{0w}} + C_{D_0,L_w} C_{L_w} + \frac{C_{L_w}^2}{\pi e_w R_{A_w}}$$

$$C_{D_h} = C_{D_{0h}} + C_{D_0,L_h} C_{L_h} + \frac{C_{L_h}^2}{\pi e_h R_{A_h}}$$

$$C_{m_h} = C_{m_h 0} + C_{m_h,\delta_e}\,\delta_e$$

Since the trim conditions are nonlinear in both α and δ_e, we use an iterative procedure to find the angle of attack and elevator deflection that will satisfy both conditions simultaneously. This nonlinear system is easily solved with Newton's method. The solution can be obtained quickly with a digital computer or a programmable calculator. Here we shall outline the procedure and give some example computations. The reader is cautioned that since Newton's method will involve numerical differentiation, round-off error will be amplified by several orders of magnitude and could result in numerical instability. Thus, high precision is required for the intermediate computations.

To facilitate finding the solution, it is convenient to write the trim conditions in the form

$$C_{L_w}\cos\alpha + C_{D_w}\sin\alpha + \frac{S_h}{S_w}\left[C_{L_h}\cos(\alpha-\varepsilon_d) + C_{D_h}\sin(\alpha-\varepsilon_d)\right] - \frac{W}{\frac{1}{2}\rho V_\infty^2 S_w}\cos\alpha \equiv R_L(\alpha,\delta_e)$$

$$C_{m_w} - \frac{l_w}{\bar{c}_w}\left(C_{L_w}\cos\alpha + C_{D_w}\sin\alpha\right) + \frac{S_h\bar{c}_h}{S_w\bar{c}_w}C_{m_h} - \frac{S_h l_h}{S_w\bar{c}_w}\left[C_{L_h}\cos(\alpha-\varepsilon_d) + C_{D_h}\sin(\alpha-\varepsilon_d)\right] \equiv R_m(\alpha,\delta_e)$$

where R_L and R_m are called *residuals*. We wish to find the values of α and δ_e that will make R_L and R_m simultaneously go to zero. For any other values of α and/or δ_e one or both of the residuals will be nonzero.

To demonstrate how the trim computations are carried out, consider the case of level flight at 80 mph. For this airspeed, the total lift coefficient is

$$\frac{W}{\frac{1}{2}\rho V_\infty^2 S_w} = \frac{2{,}700}{\frac{1}{2}0.0023769(80\times 5{,}280/3{,}600)^2 180} = 0.916785$$

We start with initial estimates for α and δ_e, say, $\alpha = 0$ and $\delta_e = 0$. This gives

$$\varepsilon_d = 0.04041 + 0.44033(0.0) = 0.040410$$

$$C_{L_w} = 4.44(0.0 + 0.05338 + 0.03840) = 0.407503$$

$$C_{L_h} = 3.97[0.0 + 0.04041 - 0.0 - 0.04041 + 0.60(0.0)] = 0.000000$$

$$C_{D_w} = 0.01 + \frac{(0.4075032)^2}{\pi(0.95)(6.05)} = 0.019197$$

$$C_{D_h} = 0.015 + \frac{(0.0)^2}{\pi(0.97)(4.0)} = 0.015000$$

$$C_{m_h} = 0.0 - 0.55(0.0) = 0.000000$$

Using these values, the residuals are found to be

$$R_L(0.0,0.0) = -0.509403$$

$$R_m(0.0,0.0) = 0.000316$$

To make an intelligent refinement to our initial guess, we must estimate the change in both residuals, R_L and R_m, with respect to both of the independent variables, α and δ_e. These four derivatives can be estimated numerically as

$$R_{L,\alpha}(\alpha,\delta_e) \equiv \frac{\partial R_L}{\partial \alpha}(\alpha,\delta_e) \cong \frac{R_L(\alpha+0.001,\delta_e)-R_L(\alpha-0.001,\delta_e)}{0.002}$$

$$R_{L,\delta_e}(\alpha,\delta_e) \equiv \frac{\partial R_L}{\partial \delta_e}(\alpha,\delta_e) \cong \frac{R_L(\alpha,\delta_e+0.001)-R_L(\alpha,\delta_e-0.001)}{0.002}$$

$$R_{m,\alpha}(\alpha,\delta_e) \equiv \frac{\partial R_m}{\partial \alpha}(\alpha,\delta_e) \cong \frac{R_m(\alpha+0.001,\delta_e)-R_m(\alpha-0.001,\delta_e)}{0.002}$$

$$R_{m,\delta_e}(\alpha,\delta_e) \equiv \frac{\partial R_m}{\partial \delta_e}(\alpha,\delta_e) \cong \frac{R_m(\alpha,\delta_e+0.001)-Rm(\alpha,\delta_e-0.001)}{0.002}$$

Recalculating the residuals for $\alpha = 0.001$ and $\delta_e = 0$ gives

$$R_L(0.001,0.0) = -0.504498$$

$$R_m(0.001,0.0) = -0.000271$$

and for $\alpha = -0.001$ and $\delta_e = 0$, we have

$$R_L(-0.001,0.0) = -0.514307$$

$$R_m(-0.001,0.0) = 0.000904$$

Thus

$$R_{L,\alpha}(0.0,0.0) \cong \frac{-0.504498-(-0.514307)}{0.002} = 4.904888^*$$

$$R_{m,\alpha}(0.0,0.0) \cong \frac{-0.000271-0.000904}{0.002} = -0.587747^*$$

In a similar manner, we obtain

$$R_{L,\delta_e}(0.0,0.0) \cong 0.476011$$

$$R_{m,\delta_e}(0.0,0.0) \cong -1.307633$$

---

* The computations used to obtain the numbers in this example were carried out with much greater precision than the reported six-place accuracy. By comparing these reported results with those obtained using six-place computation, it can be seen that three significant digits of accuracy are lost in this computation. This is one example of why intermediate computations should always be carried out with the full precision of the tools at hand. Only in reporting the final result should the output be rounded back to the precision of the input. If computations in this example were carried out to only two-place accuracy, these computations would produce only random numbers.

If both R_L and R_m were linear functions of α and δ_e, then the change in angle of attack, $\Delta\alpha$, and the change in elevator deflection, $\Delta\delta_e$, required to make both residuals zero would be found from

$$\begin{bmatrix} R_{L,\alpha} & R_{L,\delta_e} \\ R_{m,\alpha} & R_{m,\delta_e} \end{bmatrix} \begin{Bmatrix} \Delta\alpha \\ \Delta\delta_e \end{Bmatrix} = \begin{Bmatrix} -R_L \\ -R_m \end{Bmatrix}$$

Even though the residuals are not linear functions of α and δ_e, an improved estimate for the solution can be found by computing these changes and updating our estimates according to the relation

$$\begin{Bmatrix} \alpha \\ \delta_e \end{Bmatrix}_{\text{new}} = \begin{Bmatrix} \alpha \\ \delta_e \end{Bmatrix}_{\text{old}} + \begin{Bmatrix} \Delta\alpha \\ \Delta\delta_e \end{Bmatrix}$$

For the present case this gives

$$\begin{bmatrix} 4.904888 & 0.476011 \\ -0.587747 & -1.307633 \end{bmatrix} \begin{Bmatrix} \Delta\alpha \\ \Delta\delta_e \end{Bmatrix} = \begin{Bmatrix} 0.509403 \\ -0.000316 \end{Bmatrix}$$

$$\begin{Bmatrix} \Delta\alpha \\ \Delta\delta_e \end{Bmatrix} = \begin{Bmatrix} 0.108569 \\ -0.048557 \end{Bmatrix}$$

$$\begin{Bmatrix} \alpha \\ \delta_e \end{Bmatrix} = \begin{Bmatrix} 0.000000 \\ 0.000000 \end{Bmatrix} + \begin{Bmatrix} 0.108569 \\ -0.048557 \end{Bmatrix} = \begin{Bmatrix} 0.108569 \\ -0.048557 \end{Bmatrix}$$

With these improved estimates for the angle of attack and elevator deflection, the residuals can be recomputed. This gives

$$\begin{Bmatrix} R_L \\ R_m \end{Bmatrix} = \begin{Bmatrix} 0.003929 \\ -0.000248 \end{Bmatrix}$$

With the improved estimates for α and δ_e, the residuals are now smaller but not zero. Repeating the process to refine the estimates a second time, we obtain

$$\begin{Bmatrix} \alpha \\ \delta_e \end{Bmatrix} = \begin{Bmatrix} 0.107760 \\ -0.048379 \end{Bmatrix} = \underline{\begin{Bmatrix} 6.2^\circ \\ -2.8^\circ \end{Bmatrix}}, \quad \begin{Bmatrix} R_L \\ R_m \end{Bmatrix} = \begin{Bmatrix} 0.000000 \\ 0.000000 \end{Bmatrix}$$

The solution found in Example 4.3.1 using the simplified linear analysis was

$$\begin{Bmatrix} \alpha \\ \delta_e \end{Bmatrix} = \begin{Bmatrix} 0.10904 \\ -0.04889 \end{Bmatrix} = \underline{\begin{Bmatrix} 6.2^\circ \\ -2.8^\circ \end{Bmatrix}}$$

For this airplane with h_w, h_h, and h_T all zero, the simplified linear analysis agrees with the more exact solution to within about 1 percent. This is well within the accuracy to which we could expect to estimate the aerodynamic parameters from which this solution was obtained.

Using the computed values for the angle of attack and elevator deflection at trim, the lift on the horizontal tail of this airplane in trimmed flight at 80 mph is found to be

$$L_t = \tfrac{1}{2}\rho V_\infty^2 S_h C_{L_h,\alpha}[(1-\varepsilon_{d,\alpha})\alpha + \alpha_{0h} - \alpha_{L0h} - \varepsilon_{d0} + \varepsilon_e \delta_e] = \underline{73 \text{ lbf}}$$

This compares to a value of 74 lbf, which was computed in Example 4.3.1 using the simplified linear analysis.

Repeating these calculations at different airspeeds, the data plotted in Fig. 4.7.3 are obtained. In this figure, the dashed lines are the results computed in Example 4.3.1 using the simplified linear analysis. The solid lines are the results computed in the present example, using the full nonlinear trim conditions. The difference is insignificant.

From Example 4.7.1, we see that the approximate linear analysis gives good agreement with the more exact analysis when the wing, the horizontal surface, and the thrust vector are all in close vertical alignment with the center of gravity. When these conditions are not met, the nonlinear effects that result from drag become more significant. This is demonstrated in the following example.

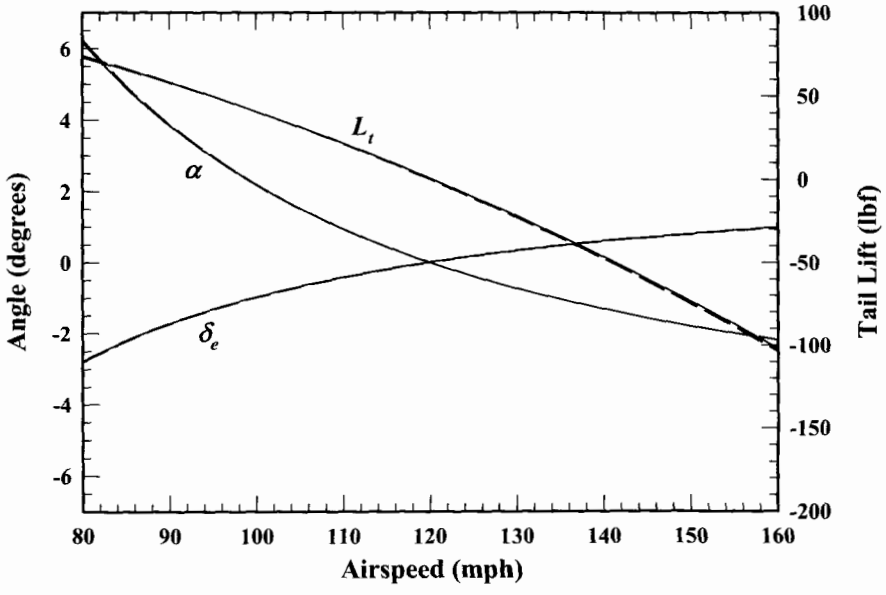


Figure 4.7.3. Conditions at level trim for the airplane in Example 4.7.1.

EXAMPLE 4.7.2. Repeat Example 4.7.1 for the case where the thrust vector is 5 feet above the center of gravity. Assume that all other properties of the airplane remain unchanged. For this airplane the wing and the horizontal tail have the following properties:

$$S_w = 180\ \text{ft}^2,\quad \bar{c}_w = 5.4545\ \text{ft},\quad R_{A_w} = 6.05,\quad e_w = 0.95,\quad l_w = -0.7094\ \text{ft},$$
$$h_w = 0.0\ \text{ft},\quad W = 2{,}700\ \text{lbf},\quad C_{L_w,\alpha} = 4.44,\quad \alpha_{0w} = 0.05338,$$
$$\alpha_{L0w} = -0.03840,\quad C_{m_w} = -0.053,\quad C_{D_{0w}} = 0.01,\quad C_{D_0,L_w} = 0.00,$$
$$S_h = 36\ \text{ft}^2,\quad \bar{c}_h = 3.0\ \text{ft},\quad R_{A_h} = 4.0,\quad e_h = 0.97,\quad l_h = 14.2906\ \text{ft},$$
$$h_h = 0.0\ \text{ft},\quad \eta_h = 1.0,\quad C_{L_h,\alpha} = 3.97,\quad \alpha_{0h} = 0.04041,$$
$$\alpha_{L0h} = 0.0,\quad \varepsilon_e = 0.60,\quad C_{m_h 0} = 0.0,\quad C_{m_h,\delta_e} = -0.55,\quad C_{D_{0h}} = 0.015,$$
$$C_{D_0,L_h} = 0.00,\quad \varepsilon_{d0} = 0.04041,\quad \varepsilon_{d,\alpha} = 0.44033,\quad h_T = 5.0\ \text{ft}$$

Solution. A free-body diagram of this wing-tail combination is shown in Fig. 4.7.4. The force balance for this example is exactly the same as that for Example 4.7.1. The only difference is that the aerodynamic pitching moment is no longer zero at trim but must balance the moment produced by the thrust of the engine. In dimensionless form, the trim requirement for pitch now becomes

$$C_{m_w} - \frac{l_w}{\bar{c}_w}\left(C_{L_w}\cos\alpha + C_{D_w}\sin\alpha\right) + \frac{S_h\bar{c}_h}{S_w\bar{c}_w}C_{m_h}$$
$$- \frac{S_h l_h}{S_w\bar{c}_w}\left[C_{L_h}\cos(\alpha-\varepsilon_d) + C_{D_h}\sin(\alpha-\varepsilon_d)\right] = \frac{h_T}{\bar{c}_w}\frac{T}{\frac{1}{2}\rho V_\infty^2 S_w}$$

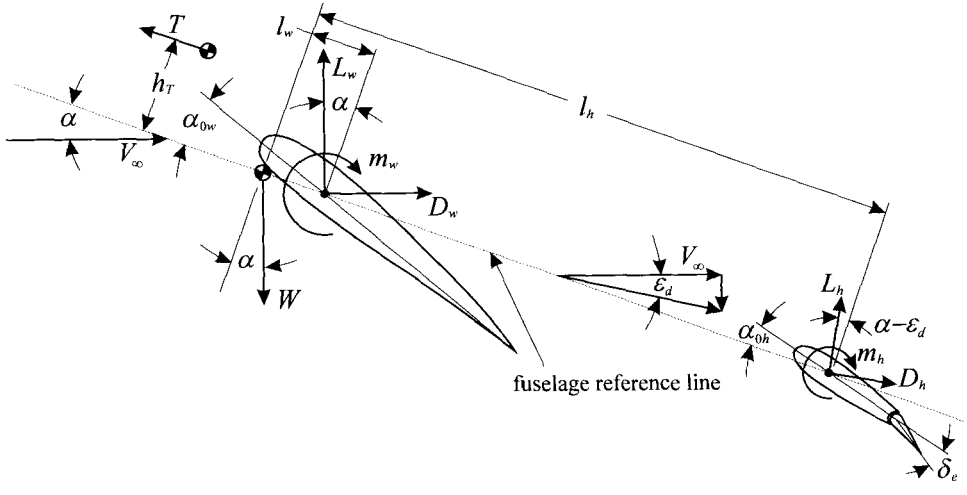


Figure 4.7.4. Free-body diagram of the wing-tail combination in Example 4.7.2.

For this geometry and level flight, the trim residual equations are

$$C_{L_w}\cos\alpha + C_{D_w}\sin\alpha + \frac{S_h}{S_w}\left[C_{L_h}\cos(\alpha-\varepsilon_d) + C_{D_h}\sin(\alpha-\varepsilon_d)\right] - \frac{W}{\frac{1}{2}\rho V_\infty^2 S_w}\cos\alpha \equiv R_L(\alpha,\delta_e)$$

$$C_{m_w} - \frac{l_w}{\bar{c}_w}\left(C_{L_w}\cos\alpha + C_{D_w}\sin\alpha\right) + \frac{S_h\bar{c}_h}{S_w\bar{c}_w}C_{m_h} - \frac{S_h l_h}{S_w\bar{c}_w}\left[C_{L_h}\cos(\alpha-\varepsilon_d) + C_{D_h}\sin(\alpha-\varepsilon_d)\right] - \frac{h_T}{\bar{c}_w}\frac{T}{\frac{1}{2}\rho V_\infty^2 S_w} \equiv R_m(\alpha,\delta_e)$$

where

$$\varepsilon_d = \varepsilon_{d0} + \varepsilon_{d,\alpha}\alpha$$

$$C_{L_w} = C_{L_w,\alpha}(\alpha + \alpha_{0w} - \alpha_{L0w})$$

$$C_{L_h} = C_{L_h,\alpha}(\alpha + \alpha_{0h} - \alpha_{L0h} - \varepsilon_d + \varepsilon_e\delta_e)$$

$$C_{D_w} = C_{D_{0w}} + C_{D_0,L_w}C_{L_w} + \frac{C_{L_w}^2}{\pi e_w R_{A_w}}$$

$$C_{D_h} = C_{D_{0h}} + C_{D_0,L_h}C_{L_h} + \frac{C_{L_h}^2}{\pi e_h R_{A_h}}$$

$$C_{m_h} = C_{m_h 0} + C_{m_h,\delta_e}\delta_e$$

and

$$\frac{T}{\frac{1}{2}\rho V_\infty^2 S_w} = \frac{W}{\frac{1}{2}\rho V_\infty^2 S_w}\sin\alpha + C_{D_w}\cos\alpha - C_{L_w}\sin\alpha + \frac{S_h}{S_w}\left[C_{D_h}\cos(\alpha-\varepsilon_d) - C_{L_h}\sin(\alpha-\varepsilon_d)\right]$$

Following the procedure used in Example 4.7.1 with an initial estimate of $\alpha = 0$ and $\delta_e = 0$, for an airspeed of 80 mph we have

$$\begin{Bmatrix}\alpha\\ \delta_e\end{Bmatrix} = \begin{Bmatrix}0.000000\\ 0.000000\end{Bmatrix}, \quad \begin{Bmatrix}R_L\\ R_m\end{Bmatrix} = \begin{Bmatrix}-0.509403\\ -0.020028\end{Bmatrix}$$

After one refinement we obtain

$$\begin{Bmatrix} \alpha \\ \delta_e \end{Bmatrix} = \begin{Bmatrix} 0.115980 \\ -0.124927 \end{Bmatrix}, \quad \begin{Bmatrix} R_L \\ R_m \end{Bmatrix} = \begin{Bmatrix} 0.004343 \\ 0.040916 \end{Bmatrix}$$

Two more iterations produce

$$\begin{Bmatrix} \alpha \\ \delta_e \end{Bmatrix} = \begin{Bmatrix} 0.111922 \\ -0.091746 \end{Bmatrix} = \underline{\begin{Bmatrix} 6.4^\circ \\ -5.3^\circ \end{Bmatrix}}, \quad \begin{Bmatrix} R_L \\ R_m \end{Bmatrix} = \begin{Bmatrix} 0.000000 \\ 0.000000 \end{Bmatrix}$$

Thus, the lift on the horizontal tail at trim is

$$L_h = \tfrac{1}{2}\rho V_\infty^2 S_h C_{L_h,\alpha}[(1-\varepsilon_{d,\alpha})\alpha + \alpha_{0h} - \alpha_{L0h} - \varepsilon_{d0} + \varepsilon_e \delta_e] = \underline{18 \text{ lbf}}$$

which differs greatly from the 74 lbf predicted from the simplified linear analysis. Repeating the calculations at different airspeeds, the data plotted in Fig. 4.7.5 are obtained. Again, the dashed lines are from the simplified linear analysis and the solid lines come from the full nonlinear trim conditions.

We have seen that aircraft drag has a significant effect on trim when the wing, the horizontal surface, and the thrust vector are not vertically aligned with the center of gravity. In general, the nonlinear drag can have a significant effect on aircraft stability as well. For the more general airplane configuration being considered in this section, the pitch stability derivative is evaluated by differentiating Eq. (4.7.6) with respect to α.

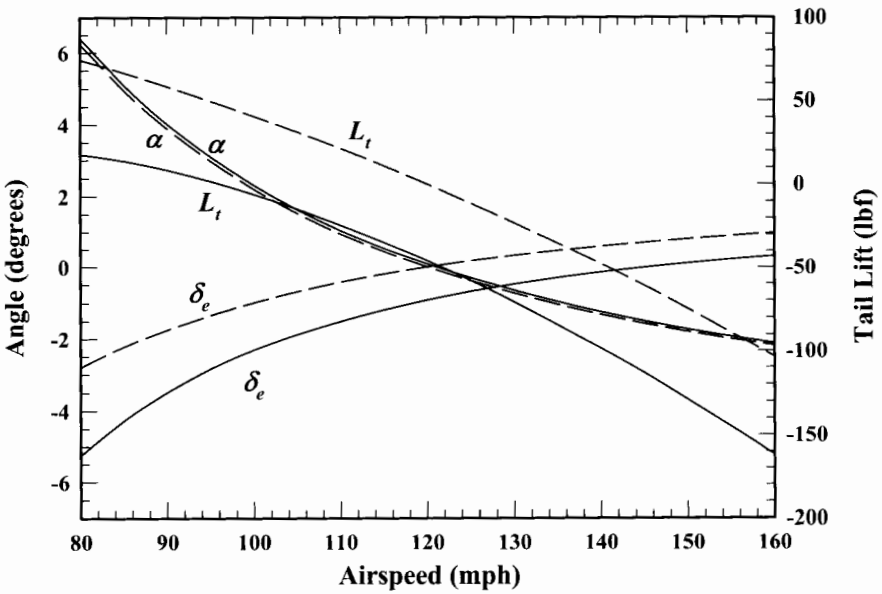


Figure 4.7.5. Conditions at level trim for the airplane in Example 4.7.2.

Since C_{m_w} and C_{m_h} are the moment coefficients relative to the aerodynamic centers of the wing and the horizontal surface, these terms in Eq. (4.7.6) are independent of angle of attack. From Eqs. (4.7.9) and (4.7.10), the changes in the drag coefficients with respect to angle of attack are

$$\frac{\partial C_{D_w}}{\partial \alpha} = \left(C_{D_0,L_w} + \frac{2C_{L_w}}{\pi e_w R_{A_w}} \right) \frac{\partial C_{L_w}}{\partial \alpha} = \left(C_{D_0,L_w} + \frac{2C_{L_w}}{\pi e_w R_{A_w}} \right) C_{L_w,\alpha} \tag{4.7.12}$$

$$\frac{\partial C_{D_h}}{\partial \alpha} = \left(C_{D_0,L_h} + \frac{2C_{L_h}}{\pi e_h R_{A_h}} \right) \frac{\partial C_{L_h}}{\partial \alpha} = \left(C_{D_0,L_h} + \frac{2C_{L_h}}{\pi e_h R_{A_h}} \right) C_{L_h,\alpha}(1-\varepsilon_{d,\alpha}) \tag{4.7.13}$$

Thus, assuming constant thrust, the pitch stability derivative is

$$\begin{aligned}
\frac{\partial C_m}{\partial \alpha} &= \left(\frac{l_w}{\bar{c}_w}\sin\alpha - \frac{h_w}{\bar{c}_w}\cos\alpha \right) C_{L_w} - \left(\frac{h_w}{\bar{c}_w}\sin\alpha + \frac{l_w}{\bar{c}_w}\cos\alpha \right) C_{D_w} \\
&- \left(\frac{l_w}{\bar{c}_w}\cos\alpha + \frac{h_w}{\bar{c}_w}\sin\alpha \right) C_{L_w,\alpha} + \left(\frac{h_w}{\bar{c}_w}\cos\alpha - \frac{l_w}{\bar{c}_w}\sin\alpha \right) \left(C_{D_0,L_w} + \frac{2C_{L_w}}{\pi e_w R_{A_w}} \right) C_{L_w,\alpha} \\
&+ \left[\frac{S_h l_h}{S_w \bar{c}_w}\sin(\alpha-\varepsilon_d) - \frac{S_h h_h}{S_w \bar{c}_w}\cos(\alpha-\varepsilon_d) \right] \eta_h C_{L_h}(1-\varepsilon_{d,\alpha}) \\
&- \left[\frac{S_h h_h}{S_w \bar{c}_w}\sin(\alpha-\varepsilon_d) + \frac{S_h l_h}{S_w \bar{c}_w}\cos(\alpha-\varepsilon_d) \right] \eta_h C_{D_h}(1-\varepsilon_{d,\alpha}) \\
&- \left[\frac{S_h l_h}{S_w \bar{c}_w}\cos(\alpha-\varepsilon_d) + \frac{S_h h_h}{S_w \bar{c}_w}\sin(\alpha-\varepsilon_d) \right] \eta_h C_{L_h,\alpha}(1-\varepsilon_{d,\alpha}) \\
&+ \left[\frac{S_h h_h}{S_w \bar{c}_w}\cos(\alpha-\varepsilon_d) - \frac{S_h l_h}{S_w \bar{c}_w}\sin(\alpha-\varepsilon_d) \right] \left(C_{D_0,L_h} + \frac{2C_{L_h}}{\pi e_h R_{A_h}} \right) \eta_h C_{L_h,\alpha}(1-\varepsilon_{d,\alpha})
\end{aligned} \tag{4.7.14}$$

For this more general case, notice that even in the range of linear lift, the stability derivative is not constant but varies with angle of attack. Thus, it is possible that an airplane could be stable for some angles of attack and be unstable for others.

EXAMPLE 4.7.3. Consider a wing-canard airplane that is similar to the one described in Example 4.6.1, except that this airplane has a high wing. The wing and the canard are geometrically similar, having the same aspect ratio and airfoil section with no sweep. The wing, canard, and engine are mounted so that, when the airplane is in level flight at the design airspeed and altitude, trim is attained with no elevator deflection and a zero angle of attack for the fuselage reference line, which passes through the center of gravity parallel to the thrust vector. At this operating condition, the following properties are known:

$$S_w = 180\ \text{ft}^2, \quad S_h = 36\ \text{ft}^2, \quad b_w = 33.0\ \text{ft}, \quad b_h = 14.758\ \text{ft}, \quad \bar{c}_w = 5.455\ \text{ft},$$
$$\bar{c}_h = 2.439\ \text{ft}, \quad R_{A_w} = R_{A_h} = 6.05, \quad R_{T_w} = R_{T_h} = 0.40, \quad C_{L_w,\alpha} = C_{L_h,\alpha} = 4.44,$$

$$C_{D_{0w}} = C_{D_{0h}} = 0.008, \quad C_{D_0,L_w} = C_{D_0,L_h} = 0.0, \quad e_w = e_h = 0.95,$$
$$C_{m_w} = C_{m_h} = -0.053, \quad \alpha_{L0w} = \alpha_{L0h} = -2.2°, \quad \alpha_{0w} = 1.8°, \quad \alpha_{0h} = 4.0°,$$
$$l_w = 3.0 \text{ ft}, \quad l_h = -12.0 \text{ ft}, \quad h_w = 4.0 \text{ ft}, \quad h_h = 0.0, \quad \eta_h = 1.0$$

With the controls fixed at this design trim condition, plot the pitching moment coefficient as a function of angle of attack from –20 to +10 degrees. Assume that the force produced by the propeller is independent of angle of attack and that neither the wing nor the canard stalls.

Solution. From Figs. 4.5.2 and 4.5.3 along with Eqs. (4.5.6) and (4.5.12) (or using a computer program), for a wing aspect ratio of 6.05, a wing taper ratio of 0.40, a wing sweep of $\Lambda = 0.0$, a canard position having $\bar{x} = -0.909$, and $\bar{y} = -0.242$, the following results are obtained:

$$\kappa_v = 1.035, \quad \kappa_b = 0.759, \quad \kappa_p = -0.054, \quad \kappa_s = 1.0$$

From Eq. (4.5.11), the downwash at the position of the canard is

$$\varepsilon_d = \frac{\kappa_v \kappa_p \kappa_s}{\kappa_b} \frac{C_{L_w}}{R_{A_w}} = \frac{1.035(-0.054)1.0}{0.759} \frac{C_{L_w}}{6.05} = -0.012\, C_{L_w}$$

At trim, the lift coefficients for the wing and the canard are

$$C_{L_w} = C_{L_w,\alpha}(\alpha + \alpha_{0w} - \alpha_{L0w}) = 4.44\left(0.0 + \frac{1.8\pi}{180} - \frac{-2.2\pi}{180}\right)$$
$$= 0.3100$$

$$\varepsilon_d = -0.012\, C_{L_w} = -0.012\,(0.3100) = -0.00372 = -0.21°$$

$$C_{L_h} = C_{L_h,\alpha}(\alpha + \alpha_{0h} - \alpha_{L0h} - \varepsilon_d)$$
$$= 4.44\left[0.0 + \frac{4.0\pi}{180} - \frac{-2.2\pi}{180} - (-0.00372)\right] = 0.4970$$

and the drag coefficients at trim are

$$C_{D_w} = C_{D_{0w}} + \frac{C_{L_w}^2}{\pi e_w R_{A_w}} = 0.008 + \frac{(0.3100)^2}{\pi(0.95)(6.05)} = 0.01332$$

$$C_{D_h} = C_{D_{0h}} + \frac{C_{L_h}^2}{\pi e_h R_{A_h}} = 0.008 + \frac{(0.4970)^2}{\pi(0.95)(6.05)} = 0.02168$$

The moment coefficient at trim is then

$$C_m = C_{m_w} - \left(\frac{l_w}{\bar{c}_w}\cos\alpha + \frac{h_w}{\bar{c}_w}\sin\alpha\right)C_{L_w} + \left(\frac{h_w}{\bar{c}_w}\cos\alpha - \frac{l_w}{\bar{c}_w}\sin\alpha\right)C_{D_w}$$
$$+ \frac{S_h\bar{c}_h}{S_w\bar{c}_w}C_{m_h} - \left[\frac{S_h l_h}{S_w\bar{c}_w}\cos(\alpha-\varepsilon_d) + \frac{S_h h_h}{S_w\bar{c}_w}\sin(\alpha-\varepsilon_d)\right]C_{L_h}$$
$$+ \left[\frac{S_h h_h}{S_w\bar{c}_w}\cos(\alpha-\varepsilon_d) - \frac{S_h l_h}{S_w\bar{c}_w}\sin(\alpha-\varepsilon_d)\right]C_{D_h}$$
$$= -0.053 - \left[\frac{3.0}{5.455}\cos(0) + \frac{4.0}{5.455}\sin(0)\right]0.3100$$
$$+ \left[\frac{4.0}{5.455}\cos(0) - \frac{3.0}{5.455}\sin(0)\right]0.01332$$
$$- \frac{36(2.439)}{180(5.455)}0.053 - \left[\frac{36(-12.0)}{180(5.455)}\cos(0+0.00372)\right]0.4970$$
$$+ \left[-\frac{36(-12.0)}{180(5.455)}\sin(0+0.00372)\right]0.02168 = \underline{0.00024}$$

Since this is the trim angle of attack, this small moment must exactly balance the pitching moment that is produced by the thrust vector. From this moment and the computations for the drag, we could compute the vertical offset for the thrust vector if that were desired.

Following the same procedure that was used for zero angle of attack, the lift coefficients for the wing and the canard at a 1.0-degree angle of attack are

$$C_{L_w} = C_{L_w,\alpha}(\alpha + \alpha_{0w} - \alpha_{L0w}) = 4.44\left(\frac{1.0\pi}{180} + \frac{1.8\pi}{180} - \frac{-2.2\pi}{180}\right) = 0.3875$$

$$\varepsilon_d = -0.012\,C_{L_w} = -0.012\,(0.3875) = -0.00465$$

$$C_{L_h} = C_{L_h,\alpha}(\alpha + \alpha_{0h} - \alpha_{L0h} - \varepsilon_d)$$
$$= 4.44\left[\frac{1.0\pi}{180} + \frac{4.0\pi}{180} - \frac{-2.2\pi}{180} - (-0.00465)\right] = 0.5786$$

and the drag coefficients are

$$C_{D_w} = C_{D_{0w}} + \frac{C_{L_w}^2}{\pi e_w R_{A_w}} = 0.008 + \frac{(0.3875)^2}{\pi(0.95)(6.05)} = 0.01632$$

$$C_{D_h} = C_{D_{0h}} + \frac{C_{L_h}^2}{\pi e_h R_{A_h}} = 0.008 + \frac{(0.5786)^2}{\pi(0.95)(6.05)} = 0.02654$$

Thus, with the controls fixed at the trim settings but with an angle of attack of 1.0 degree, the pitching moment coefficient would be

$$C_m = C_{m_w} - \left(\frac{l_w}{\bar{c}_w}\cos\alpha + \frac{h_w}{\bar{c}_w}\sin\alpha\right)C_{L_w} + \left(\frac{h_w}{\bar{c}_w}\cos\alpha - \frac{l_w}{\bar{c}_w}\sin\alpha\right)C_{D_w}$$
$$+ \frac{S_h\bar{c}_h}{S_w\bar{c}_w}C_{m_h} - \left[\frac{S_h l_h}{S_w\bar{c}_w}\cos(\alpha-\varepsilon_d) + \frac{S_h h_h}{S_w\bar{c}_w}\sin(\alpha-\varepsilon_d)\right]C_{L_h}$$
$$+ \left[\frac{S_h h_h}{S_w\bar{c}_w}\cos(\alpha-\varepsilon_d) - \frac{S_h l_h}{S_w\bar{c}_w}\sin(\alpha-\varepsilon_d)\right]C_{D_h}$$
$$= -0.053 - \left[\frac{3.0}{5.455}\cos\left(\frac{1.0\pi}{180}\right) + \frac{4.0}{5.455}\sin\left(\frac{1.0\pi}{180}\right)\right]0.3875$$
$$+ \left[\frac{4.0}{5.455}\cos\left(\frac{1.0\pi}{180}\right) - \frac{3.0}{5.455}\sin\left(\frac{1.0\pi}{180}\right)\right]0.01632$$
$$- \frac{36(2.439)}{180(5.455)}0.053 - \left[\frac{36(-12.0)}{180(5.455)}\cos\left(\frac{1.0\pi}{180} + 0.00465\right)\right]0.5786$$
$$+ \left[-\frac{36(-12.0)}{180(5.455)}\sin\left(\frac{1.0\pi}{180} + 0.00465\right)\right]0.02654 = \underline{-0.00920}$$

It is important to recognize that this operating condition does not correspond to a trim point. At this angle of attack the airplane is not in trim, because the lift is not equal to the weight and the aerodynamic pitching moment does not balance the pitching moment that is produced as a result of the thrust developed by the engine. This does not mean that the airplane could not be at this angle of attack with the controls in this position. It simply means that since this is not a trim point, the airplane must be accelerating. Atmospheric turbulence can cause the angle of attack to deviate significantly from trim with no control input.

Repeating these calculations at different angles of attack, the data plotted in Fig. 4.7.6 are obtained. In addition to the moment coefficient, this figure also shows the lift coefficients for the wing and the canard over the same range of angle of attack. Notice that the maximum lift coefficient for the canard is slightly greater than 1.3, while the minimum lift coefficient for the wing is about −1.2. Thus, the angle of attack range that is shown in Fig. 4.7.6 corresponds roughly to the range between negative and positive stall.

The slope of the moment coefficient curve in Fig. 4.7.6 is the pitch stability derivative. Notice that the change in the moment coefficient with respect to angle of attack is negative for angles of attack greater than about −6 degrees. However, the slope becomes positive when the angle of attack is less than −6 degrees. This does not mean that the airplane is unstable according to our mathematical definition of stability. Stability is always defined relative to a trim point. The only trim point on this curve is that for zero fuselage angle of attack. The moment slope is negative at this trim point, so this equilibrium flight condition is mathematically stable in pitch. However, this simply means that the airplane is stable with respect to an infinitesimal pitch disturbance. Unfortunately, the atmosphere cares little for mathematics, and as anyone who has spent much time in an airplane knows, disturbances are not always infinitesimal.

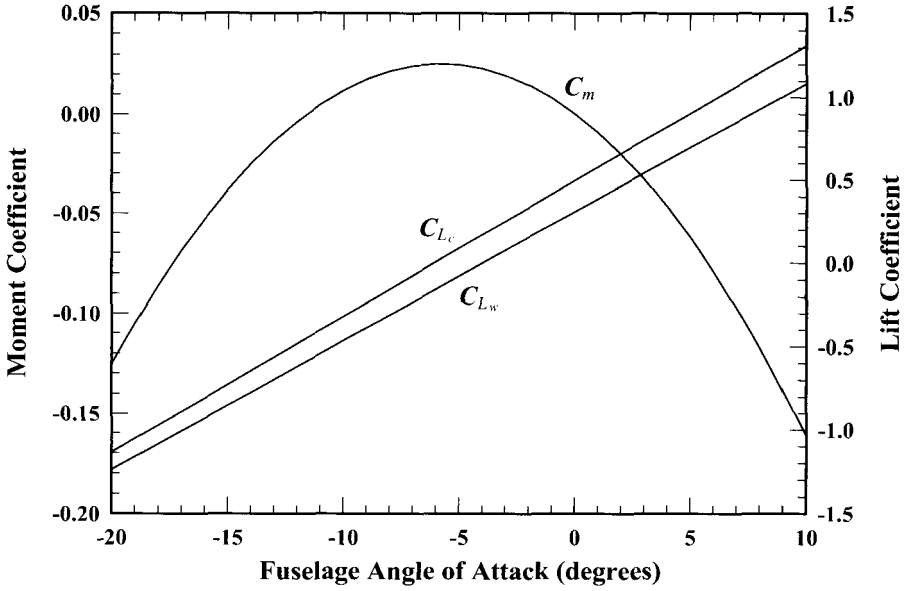


Figure 4.7.6. Pitching moment and lift coefficients for the airplane in Example 4.7.3, with a vertical wing offset of 4.0 feet.

The stable trimmed flight condition described in Example 4.7.3 is like the stable equilibrium shown in Fig. 4.1.2d. From Fig. 4.7.6, we see that large negative disturbances in angle of attack do not produce a restoring moment. When the airplane is flying at trim ($\alpha = 0$), a pitch disturbance of -6 degrees produces a maximum in the restoring moment. For larger negative disturbances, the restoring moment decreases. A pitch disturbance of about -12 degrees produces no restoring moment, and larger negative disturbances will produce divergence. This trait could not be exposed using the simplified linear stability analysis presented in Sec. 4.6.

The condition shown in Fig. 4.7.6 can be dangerous. The airplane is stable for the angles of attack that are usually encountered in normal flight, but it is unstable for large negative disturbances in angles of attack. Under normal flying conditions, the airplane could be flown for years and never encounter the large negative angles of attack that are required to expose this "instability." However, in turbulence the angle of attack can change vary rapidly, with no control input from the pilot. Under such conditions, large negative angles of attack may be unavoidable. With an airplane that displays the characteristic that is shown in Fig. 4.7.6, the airplane could suddenly and unexpectedly become inverted in severe turbulence, even though the airplane has never previously exhibited any unstable tendencies.

A similar situation sometimes occurs in ultralight hang gliders like the one shown in Fig. 4.7.7. For the angle of attack range encountered in normal flight, the glider is completely stable. However, when exiting a strong thermal the glider can suddenly pass from a region of very high lift into heavy sink, which is caused by the displaced cold air

spilling down over the outside of the warm air rising in the thermal. For obvious reasons, this is commonly called "going over the falls." When this happens, the glider can suddenly undergo a very large decrease in angle of attack. If the glider is stable at all angles of attack, the experience will simply result in a sudden decrease in the pitch attitude and a rapid downward acceleration that increases the angle of attack and eventually returns the glider to trimmed flight. However, if the glider is not stable at large negative angles of attack, which are not normally encountered in flight, "going over the falls" can cause the glider to flip and incur significant structural damage. Hang gliders are naturally susceptible to this trait because of the large vertical separation between the aerodynamic center of the wing and the center of gravity. This design flaw can be avoided with proper use of sweep and washout.

The characteristic that is shown in Fig. 4.7.6 is most likely to occur in a canard or tailless aircraft having a high-wing design and is sometimes called *canard tuck*. This condition can be avoided with proper design, even with a moderately high wing. However, the easiest way to avoid the characteristic is by keeping both the center of gravity and the aerodynamic center of the wing closely aligned with an axis that is approximately parallel with the direction of flight. To demonstrate this fact, Example 4.7.3 can be reworked with the wing moved down to the fuselage reference line ($h_w = 0$). The results of such computations are shown Fig. 4.7.8. Notice that for this configuration, the pitching moment coefficient remains quite linear with angle of attack, from negative to positive stall.



Figure 4.7.7. Ultralight hang gliders sometimes exhibit pitch instability at large negative angles of attack. (Photograph by Barry Santana)

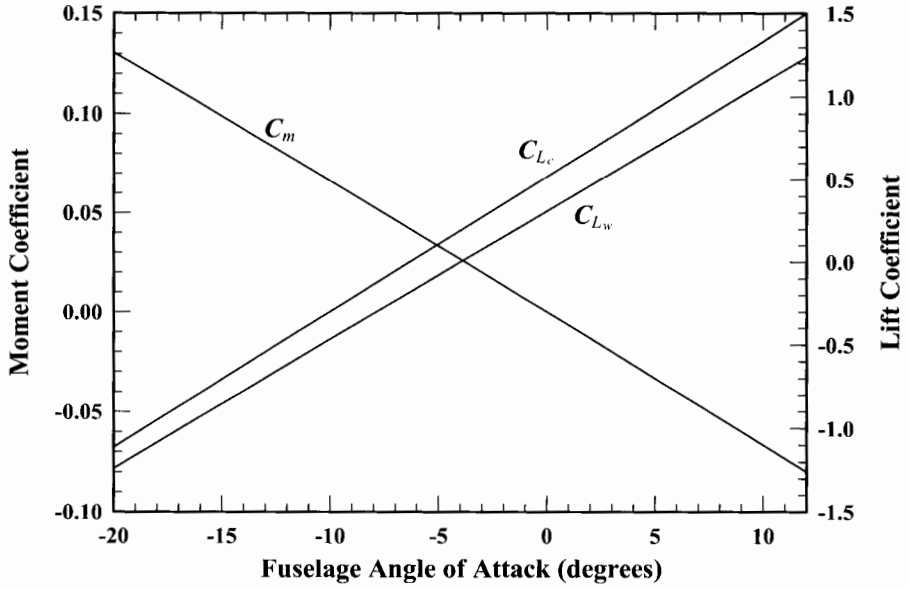


Figure 4.7.8. Pitching moment and lift coefficients for the airplane in Example 4.7.3, with no vertical wing offset.

A significant nonlinear variation in the pitching moment coefficient with angle of attack will occur whenever the center of gravity is not in close vertical alignment with the aerodynamic center of the airplane. The aerodynamic pressure and shear forces acting on an airplane can always be resolved into a lift force, a drag force, and an aerodynamic moment, all acting at the aerodynamic center, as is shown in Fig. 4.7.9. Here we let m_{ac} denote the aerodynamic pitching moment about the aerodynamic center.

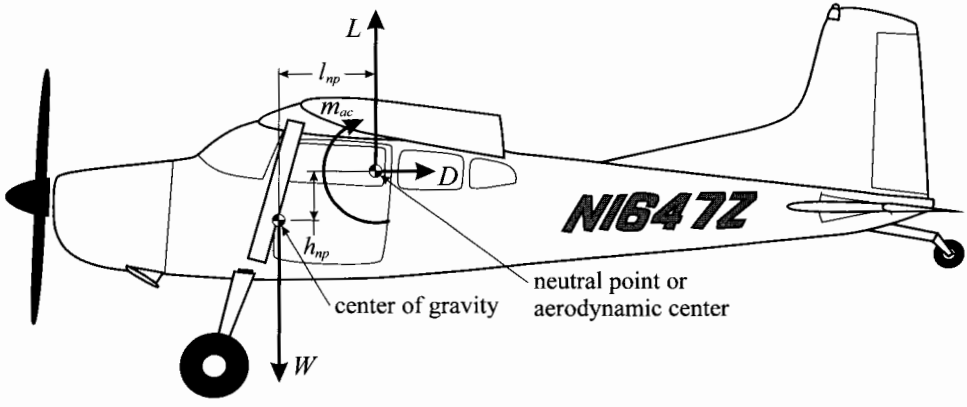


Figure 4.7.9. Vertical offset between the aerodynamic center and the center of gravity.

According to our usual notation, we use m to represent the aerodynamic pitching moment about the center of gravity. Then from the free-body diagram in Fig. 4.7.9, a summation of moments about the center of gravity gives

$$m = m_{ac} - l_{np}L + h_{np}D \tag{4.7.15}$$

Nondimensionalizing Eq. (4.7.15), we have

$$C_m = C_{m_{ac}} - \frac{l_{np}}{\bar{c}_w}C_L + \frac{h_{np}}{\bar{c}_w}C_D \tag{4.7.16}$$

By definition, the aerodynamic center is the point on the airplane where the aerodynamic moment does not change with angle of attack. Thus, differentiating Eq. (4.7.16) with respect to angle of attack results in

$$C_{m,\alpha} = -\frac{l_{np}}{\bar{c}_w}C_{L,\alpha} + \frac{h_{np}}{\bar{c}_w}C_{D,\alpha} \tag{4.7.17}$$

Equation (4.7.17) provides a more general relation for the pitch stability derivative than does the more commonly used result given by Eq. (4.4.13). Because the drag coefficient is not linear with angle of attack, a vertical offset between the aerodynamic center and the center of gravity will produce a nonlinear pitching moment coefficient.

Potential problems can also arise when the thrust vector has a significant vertical offset from the center of gravity. For example, consider the amphibian shown in Fig. 4.7.10. This airplane has a thrust vector that is considerably above the center of gravity. This condition frequently occurs with amphibians, because of the need to keep the propeller out of the water. When the thrust vector has a large vertical offset from the



Figure 4.7.10. Example of an airplane with a high thrust vector. (Photographs by Barry Santana)

CG, a large aerodynamic pitching moment is required to trim the airplane against the pitching moment produced by the engine. In the case of the airplane that is shown in Fig. 4.7.10, the thrust developed by the engine produces a negative pitching moment about the center of gravity. To offset this negative pitching moment, the airplane must be trimmed so that the airframe produces a balancing positive moment. At takeoff, when the engine is producing maximum thrust, the positive pitching moment needed to trim the airplane is greatest. If the engine should suddenly fail just after liftoff, the thrust developed by the engine would be replaced with drag. Thus, the negative pitching moment produced by the engine would be replaced with a positive pitching moment. This moment, combined with the additional positive pitching moment that is being applied to trim the airplane at full throttle, will cause a rapid nose-up rotation of the airplane. If the pilot does not respond with a rapid nose-down control input, the wing could easily stall. Engine failure just after liftoff is always dangerous. However, the danger is greatly amplified if the wing should stall.

Such a high thrust vector can also cause some potential difficulties on landing, should a go-around become necessary. On a typical landing the thrust is considerably less than maximum thrust. When the pilot decides that a go-around is prudent, full throttle is applied as rapidly as possible. With a high thrust vector, this rapid increase in thrust causes a negative pitching moment, which puts the airplane out of trim and pitches the nose down. Rapid nose-up control input is needed just to keep the airplane in trim. This tendency for the airplane to pitch down when the throttle is increased makes it more difficult for the pilot to climb out quickly after the go-around is initiated. Greater pitch control authority is needed for such designs.

As we have seen from the material presented in this section, the moments associated with the vertical offset of the wing, tail, and thrust vector can be important. While accounting for these moments will increase the complexity of the trim and stability analysis, it is not conceptually difficult. However, the added bookkeeping does increase the possibility of making an error. To minimize this possibility, **the student should always draw a good free-body diagram**. It also helps to use a consistent notation for labeling the axial and vertical offsets. In this text it is suggested that **the variable *l* should always be used to denote a distance measured aft of the center of gravity, and the variable *h* should always be used to denote a distance measured above the center of gravity**.

4.8. Contribution of the Fuselage and Nacelles

The contribution of the fuselage and nacelles to the static stability of an airplane is typically destabilizing. Furthermore, in some cases this destabilizing effect can be quite significant. Thus, the fuselage and nacelles should be included in the trim and stability analysis during all phases of the airplane design process.

The aerodynamic forces and moments generated on the fuselage and nacelles are extremely complex, and are significantly affected by aerodynamic interactions with the wing and the tail. To estimate these forces and moments accurately, we must make use of computer simulations and/or wind tunnel tests. Such methods should always be employed in the later phases of the airplane design process. However, for the purpose of

preliminary design, it is useful to have some method that can be used to easily obtain a first approximation for these effects.

As a first approximation, the effect of the fuselage and nacelles on airplane lift is usually neglected. However, even for preliminary design, some estimation of the effect of the fuselage and nacelles on the airplane moments should be made. The method to be presented here is taken from Hoak (1960). The method is presented in terms of the fuselage, but exactly the same approach can be used for the nacelles.

Consider the fuselage geometry shown in Fig. 4.8.1. As has been our usual convention, l will indicate a distance measured aft of the CG and c will indicate the total length of an object in the chordwise direction. While the characteristic area for a lifting surface such as the wing or the tail is always taken as the planform area, the characteristic area for a fuselage or nacelle is typically defined to be the projected frontal area. This is the maximum cross-sectional area of the body in a plane normal to the axial chord.

A rough estimate of the fuselage pitching moment coefficient about the airplane center of gravity can be made from the experimental correlation,

$$C_{m_f} \equiv \frac{m_{cg_f}}{\frac{1}{2}\rho V_\infty^2 S_f c_f} = -2\frac{l_f}{c_f}\left[1 - 1.76\left(\frac{d_f}{c_f}\right)^{3/2}\right]\alpha_f \tag{4.8.1}$$

where S_f is the maximum cross-sectional area of the fuselage, c_f is the chord length of the fuselage, l_f is the distance that the fuselage center of pressure is aft of the airplane center of gravity, d_f is the diameter of a circle having the same area as the maximum cross-sectional area of the fuselage,

$$d_f \equiv 2\sqrt{S_f/\pi} \tag{4.8.2}$$

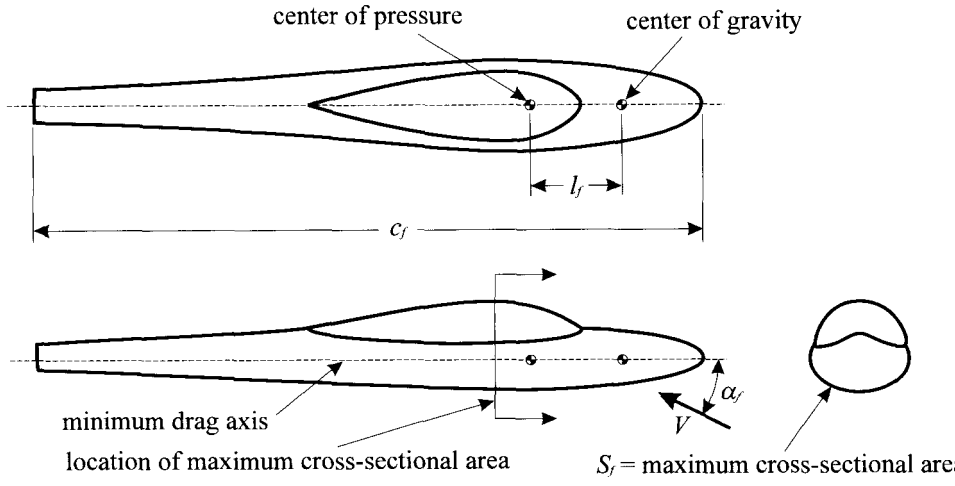


Figure 4.8.1. Fuselage geometry.

and α_f is the angle of attack for the minimum drag axis of the fuselage. As a first estimate, the fuselage center of pressure can be assumed to be halfway between the nose and the point of maximum cross-sectional area. Since this point is normally forward of the airplane center of gravity, l_f is typically negative.

The pitching moment computed from Eq. (4.8.1) can be added to the contributions from the wing and the tail to obtain an estimate for the complete airframe. However, the characteristic area for the complete airplane was defined to be the area of the main wing, and the characteristic length was defined to be the mean chord length of the main wing. Thus, the contribution of the fuselage to the total airplane pitching moment coefficient can be approximated by multiplying the result from Eq. (4.8.1) by the product $S_f c_f$ and dividing by the product $S_w \bar{c}_w$:

$$(\Delta C_m)_f \equiv \frac{m_{cg_f}}{\frac{1}{2}\rho V_\infty^2 S_w \bar{c}_w} = \frac{S_f c_f}{S_w \bar{c}_w} C_{m_f} = -2\frac{S_f l_f}{S_w \bar{c}_w}\left[1 - 1.76\left(\frac{d_f}{c_f}\right)^{3/2}\right]\alpha_f \quad (4.8.3)$$

This can be written as

$$(\Delta C_m)_f = (\Delta C_{m0})_f + (\Delta C_{m,\alpha})_f \alpha \quad (4.8.4)$$

where

$$(\Delta C_{m0})_f = -2\frac{S_f l_f}{S_w \bar{c}_w}\left[1 - 1.76\left(\frac{d_f}{c_f}\right)^{3/2}\right]\alpha_{0f} \quad (4.8.5)$$

and

$$(\Delta C_{m,\alpha})_f = -2\frac{S_f l_f}{S_w \bar{c}_w}\left[1 - 1.76\left(\frac{d_f}{c_f}\right)^{3/2}\right] \quad (4.8.6)$$

α is the airplane angle of attack relative to the fuselage reference line, and α_{0f} is the angle that the minimum drag axis of the fuselage makes with the fuselage reference line. Since the fuselage center of pressure is usually forward of the airplane center of gravity making l_f negative, the fuselage contribution to the pitch stability derivative is typically destabilizing.

It is important to remember that this method gives only a very rough estimate of the aerodynamic pitching moment generated on the fuselage, and it should only be used as a first estimate for preliminary design. Wind tunnel tests and/or computer simulations should always be used in the later phases of design. Because the aerodynamic moments generated on the fuselage are primarily the result of pressure forces, panel methods will give a reasonable estimate for these moments. However, for best results, viscous computational fluid dynamics (CFD) or wind tunnel tests should be used.

EXAMPLE 4.8.1. The airplane described in Example 4.4.1 has a fuselage that is 23 ft long. The point of maximum cross-section is located 9 ft aft of the nose and the airplane center of gravity is 8 ft aft of the nose. The maximum cross-sectional area of the fuselage is 21 ft^2. Estimate the static margin in the linear lift range for the complete airframe, including the effect of the fuselage.

Solution. For this airplane we have

$$S_w = 180\,\text{ft}^2, \quad b_w = 33\,\text{ft}, \quad C_{L_w,\alpha} = 4.44, \quad l_w = -0.71\,\text{ft},$$
$$S_t = 36\,\text{ft}^2, \quad b_t = 12\,\text{ft}, \quad C_{L_t,\alpha} = 3.97, \quad l_t = 14.29\,\text{ft},$$
$$\eta_t = 1.0, \quad \varepsilon_{d,\alpha} = 0.44, \quad S_f = 21\,\text{ft}^2, \quad d_f = 2\sqrt{21\,\text{ft}^2/\pi} = 5.17\,\text{ft},$$
$$c_f = 23\,\text{ft}, \quad l_f = (9\,\text{ft}/2) - 8\,\text{ft} = -3.5\,\text{ft}$$

By definition, the moment slope relative to the stick-fixed neutral point is zero. Thus, using Eq. (4.8.6) to estimate the fuselage contribution yields

$$\frac{\partial C_{m_{np}}}{\partial \alpha} = -\frac{l_w - l_{np}}{\bar{c}_w} C_{L_w,\alpha} - \frac{S_t(l_t - l_{np})}{S_w \bar{c}_w} \eta_t (1 - \varepsilon_{d,\alpha}) C_{L_t,\alpha}$$
$$- 2\frac{S_f(l_f - l_{np})}{S_w \bar{c}_w}\left[1 - 1.76\left(\frac{d_f}{c_f}\right)^{3/2}\right] = 0$$

Solving for the static margin gives

$$\frac{l_{np}}{\bar{c}_w} = \frac{l_w C_{L_w,\alpha} + \dfrac{S_t l_t}{S_w}\eta_t(1-\varepsilon_{d,\alpha})C_{L_t,\alpha} + 2\dfrac{S_f l_f}{S_w}\left[1 - 1.76\left(\dfrac{d_f}{c_f}\right)^{3/2}\right]}{\bar{c}_w\left\{C_{L_w,\alpha} + \dfrac{S_t}{S_w}\eta_t(1-\varepsilon_{d,\alpha})C_{L_t,\alpha} + 2\dfrac{S_f}{S_w}\left[1 - 1.76\left(\dfrac{d_f}{c_f}\right)^{3/2}\right]\right\}}$$

$$= \frac{(-0.71)4.44 + \dfrac{36(14.29)}{180}1.0(1-0.44)3.97 + 2\dfrac{21(-3.5)}{180}\left[1 - 1.76\left(\dfrac{5.17}{23}\right)^{3/2}\right]}{\dfrac{180}{33}\left\{4.44 + \dfrac{36}{180}1.0(1-0.44)3.97 + 2\dfrac{21}{180}\left[1 - 1.76\left(\dfrac{5.17}{23}\right)^{3/2}\right]\right\}}$$

$$= \underline{9\%}$$

Comparing this result with that from Example 4.4.1, we see that the destabilizing effect of the fuselage was to move the neutral point forward by about 3 percent of the wing chord. This is significant when one considers that the minimum design criterion for static margin is only 5 percent of the wing chord.

4.9. Contribution of Running Propellers

Running propellers can have a profound effect on the trim and static stability of an airplane. The contributions of a running propeller to trim and static stability can be divided into two main categories. These are the direct effects, arising from the aerodynamic forces and moments on the propeller itself, and the indirect effects, which result from the interaction of the propeller slipstream with other surfaces of the airplane.

The effects of the propeller slipstream on other airplane surfaces such as the wing, tail, and fuselage are very complex and do not lend themselves to accurate analytical treatment. These effects can be accurately evaluated only from powered wind tunnel tests. Such tests are commonly performed in the final phase of the airplane design process. Simply because of complexity, the slipstream effects are usually neglected in the preliminary design phase. It should be remembered, however, that the slipstream effects can be significant.

The direct effects of the propeller forces and moments, on the other hand, can be estimated analytically using the method presented in Chapter 2. When a rotating propeller is advancing through the air so that the axis of rotation make some angle of attack with the freestream, in addition to the thrust, a normal force is produced that is proportional to the angle of attack. This is shown in Figs. 4.9.1 and 4.9.2. The pitching moment that the propeller produces about the airplane's center of gravity is a result of the thrust and normal force, each multiplied by the appropriate moment arm,

$$m_{cg_p} = -h_p T - l_p N_p \tag{4.9.1}$$

where T and N_p are, respectively, the propeller thrust and normal force. For consistency, we are defining l_p as the axial distance that the propeller is mounted aft of the CG and h_p is the vertical distance that the propeller axis is above the CG. For a conventional tractor prop, l_p is typically negative, and for a pusher prop, l_p is usually positive.



Figure 4.9.1. Forces generated by an aft propeller. (Photograph by Barry Santana)

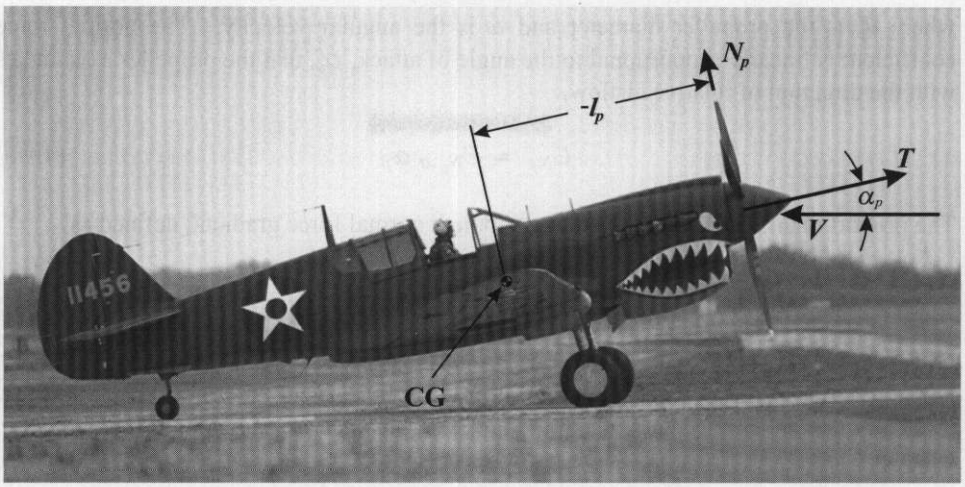


Figure 4.9.2. Forces generated by a forward propeller. (Photograph by Barry Santana)

The pitching moment computed from Eq. (4.9.1) can be added to the pitching moment obtained for all of the other airplane components to determine the pitching moment for the complete airplane. Thus, the contribution of the propeller to the total airplane pitching moment coefficient is found by nondimensionalizing Eq. (4.9.1),

$$\left(\Delta C_m\right)_p = \frac{m_{cg_p}}{\frac{1}{2}\rho V_\infty^2 S_w \bar{c}_w} = -\frac{h_p}{\bar{c}_w}\frac{T}{\frac{1}{2}\rho V_\infty^2 S_w} - \frac{l_p}{\bar{c}_w}\frac{N_p}{\frac{1}{2}\rho V_\infty^2 S_w} \tag{4.9.2}$$

For small thrust angles the equilibrium thrust is nearly equal to the drag and Eq. (4.9.2) can be closely approximated as

$$\left(\Delta C_m\right)_p = \frac{m_{cg_p}}{\frac{1}{2}\rho V_\infty^2 S_w \bar{c}_w} = -\frac{h_p}{\bar{c}_w} C_D - \frac{l_p}{\bar{c}_w}\frac{N_p}{\frac{1}{2}\rho V_\infty^2 S_w} \tag{4.9.3}$$

While the equilibrium thrust developed by an airplane's propeller can be related to the airplane drag, this cannot be said for the propeller normal force. To evaluate the propeller normal force, we return to the material presented in Chapter 2.

Propeller forces are conventionally expressed in terms of the thrust coefficient and the normal force coefficient,

$$C_T \equiv \frac{T}{\rho(\omega/2\pi)^2 d_p^4} \tag{4.9.4}$$

$$C_{N_p} \equiv \frac{N_p}{\rho(\omega/2\pi)^2 d_p^4} \tag{4.9.5}$$

where d_p is the propeller diameter and ω is the angular velocity. The normal force coefficient is linearly proportional to the angle of attack, α_p, that the propeller axis makes with the direction of relative airflow,

$$C_{N_p} = C_{N_p,\alpha}\,\alpha_p \tag{4.9.6}$$

The proportionality constant is the dimensionless normal force gradient, defined as

$$C_{N_p,\alpha} \equiv \frac{1}{\rho(\omega/2\pi)^2 d_p^4}\frac{\partial N_p}{\partial \alpha_p} \tag{4.9.7}$$

For a given propeller geometry both the thrust coefficient and the dimensionless normal force gradient are strong functions of the propeller advance ratio, J, which was defined in Chapter 2 as

$$J \equiv \frac{2\pi V_\infty}{\omega d_p} \tag{4.9.8}$$

With a fixed-pitch propeller of given geometry, to attain some particular level flight airspeed, the pilot must adjust the propeller's rotational speed so that the propeller thrust will balance the drag at the desired airspeed. The advance ratio that is required to balance the drag with the thrust determines the propeller normal force gradient for a particular operating condition. Since the thrust coefficient decreases with increasing advance ratio while the dimensionless normal force gradient increases with increasing advance ratio, the propeller's effect on static stability and trim will vary significantly with propeller advance ratio.

Using Eqs. (4.9.5) through (4.9.8) in Eq. (4.9.3), the contribution of the propeller to the total airplane pitching moment coefficient is

$$(\Delta C_m)_p = -\frac{h_p}{\bar{c}_w} C_D - \frac{2 d_p^2 l_p}{S_w \bar{c}_w}\frac{C_{N_p,\alpha}}{J^2}\alpha_p \tag{4.9.9}$$

The dimensionless normal force gradient, which appears in Eq. (4.9.9), depends on the number and geometry of the propeller blades, as well as the advance ratio. For known propeller geometry, the normal force gradient can be determined as a function of advance ratio using the method presented in Chapter 2. For example, Fig. 4.9.3 shows the dimensionless normal force gradient divided by the advance ratio squared, plotted as a function of advance ratio and pitch-to-diameter ratio, K_c, for one particular propeller blade geometry.

The propeller angle of attack in Eq. (4.9.9) is affected by the airflow around the wing. If the propeller is aft of the wing, it is located in a region of downwash and the propeller angle of attack is decreased. If the propeller is forward of the wing, it is in a region of upwash and the propeller angle of attack is increased. The angle of attack that the propeller axis makes with the local relative airflow can be written as

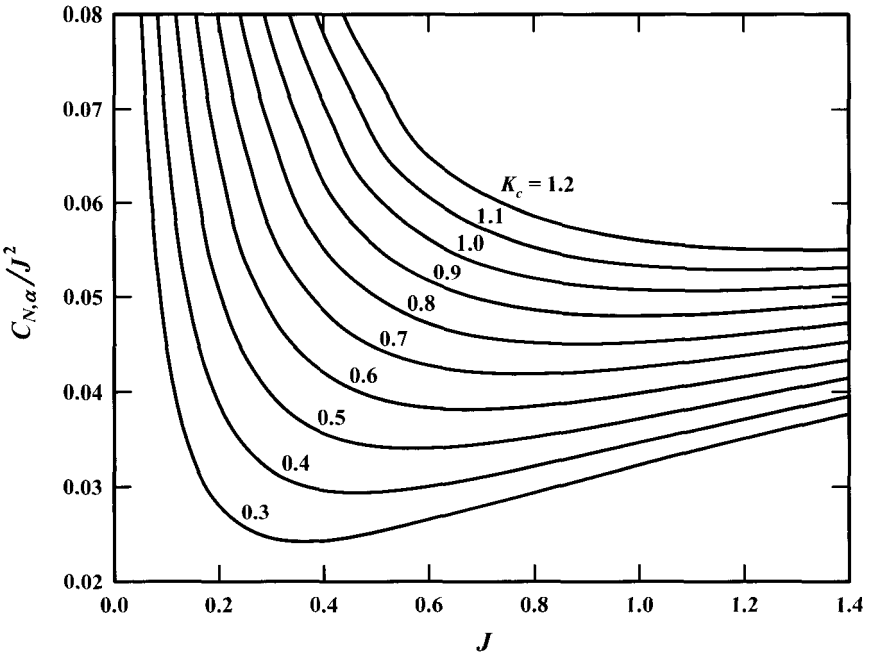


Figure 4.9.3. Dimensionless normal force gradient divided by the advance ratio squared.

$$\alpha_p = \alpha - \varepsilon_{dp} + \alpha_{0p} \tag{4.9.10}$$

where α is the airplane angle of attack relative to the fuselage reference line, ε_{dp} is the local downwash angle at the position of the propeller, and α_{0p} is the angle that the propeller axis makes with the fuselage reference line. It should be noted that in some textbooks, a propeller upwash angle is used in Eq. (4.9.10), because propellers are most commonly mounted ahead of the wing. For consistency with the material presented in Sec. 4.5, in this textbook we are defining ε_{dp} as the propeller downwash angle. With the present definition, if the propeller is forward of the wing, ε_{dp} is negative. If the propeller is aft of the wing, ε_{dp} is positive.

Using Eq. (4.9.10) with Eq. (4.9.9), the contribution of the propeller to the total airplane pitching moment coefficient can be written as

$$(\Delta C_m)_p = (\Delta C_{m0})_p + (\Delta C_{m,\alpha})_p \alpha \tag{4.9.11}$$

where

$$(\Delta C_{m0})_p = -\frac{h_p}{\bar{c}_w} C_D - \frac{2 d_p^2 l_p}{S_w \bar{c}_w} \frac{C_{N_p,\alpha}}{J^2} (\alpha_{0p} - \varepsilon_{d0p}) \tag{4.9.12}$$

$$\left(\Delta C_{m,\alpha}\right)_p = -\frac{2d_p^2 l_p}{S_w \bar{c}_w}(1-\varepsilon_{d,\alpha})_p \frac{C_{N_p,\alpha}}{J^2} \tag{4.9.13}$$

ε_{d0p} is the propeller downwash angle with the fuselage reference line at zero angle of attack and $(\varepsilon_{d,\alpha})_p$ is the downwash gradient at the position of the propeller. Since the change in the normal force coefficient with angle of attack is positive, if the propeller is forward of the center of gravity, l_p is negative and the propeller contribution to the pitch stability derivative is destabilizing. If the propeller is aft of the center of gravity, l_p is positive and the propeller contribution to the pitch stability derivative is stabilizing.

EXAMPLE 4.9.1. The airplane described in Examples 4.4.1 and 4.8.1 is powered by a piston engine turning a 74-inch propeller at 2,350 rpm and is flying at 80 mph. The change in normal force coefficient with propeller angle of attack for this propeller and operating condition is 0.04. The propeller is mounted in front of the fuselage and is 9 feet forward of the center of gravity. Estimate the static margin in the linear lift range for the complete airplane, including the effect of the fuselage and propeller.

Solution. For this airplane we have

$$S_w = 180\ \text{ft}^2, \quad b_w = 33\ \text{ft}, \quad C_{L_w,\alpha} = 4.44, \quad l_w = -0.71\ \text{ft},$$
$$S_t = 36\ \text{ft}^2, \quad b_t = 12\ \text{ft}, \quad C_{L_t,\alpha} = 3.97, \quad l_t = 14.29\ \text{ft},$$
$$R_{T_w} = 0.40, \quad \Lambda_w = 0°, \quad \eta_t = 1.0, \quad (\varepsilon_{d,\alpha})_t = 0.44,$$
$$S_f = 21\ \text{ft}^2, \quad d_f = 2\sqrt{21\ \text{ft}^2/\pi} = 5.17\ \text{ft}, \quad c_f = 23\ \text{ft}, \quad l_f = -3.5\ \text{ft},$$
$$d_p = 74/12\ \text{ft}, \quad \omega/2\pi = 2{,}350\ \text{rpm}, \quad l_p = -9\ \text{ft}, \quad V_\infty = 80\ \text{mph}, \quad C_{N_p,\alpha} = 0.04$$

For this propeller and airspeed the advance ratio is

$$J = \frac{V_\infty}{(\omega/2\pi)d_p} = \frac{80\times 5{,}280/3{,}600}{(2{,}350/60)(74/12)} = 0.4858$$

The downwash angle for the propeller can be estimated using the method presented in Sec. 4.5. For this wing and propeller position, we have

$$R_{Aw} = 6.05, \quad R_{Tw} = 0.40, \quad \bar{x} = \frac{l_p - l_w}{b_w/2} = -0.502, \quad \bar{y} = 0.0, \quad \Lambda_w = 0°$$

and the propeller downwash angle is

$$\varepsilon_{dp} = \frac{\kappa_v \kappa_p \kappa_s}{\kappa_b}\frac{C_{L_w}}{R_{A_w}} = \frac{1.035(-0.165)1.0}{0.759}\frac{C_{L_w}}{R_{A_w}} = -0.225\frac{C_{L_w}}{R_{A_w}}$$

The propeller downwash gradient is then

$$(\varepsilon_{d,\alpha})_p = -0.225\frac{C_{L_w,\alpha}}{R_{A_w}} = -0.225\frac{4.44}{6.05} = -0.165$$

By definition, the moment slope relative to the neutral point is zero. Thus, using Eqs. (4.8.6) and (4.9.12) to estimate the fuselage and propeller contributions to the moment slope,

$$\frac{\partial C_{m_{np}}}{\partial \alpha} = -\frac{(l_w - l_{np})}{\bar{c}_w}C_{L_w,\alpha} - \frac{S_t(l_t - l_{np})}{S_w\bar{c}_w}\eta_t(1-\varepsilon_{d,\alpha})_t C_{L_t,\alpha} + \frac{l_f - l_{np}}{l_f}(\Delta C_{m,\alpha})_f - \frac{2d_p^2(l_p - l_{np})}{J^2 S_w\bar{c}_w}(1-\varepsilon_{d,\alpha})_p C_{N_p,\alpha} = 0$$

where

$$(\Delta C_{m,\alpha})_f = -2\frac{S_f l_f}{S_w\bar{c}_w}\left[1-1.76\left(\frac{d_f}{c_f}\right)^{3/2}\right] = -2\frac{21(-3.5)}{180(180/33)}\left[1-1.76\left(\frac{5.17}{23}\right)^{3/2}\right] = 0.1216$$

Solving for the static margin gives

$$\frac{l_{np}}{\bar{c}_w} = \frac{l_w C_{L_w,\alpha} + \frac{S_t l_t}{S_w}\eta_t(1-\varepsilon_{d,\alpha})_t C_{L_t,\alpha} - \bar{c}_w(\Delta C_{m,\alpha})_f + \frac{2d_p^2 l_p}{J^2 S_w}(1-\varepsilon_{d,\alpha})_p C_{N_p,\alpha}}{\bar{c}_w\left\{C_{L_w,\alpha} + \frac{S_t}{S_w}\eta_t(1-\varepsilon_{d,\alpha})_t C_{L_t,\alpha} - \frac{\bar{c}_w}{l_f}(\Delta C_{m,\alpha})_f + \frac{2d_p^2}{J^2 S_w}(1-\varepsilon_{d,\alpha})_p C_{N_p,\alpha}\right\}}$$

$$= \frac{(-.71)4.44 + \frac{36(14.29)}{180}1.(1-.44)3.97 - \frac{180}{33}.1216 + \frac{2(74/12)^2(-9)}{(.4858)^2 180}(1.165).04}{\frac{180}{33}\left\{4.44 + \frac{36}{180}1.(1-.44)3.97 - \frac{180/33}{-3.5}.1216 + \frac{2(74/12)^2}{(.4858)^2 180}(1.165).04\right\}} = \underline{6\%}$$

Comparing this result with that from Example 4.8.1, we see that the destabilizing effect of the propeller was to move the neutral point forward by about 3 percent of the wing chord. This is quite typical of what might be expected for an airplane with low thrust-to-weight ratio. However, an even greater destabilizing effect can be encountered for airplanes with higher thrust-to-weight ratio, such as the fighter planes of World War II.

4.10. Contribution of Jet Engines

Turbojet or turbofan engines can also make a significant contribution to the trim and static stability of an airplane. These effects are also divided into two categories, those arising directly from the forces and moments produced by the engine and those which result from the interaction of the exhaust jet with other surfaces of the airplane.

Even if the exhaust jet does not impinge directly upon any surface of the airplane, the jet can still have significant indirect effects resulting from the entrained flow. Because the velocity of the exhaust gas is much greater than that of the surrounding air, a turbulent shear layer develops between the exhaust jet and the freestream. The viscous shear and turbulent mixing that occur between the exhaust jet and the surrounding air decrease the velocity of the exhaust gas and increase the velocity of the adjacent air. This entrainment of freestream air into the exhaust jet causes the jet to broaden as it moves downstream and induces a flow of ambient air toward the axis of the jet, as is shown in Fig. 4.10.1. If the tail or any other surface of the airplane is placed in this entrainment flow field, the local angle of attack will be modified by the entrained flow. For example, if the horizontal tail is above the exhaust jet, as shown in Fig. 4.10.1, the angle of attack will be decreased as a result of the entrainment.

The indirect effects of the exhaust jet on other airplane surfaces, such as the wing, the tail, and the fuselage, are very complex and can only be evaluated analytically with the use of computational methods on a digital computer. Because entrainment is a viscous phenomenon, inviscid methods such as panel codes cannot be used for this analysis. A viscous CFD code must be used. Such methods can be used in the final phase of the airplane design process. However, because of complexity, the indirect effects of jet exhaust are usually neglected in the preliminary design phase. It should be remembered, however, that such effects could be significant.

The direct effects of the forces and moments produced by a jet or turbofan engine are essentially identical to those produced by an engine-propeller combination. Like a propeller, a turbojet or turbofan engine produces both an axial thrust and an off-axis normal force. The normal force is proportional to the angle that the axis of the exhaust jet makes with the local freestream at the engine inlet. As was the case for a propeller, the pitching moment that a jet engine produces about the airplane center of gravity is

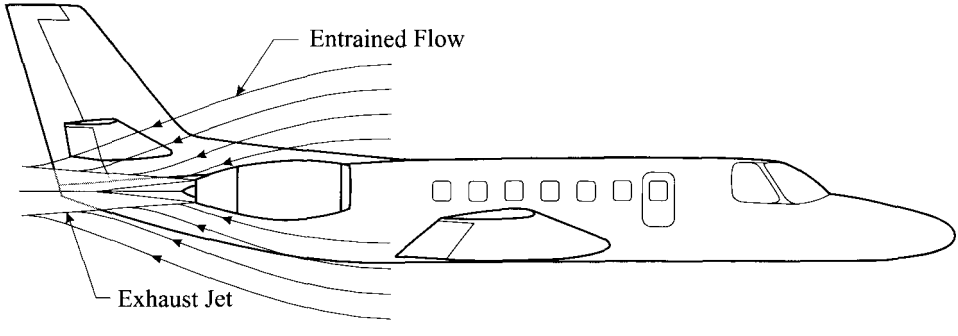


Figure 4.10.1. Flow entrained by the exhaust of a turbojet or turbofan engine.

simply a result of the thrust and the normal force, each multiplied by the appropriate moment arm. The only difference between computing the pitching moment contribution for a jet engine and that for propeller is the manner in which the normal force is computed.

The velocity of the air passing through a turbojet or turbofan engine can undergo a change in direction as well as a change in magnitude. The thrust and normal forces exerted on the airplane by the engine result directly from these changes in the velocity vector. Consider a control volume that encloses the engine of the airplane that is shown in Fig. 4.10.2. This control volume extends everywhere sufficiently far from the engine so that ambient pressure exists on the entire enclosing surface. Writing the vector form of Newton's second law for this nonaccelerating control volume, we have

$$\mathbf{F}_j = \dot{m}_j(\mathbf{V}_i - \mathbf{V}_j) \tag{4.10.1}$$

where $\mathbf{F}_j$ is the resultant force exerted on the airplane by the engine, $\mathbf{V}_i$ and $\mathbf{V}_j$ are, respectively, the inlet and exit velocities, and $\dot{m}_j$ is the mass flow rate passing through the engine. The axial and normal components of this vector equation result in

$$T = \dot{m}_j(V_j - V_i \cos\alpha_j) \tag{4.10.2}$$

$$N_j = \dot{m}_j V_i \sin\alpha_j \tag{4.10.3}$$

where V_j is the magnitude of the exhaust jet velocity, V_i is the magnitude of the local freestream velocity at the inlet, and α_j is the angle of attack that the axis of the exhaust jet makes with the direction of the local freestream at the inlet. For small angles, Eqs. (4.10.2) and (4.10.3) can be approximated as

$$T = \dot{m}_j(V_j - V_\infty) \tag{4.10.4}$$

$$N_j = \dot{m}_j V_\infty \alpha_j \tag{4.10.5}$$

where V_∞ is the far-field airspeed. Solving Eq. (4.10.4) for the mass flow rate and using the result in Eq. (4.10.5) gives

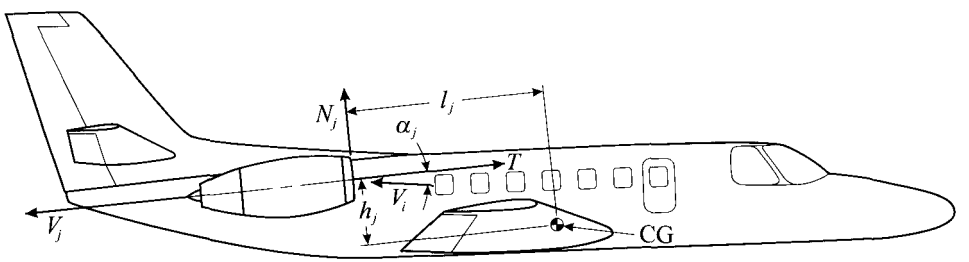


Figure 4.10.2. Forces generated by a turbojet or turbofan engine.

$$N_j = \frac{V_\infty T}{V_j - V_\infty}\alpha_j \tag{4.10.6}$$

From the geometry in Fig 4.10.2, the pitching moment that the engine produces about the airplane center of gravity is

$$m_{cg_j} = -Th_j - N_j l_j \tag{4.10.7}$$

Nondimensionalizing Eq. (4.10.7) and applying Eq. (4.10.6), the contribution of the jet engine to the total airplane pitching moment coefficient is

$$(\Delta C_m)_j = \frac{m_{cg_j}}{\frac{1}{2}\rho V_\infty^2 S_w \bar{c}_w} = -\frac{T}{\frac{1}{2}\rho V_\infty^2 S_w}\left(\frac{h_j}{\bar{c}_w} + \frac{V_\infty l_j}{(V_j - V_\infty)\bar{c}_w}\alpha_j\right) \tag{4.10.8}$$

The local angle of attack in Eq. (4.10.8) is affected by the airflow around the wing. If the engine inlet is aft of the wing, it is located in a region of downwash and the local angle of attack is decreased. If the inlet is forward of the wing, it is in a region of upwash and the local angle of attack is increased. The angle of attack that the exhaust jet axis makes with the local relative airflow at the engine inlet can be written as

$$\alpha_j = \alpha - \varepsilon_{dj} + \alpha_{0j} \tag{4.10.9}$$

where α is the airplane angle of attack relative to the fuselage reference line, ε_{dj} is the local downwash angle at the position of the engine inlet, and α_{0j} is the angle that the exhaust jet axis makes with the fuselage reference line.

Using Eq. (4.10.9) in Eq. (4.10.8), the contribution of a jet engine to the total airplane pitching moment coefficient can be written as

$$(\Delta C_m)_j = (\Delta C_{m0})_j + (\Delta C_{m,\alpha})_j \alpha \tag{4.10.10}$$

where

$$(\Delta C_{m0})_j = -\frac{T}{\frac{1}{2}\rho V_\infty^2 S_w}\left[\frac{h_j}{\bar{c}_w} + \frac{V_\infty l_j}{(V_j - V_\infty)\bar{c}_w}(\alpha_{0j} - \varepsilon_{d0j})\right] \tag{4.10.11}$$

$$(\Delta C_{m,\alpha})_j = -\frac{T}{\frac{1}{2}\rho V_\infty^2 S_w}\frac{V_\infty l_j}{(V_j - V_\infty)\bar{c}_w}(1 - \varepsilon_{d,\alpha})_j \tag{4.10.12}$$

ε_{d0j} is the inlet downwash angle with the fuselage reference line at zero angle of attack, and $(\varepsilon_{d,\alpha})_j$ is the downwash gradient at the position of the engine inlet. Since the thrust is positive in normal flight, if the inlet is forward of the center of gravity, l_j is negative and the engine's contribution to the pitch stability derivative is destabilizing. If the inlet

is aft of the center of gravity, l_j is positive and the engine's contribution to the pitch stability derivative is stabilizing.

As discussed in Sec. 2.1, the ideal propulsive efficiency for a jet engine is a function only of the exhaust jet velocity and the freestream velocity,

$$\eta_{p_i} = \frac{2V_\infty}{V_\infty + V_j} = \frac{2}{1+V_j/V_\infty} \tag{4.10.13}$$

Thus, we can express the ratio of the exhaust jet velocity to the freestream velocity as a function of ideal propulsive efficiency. Rearranging Eq. (4.10.13), the velocity ratio for a jet engine can be expressed as

$$\frac{V_j}{V_\infty} = \frac{2}{\eta_{p_i}} - 1 \tag{4.10.14}$$

or

$$\frac{V_\infty}{V_j - V_\infty} = \frac{\eta_{p_i}}{2(1-\eta_{p_i})} \tag{4.10.15}$$

The velocity ratio in Eq. (4.10.15), which also appears in Eqs. (4.10.11) and (4.10.12), is plotted in Fig. 4.10.3. This figure combined with Eqs. (4.10.11) and (4.10.12) shows that increasing the propulsive efficiency of a jet engine will also increase the engine's effect on static stability and trim.

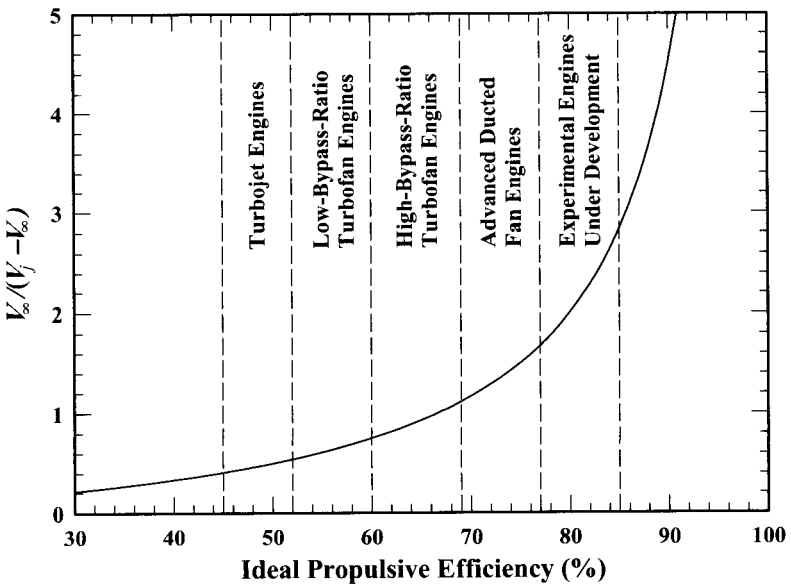


Figure 4.10.3. Velocity ratio for a jet engine as a function of ideal propulsive efficiency.

Using Eq. (4.10.15) in Eqs. (4.10.11) and (4.10.12), we have

$$(\Delta C_{m0})_j = -\frac{T}{\frac{1}{2}\rho V_\infty^2 S_w}\left[\frac{h_j}{\bar{c}_w} + \frac{\eta_{p_i} l_j}{2(1-\eta_{p_i})\bar{c}_w}(\alpha_{0j} - \varepsilon_{d0j})\right] \tag{4.10.16}$$

$$(\Delta C_{m,\alpha})_j = -\frac{T}{\frac{1}{2}\rho V_\infty^2 S_w}\frac{\eta_{p_i} l_j}{2(1-\eta_{p_i})\bar{c}_w}(1-\varepsilon_{d,\alpha})_j \tag{4.10.17}$$

For small thrust angles, the thrust is very nearly equal to the drag and Eqs. (4.10.16) and (4.10.17) can be closely approximated as

$$(\Delta C_{m0})_j = -C_D\left[\frac{h_j}{\bar{c}_w} + \frac{\eta_{p_i} l_j}{2(1-\eta_{p_i})\bar{c}_w}(\alpha_{0j} - \varepsilon_{d0j})\right] \tag{4.10.18}$$

$$(\Delta C_{m,\alpha})_j = -C_D\frac{\eta_{p_i} l_j}{2(1-\eta_{p_i})\bar{c}_w}(1-\varepsilon_{d,\alpha})_j \tag{4.10.19}$$

From Eqs. (4.10.18) and (4.10.19) we can estimate the effects of a jet engine on airplane trim and stability if we know the ideal propulsive efficiency for the engine. From knowledge of the engine type, a rough estimate for this efficiency can be made from the information in Fig. 4.10.3. After replacing Eqs. (4.9.12) and (4.9.13) with Eqs. (4.10.18) and (4.10.19), the direct contribution of a turbojet or turbofan engine to the trim and static stability of an airplane is identical to that of an engine-propeller combination, as described in Sec. 4.9.

4.11. Problems

4.1. An airplane is to weigh 2,000 pounds and its fuselage is to be 15 feet long. The center of gravity is to be 7.5 feet aft of its nose. The airplane is to be a wing-tail configuration. It is to be designed to fly at 15,000 feet at 150 mph. For this first analysis assume that all lifting surfaces are symmetric thin airfoils with infinite aspect ratio. Neglecting changes in weight with the size of the wing and tail, determine the following (there are many possible solutions):

a) The size of the wing and tail required to maintain trimmed cruise.
b) The location of the wing and tail in order to place the airplane's neutral point 0.5 ft aft of the CG.
c) The angle that the wing and the tail make with the upstream flow, taking the fuselage to make an angle of 0° with the upstream flow.

4.2. For the airplane in problem 4.1, assume that the wing has an aspect ratio of 6.0, a taper ratio of 0.4, and no sweep. Also assume that the horizontal tail has an aspect ratio of 4.0, a taper ratio of 0.4, and no sweep. Refine your design to account for downwash.

4.3. The British Spitfire Mark XVIII that is shown in Figs. 4.11.1 and 4.11.2 weighs 8,375 lbf and both the wing and horizontal tail have elliptic planform shapes. The horizontal tail has a symmetric airfoil section when the elevator is not deflected. The wing and the horizontal tail have the following properties:

$$S_w = 244 \text{ ft}^2, \quad b_w = 36.83 \text{ ft}, \quad C_{L_w,\alpha} = 4.62, \quad \alpha_{L0w} = -2.20°, \quad C_{m_w} = -0.053,$$
$$S_h = 31 \text{ ft}^2, \quad b_h = 10.64 \text{ ft}, \quad C_{L_h,\alpha} = 4.06, \quad \varepsilon_e = 0.60, \quad C_{m_h,\delta_e} = -0.55,$$
$$l_h - l_w = 18.16 \text{ ft}$$

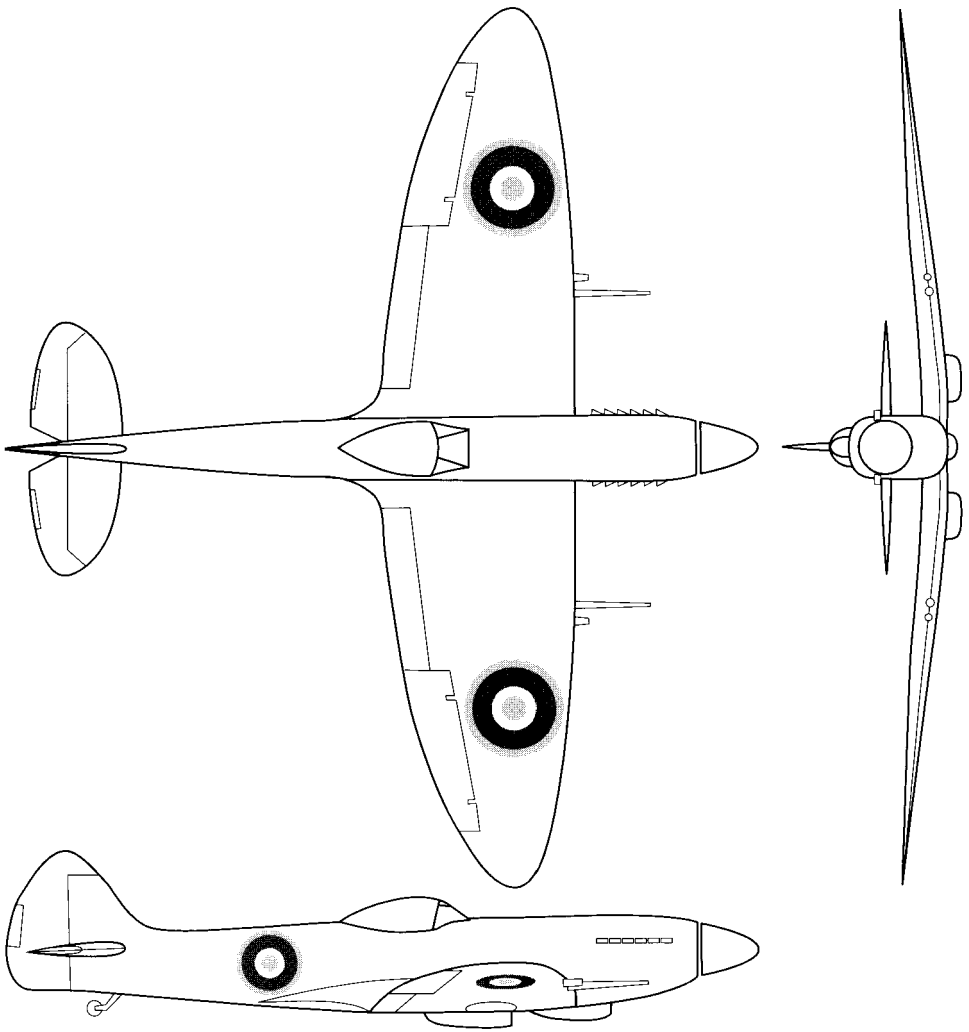


Figure 4.11.1. The British Spitfire Mark XVIII has an overall length of 32 feet 8 inches.



Figure 4.11.2. The British Spitfire Mark XVIII has an elliptic wing with a planform area of 244 square feet. The wing spans 36 feet 10 inches and supports a normal gross weight of 8,375 pounds. Later versions were powered by a liquid-cooled, 12-cylinder, Rolls-Royce Griffon engine developing 2,375 horsepower at 2,750 rpm. The 132-inch, five-blade, Rotol propeller is turned with 1.961:1 gear reduction. The airplane has a top speed in level flight of 450 miles per hour and has a rate of climb at sea level of over 5,000 feet per minute. (Photographs by Barry Santana)

For the CG located at the wing quarter-chord, the wing and the tail are mounted so that in level flight with an airspeed of 200 mph at standard sea level, trim is attained with no elevator deflection and a zero angle of attack for the fuselage reference line. Neglecting any effects associated with the propeller and fuselage, determine the mounting angles for the wing and the tail and the pitch stability derivative for the wing-tail combination. Use the simplified analysis presented in Sec. 4.3 and neglect the effects of wing downwash on the tail. In this and the following problems that deal with the spitfire, any dimensions that are not otherwise given may be scaled from Figs. 4.11.1 and 4.11.2.

4.4. Excluding the effects of wing downwash, determine the static margin in the range of linear lift for the wing-tail combination of the Spitfire Mark XVIII that is described in problem 4.3.

4.5. Using the method that was presented in Sec. 4.5, determine the relation between the downwash on the horizontal tail and the lift coefficient for the wing of the Spitfire Mark XVIII that is described in problem 4.3.

4.6. Using the results that were obtained from problem 4.5 for the downwash, recompute the mounting angles for both the wing and tail of the Spitfire Mark XVIII that is described in problem 4.3. Compare the result to that obtained in problem 4.3.

4.7. Including the effects of wing downwash but neglecting any effects associated with the propeller and fuselage, determine the static margin in the range of linear lift for the wing-tail combination of the Spitfire Mark XVIII that is described in problem 4.3. Compare the result to that obtained in problem 4.4.

4.8. Assume that the wing and the horizontal tail of the Spitfire Mark XVIII have the following properties:

$$S_w = 244\ \text{ft}^2, \quad b_w = 36.83\ \text{ft}, \quad C_{L_w,\alpha} = 4.62, \quad C_{m_w} = -0.053,$$
$$\alpha_{L0w} = -2.20°, \quad \alpha_{0w} = 2.0°, \quad l_w = 0.0\ \text{ft},$$
$$S_h = 31\ \text{ft}^2, \quad b_h = 10.64\ \text{ft}, \quad C_{L_h,\alpha} = 4.06, \quad C_{m_{h0}} = 0.000,$$
$$\alpha_{L0h} = 0.0°, \quad \alpha_{0h} = 0.0°, \quad l_h = 18.16\ \text{ft},$$
$$W = 8{,}375\ \text{lbf}, \quad \varepsilon_e = 0.60, \quad C_{m_h,\delta_e} = -0.55$$

Including the effects of wing downwash but neglecting the effects of the propeller and fuselage, find the elevator deflection and the angle of attack required for trimmed level flight at sea level for airspeeds of 100, 200, and 300 miles per hour. Also determine the lift on the horizontal tail at level trim for the same airspeeds. Assume a tail efficiency of 1.0 and use the simplified analysis that was presented in Sec. 4.3.

4.9. For the Spitfire Mark XVIII described in problem 4.8, including the effects of downwash, plot the elevator deflection required to trim the airplane at 100 mph as a function of CG location measured relative to the quarter-chord of the main wing. Neglect the effects of the propeller and fuselage.

4.10. The Spitfire described in problem 4.8 has a fuselage 32 feet 8 inches long. The point of maximum cross-section is 16 feet aft of the nose and the CG is 11 feet aft of the nose. The maximum cross-sectional area of the fuselage is 15 ft^2. Estimate the static margin in the linear lift range for the complete airframe.

4.11. A 2,375-horsepower piston engine turning a 132-inch, five-blade propeller powers the Spitfire Mark XVIII described in problem 4.8. When the airplane is flying at 200 mph the propeller is turning at 1,300 rpm. The change in normal force coefficient with propeller angle of attack for this propeller and operating condition is 0.270. The propeller is mounted 9 feet 4 inches forward of the center of gravity. Estimate the static margin in the linear lift range for the complete airplane, including the effect of the fuselage and propeller.

4.12. Assume the following properties for the Spitfire Mark XVIII:

$$S_w = 244\ \text{ft}^2, \quad b_w = 36.83\ \text{ft}, \quad C_{L_w,\alpha} = 4.62, \quad C_{m_w} = -0.053,$$
$$\alpha_{L0w} = -2.20°, \quad \alpha_{0w} = 2.0°, \quad l_w = 0.0\ \text{ft}, \quad h_w = -2.6\ \text{ft},$$
$$C_{D_{0w}} = 0.01, \quad C_{D_0,L_w} = 0.00, \quad e_w = 1.00,$$
$$S_h = 31\ \text{ft}^2, \quad b_h = 10.64\ \text{ft}, \quad C_{L_h,\alpha} = 4.06, \quad C_{m_{h0}} = 0.000,$$
$$\alpha_{L0h} = 0.0°, \quad \alpha_{0h} = 0.0°, \quad l_h = 18.16\ \text{ft}, \quad h_h = 0.0\ \text{ft},$$
$$C_{D_{0h}} = 0.01, \quad C_{D_0,L_h} = 0.00, \quad e_h = 1.00,$$
$$W = 8{,}375\ \text{lbf}, \quad \varepsilon_e = 0.60, \quad C_{m_h,\delta_e} = -0.55, \quad l_p = -9.33\ \text{ft}, \quad h_p = 0.0\ \text{ft}$$

Including the effects of downwash but neglecting the propeller and fuselage, find the elevator deflection and angle of attack required for trimmed level flight at sea level for airspeeds of 100, 200, and 300 miles per hour. Also determine the lift on the horizontal tail at level trim for the same airspeeds. Assume a tail efficiency of 1.0 and account for the effects of drag and vertical offset as discussed in Sec. 4.7. Compare the results with those obtained in problem 4.8.

4.13. Assume that the Spitfire Mark XVIII has the properties listed in problem 4.12. With the controls fixed at the 200-mph trim condition, plot the pitching moment coefficient as a function of angle of attack from –20 to +12 degrees. Include the effects of wing downwash but neglect the effects of the propeller and fuselage. Assume that neither the wing nor the horizontal tail stalls. Assume a tail efficiency of 1.0 and account for the effects of drag and vertical offset as discussed in Sec. 4.7. On the same graph plot the pitching moment coefficient as obtained from the simplified analysis presented in Sec. 4.3.

4.14. A small jet transport with an aft tail weighs 73,000 pounds. The wing and the horizontal tail have the following properties:

$$S_w = 950 \text{ ft}^2, \quad b_w = 75 \text{ ft}, \quad C_{L_w,\alpha} = 4.30, \quad \alpha_{L0_w} = -2.0°, \quad C_{m_w} = -0.050,$$
$$S_h = 207 \text{ ft}^2, \quad b_h = 31 \text{ ft}, \quad C_{L_h,\alpha} = 4.00, \quad \varepsilon_e = 0.51, \quad C_{m_h,\delta_e} = -0.49,$$
$$l_h - l_w = 42.5 \text{ ft}$$

The airplane's main wing has a taper ratio of 0.35 and a quarter-chord sweep angle of 15 degrees. The horizontal tail is mounted 17.5 feet above the wing and has a symmetric airfoil section when the elevator is not deflected. The wing and the horizontal tail are mounted so that when the airplane is in level flight with an airspeed of 400 mph at an elevation of 30,000 feet, trim is attained with no elevator deflection, no lift on the horizontal tail, and a zero angle of attack for the fuselage reference line. Neglecting any moments associated with the thrust deck and the fuselage, determine the location of the center of gravity, the mounting angles for the wing and the tail, and the pitch stability derivative for the wing-tail combination. Use the simplified analysis presented in Sec. 4.3 and assume a tail efficiency of 1.0.

4.15. Including the effects of wing downwash, determine the static margin in the range of linear lift for the wing-tail combination of the small jet transport that is described in problem 4.14. Neglect any effects associated with the thrust deck and the fuselage.

4.16. Two high-bypass-ratio turbofan engines power a small jet transport. Assume that the airplane has the following properties:

$$S_w = 950 \text{ ft}^2, \quad b_w = 75 \text{ ft}, \quad R_{T_w} = 0.35, \quad C_{L_w,\alpha} = 4.30, \quad C_{m_w} = -0.050,$$
$$\Lambda_w = 15°, \quad \alpha_{L0w} = -2.0°, \quad \alpha_{0w} = 1.5°, \quad l_w = 0.7 \text{ ft}, \quad h_w = -3.8 \text{ ft},$$
$$C_{D_{0_w}} = 0.01, \quad C_{D_0,L_w} = 0.00, \quad e_w = 0.95,$$
$$S_h = 207 \text{ ft}^2, \quad b_h = 31 \text{ ft}, \quad R_{T_h} = 0.35, \quad C_{L_h,\alpha} = 4.00, \quad C_{m_{h0}} = 0.000,$$
$$\Lambda_h = 15°, \quad \alpha_{L0h} = 0.0°, \quad \alpha_{0h} = 0.0°, \quad l_h = 43.2 \text{ ft}, \quad h_h = 13.7 \text{ ft},$$
$$C_{D_{0h}} = 0.01, \quad C_{D_0,L_h} = 0.00, \quad e_h = 0.96,$$
$$W = 73{,}000 \text{ lbf}, \quad \varepsilon_e = 0.51, \quad C_{m_h,\delta_e} = -0.49, \quad l_j = 9.4 \text{ ft}, \quad h_j = 2.4 \text{ ft},$$
$$C_{D_{L0}} = 0.020, \quad C_{D_0,L} = 0.0, \quad e = 0.67$$

Including the effects of wing downwash but neglecting effects of the thrust deck and fuselage, find the elevator deflection and the angle of attack required for trimmed level flight at 30,000 feet for airspeeds of 300, 400, and 500 miles per hour. Also determine the lift on both the wing and the horizontal tail at level trim for the same altitude and airspeeds. Assume a tail efficiency of 1.0 and use the simplified analysis that was presented in Sec. 4.3.

4.17. For the small jet transport described in problem 4.16, including the effects of downwash, plot the elevator deflection required to trim the airplane at 400 mph as a function of CG location measured relative to the quarter-chord of the main wing. Neglect the effects of the thrust deck and fuselage.

4.18. The small jet transport described in problem 4.16 has a fuselage that is 78 feet long. The point of maximum cross-section is located 37 feet aft of the nose, and the center of gravity is also 37 feet aft of the nose. The maximum cross-sectional area of the fuselage is 52 ft^2. Estimate the static margin in the range of linear lift for the complete airframe, including the effect of the fuselage.

4.19. Two high-bypass-ratio turbofan engines power the small jet transport that is described in problem 4.16. When the airplane is flying at 400 mph, the engines have an ideal propulsive efficiency of 0.64. The engine inlets are 9.4 feet aft of the center of gravity. Estimate the static margin in the linear lift range for the complete airplane, including the effect of the fuselage and thrust deck.

4.20. For the jet transport described in problem 4.16, including the effects of wing downwash but neglecting effects of thrust deck and fuselage, find the elevator deflection and the angle of attack required for trimmed level flight at 30,000 feet for airspeeds of 300, 400, and 500 miles per hour. Also determine the lift on the wing and horizontal tail at level trim for the same airspeeds. Assume a tail efficiency of 1.0 and account for the effects of drag and vertical offset as discussed in Sec. 4.7. Compare the results with those obtained in problem 4.16.

4.21. Assume that the wing and the horizontal tail of the small jet transport have the properties listed in problem 4.16. With the controls fixed at the 400-mph trim condition, plot the pitching moment coefficient as a function of angle of attack from –20 to +12 degrees. Include the effects of wing downwash but neglect the effects of the thrust deck and fuselage. Assume that neither the wing nor the horizontal tail stalls. Assume a tail efficiency of 1.0 and account for the effects of drag and vertical offset as discussed in Sec. 4.7. On the same graph plot the pitching moment coefficient as obtained from the simplified analysis presented in Sec. 4.3.

4.22. Estimate the maximum total lift coefficient and the minimum trimmed airspeed for the wing-tail combination of the jet transport described in problem 4.16. The maximum lift coefficient for the main wing is 1.40. The maximum lift coefficient for the horizontal tail varies with elevator deflection according to

$$C_{L_h \max} = 1.4 + 0.955\delta_e$$

where δ_e is in radians. Consider maximum total lift coefficient and minimum airspeed to be that for trimmed flight when either the wing or the horizontal tail carries its respective maximum lift.

4.23. A small jet transport of the wing-canard design weighs 73,000 pounds. The wing and horizontal canard have the following properties:

$$S_w = 950 \text{ ft}^2, \quad b_w = 75 \text{ ft}, \quad C_{L_w,\alpha} = 4.30, \quad \alpha_{L0w} = -2.0°, \quad C_{m_w} = -0.050,$$
$$S_h = 219 \text{ ft}^2, \quad b_h = 36 \text{ ft}, \quad C_{L_h,\alpha} = 4.30, \quad \alpha_{L0h} = -2.0°, \quad C_{m_{h0}} = -0.050,$$
$$l_w - l_h = 42.5 \text{ ft}, \quad \varepsilon_e = 0.51, \quad C_{m_h,\delta_e} = -0.49$$

Both the main wing and canard have a taper ratio of 0.35 and a quarter-chord sweep angle of 15°. The canard is mounted directly in front of the wing at the same vertical level. The wing and canard are mounted so that when the airplane is in level flight with an airspeed of 400 mph at an elevation of 30,000 feet, trim is attained with no control surface deflection and a zero angle of attack for the fuselage reference line. In the range of linear lift, the static margin for this wing-canard combination is 5 percent. Neglecting any moments associated with the thrust deck and fuselage, determine the location of the center of gravity, the mounting angles for the wing and the canard, and the pitch stability derivative for this wing-canard combination. Use the simplified analysis presented in Sec. 4.6 and assume a canard efficiency of 1.0. Include the effects of the upwash that is induced on the canard by the main wing, but neglect all other vortex interactions between the canard and the wing.

4.24. For the jet transport described in problem 4.23, recompute the mounting angles and CG location, neglecting the upwash induced on the canard by the wing.

4.25. Two high-bypass-ratio turbofan engines power the jet transport that is described in problem 4.23. Assume that the airplane has the following properties:

$$S_w = 950 \text{ ft}^2, \quad b_w = 75 \text{ ft}, \quad R_{T_w} = 0.35, \quad C_{L_w,\alpha} = 4.30, \quad C_{m_w} = -0.050,$$
$$\Lambda_w = 15°, \quad \alpha_{L0w} = -2.0°, \quad \alpha_{0w} = 1.5°, \quad l_w = 8.6 \text{ ft}, \quad h_w = -3.8 \text{ ft},$$
$$C_{D_{0w}} = 0.01, \quad C_{D_0,L_w} = 0.00, \quad e_w = 0.95,$$
$$S_h = 219 \text{ ft}^2, \quad b_h = 36 \text{ ft}, \quad R_{T_h} = 0.35, \quad C_{L_h,\alpha} = 4.30, \quad C_{m_{h0}} = -0.050,$$
$$\Lambda_h = 15°, \quad \alpha_{L0h} = -2.0°, \quad \alpha_{0h} = 2.0°, \quad l_h = -33.9 \text{ ft}, \quad h_h = -3.8 \text{ ft},$$
$$C_{D_{0h}} = 0.01, \quad C_{D_0,L_h} = 0.00, \quad e_h = 0.95,$$
$$W = 73{,}000 \text{ lbf}, \quad \varepsilon_e = 0.51, \quad C_{m_h,\delta_e} = -0.49, \quad l_j = 9.4 \text{ ft}, \quad h_j = 2.4 \text{ ft},$$
$$C_{D_{l.0}} = 0.020, \quad C_{D_0,L} = 0.0, \quad e = 0.67$$

Including the effects of wing upwash but neglecting effects of the thrust deck and fuselage, find the control surface deflection and angle of attack required for trimmed level flight at 30,000 feet for airspeeds of 300, 400, and 500 miles per hour. Also determine the lift on both the wing and the canard at level trim for the same altitude and airspeeds. Assume a canard efficiency of 1.0 and use the simplified analysis that was presented in Sec. 4.6.

4.26. For the small jet transport described in problem 4.25, including the effects of upwash, plot the control surface deflection required to trim the airplane at 400 mph as a function of CG location measured relative to the quarter-chord of the main wing. Neglect the effects of the thrust deck and fuselage.

4.27. The small jet transport described in problem 4.25 has a fuselage that is 78 feet long. The point of maximum cross-section is located 37 feet aft of the nose and the center of gravity is also 37 feet aft of the nose. The maximum cross-sectional area of the fuselage is 52 ft^2. Estimate the static margin in the range of linear lift for the complete airframe, including the effect of the fuselage.

4.28. Two high-bypass-ratio turbofan engines power the small jet transport that is described in problem 4.25. When the airplane is flying at 400 mph the engines have an ideal propulsive efficiency of 0.64. The engine inlets are 9.4 feet aft of the center of gravity. Estimate the static margin in the linear lift range for the complete airplane, including the effect of the fuselage and thrust deck.

4.29. For the jet transport described in problem 4.25, including the effects of wing upwash but neglecting the thrust deck and fuselage, find the control surface deflection and the angle of attack required for trimmed level flight at 30,000 feet for airspeeds of 300, 400, and 500 miles per hour. Also determine the lift on the wing and canard at level trim for the same airspeeds. Assume a canard efficiency of 1.0 and account for the effects of drag and vertical offset as discussed in Sec. 4.7. Compare the results with those obtained in problem 4.25.

4.30. Assume that the wing and canard of the small jet transport have the properties that are listed in problem 4.25. With the controls fixed at the 400-mph trim condition, plot the pitching moment coefficient as a function of angle of attack from –20 to +12 degrees. Include effects of wing upwash but neglect the effects of the thrust deck and fuselage. Assume that neither the wing nor the canard stalls. Assume a canard efficiency of 1.0 and account for the effects of drag and vertical offset as discussed in Sec. 4.7. On the same graph plot the pitching moment coefficient as obtained from the simplified analysis presented in Sec. 4.6.

4.31. Estimate the maximum total lift coefficient and the minimum trimmed airspeed for the wing-canard combination of the jet transport described in problem 4.25. The maximum lift coefficient for the main wing is 1.40. The maximum lift coefficient for the canard varies with control surface deflection according to

$$C_{L_h \max} = 1.4 + 0.955\delta_e$$

where δ_e is in radians. Consider maximum total lift coefficient and minimum airspeed to be that for trimmed flight when either the wing or the canard carries its respective maximum lift.

4.32. The turboprop transport shown in Fig. 4.11.3 has the following properties:

$$S_w = 1{,}745\ \text{ft}^2,\quad b_w = 132.6\ \text{ft},\quad R_{T_w} = 0.57,\quad C_{L_w,\alpha} = 5.16,\quad C_{m_w} = -0.050,$$
$$\Lambda_w = 0°,\quad \alpha_{L0w} = -2.0°,\quad \alpha_{0w} = 0.0°,\quad l_w = -2.5\ \text{ft},\quad h_w = 7.4\ \text{ft},$$
$$C_{D_{0w}} = 0.01,\quad C_{D_0,L_w} = 0.00,\quad e_w = 0.96,$$
$$S_h = 528\ \text{ft}^2,\quad b_h = 52.7\ \text{ft},\quad R_{T_h} = 0.35,\quad C_{L_h,\alpha} = 4.52,\quad C_{m_{h0}} = 0.000,$$
$$\Lambda_h = 7°,\quad \alpha_{L0h} = 0.0°,\quad \alpha_{0h} = -1.5°,\quad l_h = 44.5\ \text{ft},\quad h_h = 7.4\ \text{ft},$$
$$C_{D_{0h}} = 0.01,\quad C_{D_0,L_h} = 0.00,\quad e_h = 0.97,$$
$$W = 155{,}000\ \text{lbf},\quad \varepsilon_e = 0.58,\quad C_{m_h,\delta_e} = -0.49,\quad l_p = -11.9\ \text{ft},\quad h_p = 6.2\ \text{ft},$$
$$C_{D_{L0}} = 0.031,\quad C_{D_0,L} = 0.0,\quad e = 0.65$$

Including the effects of wing downwash but neglecting effects of the propellers and fuselage, find the elevator deflection and the angle of attack required for trimmed level flight at sea level for airspeeds of 200, 300, and 350 miles per hour. Also determine the lift on both the wing and the horizontal tail at level trim for the same altitude and airspeeds. Assume a tail efficiency of 1.0 and use the simplified analysis that was presented in Sec. 4.3.

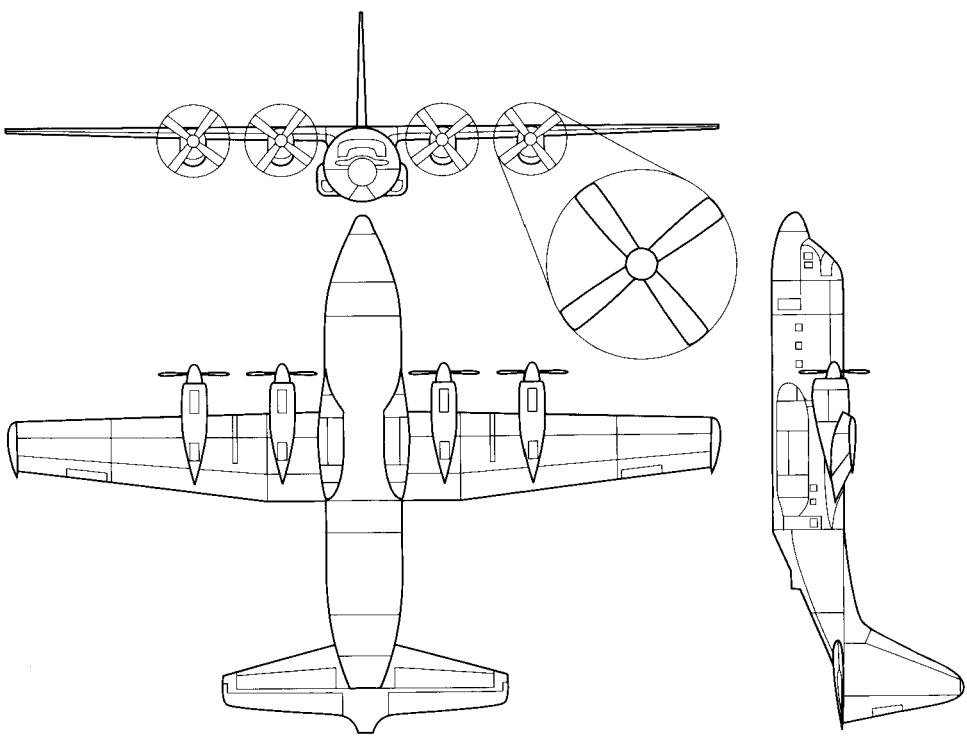


Figure 4.11.3. Turboprop transport described in problem 4.32.

4.33. For the turboprop transport described in problem 4.32, including the effects of downwash, plot the elevator deflection required to trim the airplane at 200 mph as a function of CG location measured relative to the quarter-chord of the main wing. Neglect the effects of the propellers, nacelles, and fuselage.

4.34. The turboprop transport described in problem 4.32 has a fuselage that is 87.9 feet long. The point of maximum cross-section is located 41 feet aft of the nose and the center of gravity is also 41 feet aft of the nose. The maximum cross-sectional area of the fuselage is 173 ft^2. Estimate the static margin in the range of linear lift for the complete airframe, including the effect of the fuselage.

4.35. Four 4,910-horsepower constant-speed turboprop engines turning at 13,820 rpm power the transport airplane described in problem 4.32. Each engine turns a 162-inch propeller through a gear reduction assembly having a total reduction ratio of 13.54 to 1. The engines operate at constant rotational speed, independent of flight speed. Changes in power requirements are met by changing the fuel flow and propeller pitch. As the fuel flow is changed, an automatic control system very precisely adjusts the propeller pitch to maintain constant engine rpm. For level flight at sea level with airspeeds of 200, 300, and 350 mph, the change in normal force coefficient with propeller angle of attack for these propellers and operating conditions are 0.277, 0.721, and 1.025, respectively. The propellers are mounted 11 feet 11 inches forward of the center of gravity. At all three of the above airspeeds, estimate the static margin in the linear lift range for the complete airplane, including the effect of the fuselage and propellers.

4.36. For the turboprop transport described in problem 4.32, including the effects of wing downwash but neglecting effects of the fuselage, nacelles, and propellers, find the elevator deflection and the angle of attack required for trimmed level flight at sea level for airspeeds of 200, 300, and 350 miles per hour. Also determine the lift on the wing and horizontal tail at level trim for the same airspeeds. Assume a tail efficiency of 1.0 and account for the effects of drag and vertical offset as discussed in Sec. 4.7. Compare the results with those obtained in problem 4.32.

4.37. Assume that the wing and the horizontal tail of the turboprop transport have the properties listed in problem 4.32. With the controls fixed at the 300-mph trim condition, plot the pitching moment coefficient as a function of angle of attack from –20 to +12 degrees. Include the effects of wing downwash but neglect effects of the fuselage, nacelles, and propellers. Assume that neither the wing nor the horizontal tail stalls. Assume a tail efficiency of 1.0 and account for the effects of drag and vertical offset as discussed in Sec. 4.7. On the same graph plot the pitching moment coefficient as obtained from the simplified analysis presented in Sec. 4.3.

Chapter 5
Lateral Static Stability and Trim

5.1. Introduction

In Chapter 4 our consideration of static aircraft stability and trim was limited to what is commonly called *longitudinal motion*, i.e., motion confined to the aircraft plane of symmetry. For such motion, the total aerodynamic force can be resolved into a lift force and a drag force, L and D, or a normal force and an axial force, N and A, all of which fall in the aircraft plane of symmetry. The only aerodynamic moment associated with longitudinal motion is the pitching moment, m. The velocity vector associated with longitudinal motion is completely defined by its magnitude, V, and angle of attack, α. For general three-dimensional motion, there may be a component of velocity normal to the aircraft plane of symmetry, which is called *sideslip*, and the aircraft may experience aerodynamic moments in roll and yaw as well as in pitch.

Longitudinal motion involves three degrees of freedom; axial translation, normal translation, and rotation in pitch. The other three degrees of freedom are commonly called the *lateral degrees of freedom*. These are sideslip translation, rotation in roll, and rotation in yaw. The *longitudinal degrees of freedom* constitute planar motion, which has the great simplification of being two-dimensional. However, the lateral degrees of freedom do not compose a planar motion and must be treated as three-dimensional.

There is some inconsistency in the literature regarding notation for the rolling moment. Both L and l have been commonly used to signify the rolling moment. In this text, a lowercase script ℓ will be used for the rolling moment to avoid confusion with either the lift or a distance measured aft of the CG. The yawing moment is commonly given the symbol N or n. Here, we shall choose n for the yawing moment, to avoid confusion with the normal force. With this notation, all forces are represented with uppercase letters and lowercase letters are used to denote all moments. By standard notation the sideslip angle is given the symbol β and the bank angle is denoted as ϕ. The sign convention for these moments and angles is shown in Figs. 5.1.1.

According to common practice, the aerodynamic coefficients for the rolling and yawing moments are, respectively, defined as

$$C_\ell \equiv \frac{\ell}{\frac{1}{2}\rho V_\infty^2 S_w b_w} \tag{5.1.1}$$

and

$$C_n \equiv \frac{n}{\frac{1}{2}\rho V_\infty^2 S_w b_w} \tag{5.1.2}$$

Notice that by standard convention, the characteristic length used to nondimensionalize the rolling and yawing moment is the wingspan, b_w, while the pitching moment was nondimensionalized with respect to the mean wing chord, $\bar{c}_w$.

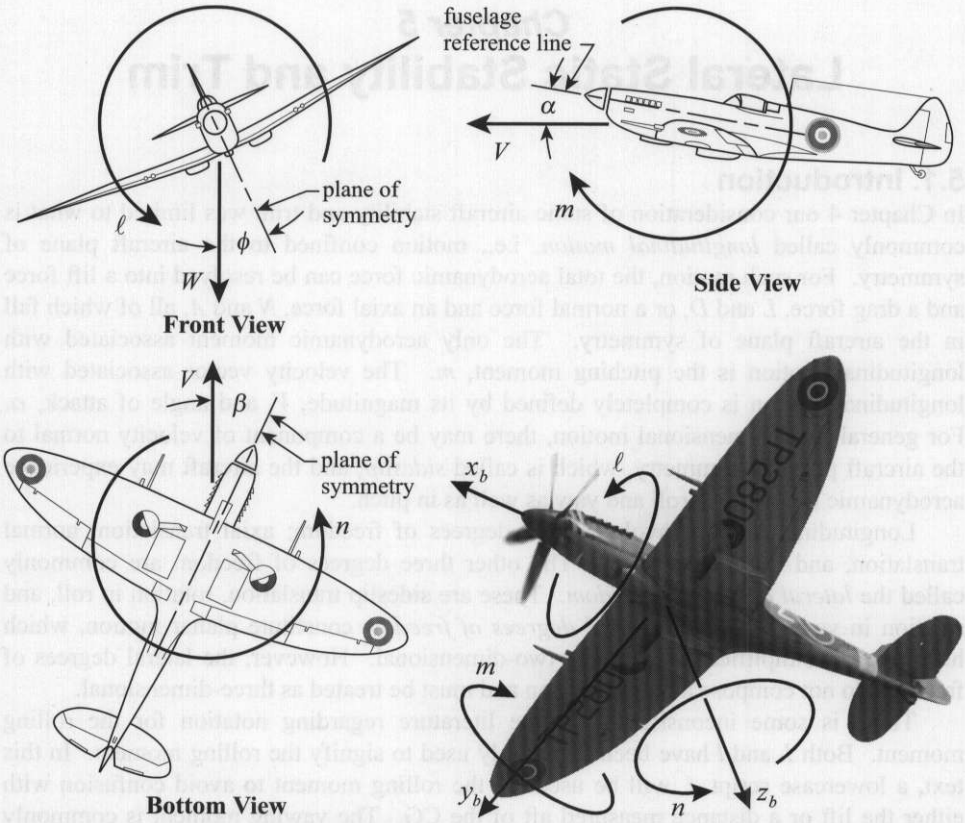


Figure 5.1.1. Sign convention for the aerodynamic angles and the moments acting on an airplane in free flight. (Photograph by Barry Santana)

At this point the reader should memorize the sign convention shown in Fig. 5.1.1. In our study of longitudinal stability and trim we were concerned with one angle and one moment: the angle of attack, α, and the pitching moment, m. It was quite easy to remember that angle of attack is positive with the nose up, in the direction of increasing lift. We then only needed to remember that the pitching moment is positive in the direction of increasing angle of attack. For our study of lateral stability and trim, we have now introduced two more angles and two more moments: the bank angle, ϕ; the sideslip angle, β; the rolling moment, ℓ; and the yawing moment, n. There seems to be no preferred direction for roll and yaw on which to base a sign convention. In fact, the choice of sign convention is arbitrary as long as we are consistent. The need to be consistent is the primary reason for defining and memorizing any sign convention. Students are often confused by the sign convention for β in Fig. 5.1.1. This confusion stems from the fact that the pitching moment is positive in the direction of increasing angle of attack, the rolling moment is positive in the direction of increasing bank angle, but the yawing moment is positive in the direction of decreasing sideslip angle.

The traditional way to remember the sign convention for angles or moments is to use the *right-hand rule* relative to some right-hand coordinate system. In this case the coordinate system is the (x_b, y_b, z_b) system shown in Fig. 5.1.1. This coordinate system is fixed to the body of the aircraft with the origin at the CG. The x_b-z_b plane is the aircraft plane of symmetry. The x_b-axis points forward and the z_b-axis points downward. The y_b-axis must then point out the right-hand side of the airplane to complete the right-hand coordinate system. Relative to this coordinate system, the aerodynamic moments ℓ, m, and n are right-hand moments about the x_b, y_b, and z_b axes, respectively.

Students are commonly confused by trying to apply a similar right-hand rule to the angles ϕ, α, and β. The bank angle, ϕ, in Fig. 5.1.1 is defined to be a right-hand rotation of the airplane about the roll axis, x_b. Similarly, a positive increase in angle of attack could be thought of as a right-hand rotation of the airplane about the pitch axis, y_b. However, to attain a positive sideslip angle, a left-hand rotation of the airplane about the yaw axis, z_b, is required. This could be viewed as an inconsistency in the sign convention shown in Fig. 5.1.1 and it often leads to confusion. To resolve this confusion, we must realize that the bank angle, ϕ, is fundamentally different from the angle of attack, α, and the sideslip angle, β. Both α and β are called *aerodynamic angles* because they are defined with respect to the airplane's velocity vector relative to the surrounding air. On the other hand, ϕ is called an orientation angle, because it defines one component of the airplane's orientation relative to the earth. The bank angle, ϕ, is completely independent of the airplane's velocity. We will later find it convenient to define two additional orientation angles. Because of the fundamental difference between the aerodynamic angles and the orientation angles, we should not expect the sign convention for β and ϕ to be defined in exactly the same way. This still does not explain the difference between the sign convention for α and β when viewed as rotations about the y_b and z_b axes. To resolve the confusion, we must think of sideslip not in terms of sideslip angle, but rather in terms of sideslip velocity. **The aircraft is defined to have positive sideslip when the y_b-component of aircraft velocity relative to the surrounding air is positive.** This is consistent with the sign convention for α, since a positive z_b-component of aircraft velocity relative to the surrounding air gives a positive angle of attack.

For equilibrium longitudinal motion, the side force, rolling moment, and yawing moment must all be zero. All three of these equilibrium requirements can be naturally satisfied with spanwise airplane symmetry. Furthermore, in level flight the gravity vector is in the plane of symmetry and produces no side force. Hence, for a completely spanwise symmetric airplane, there is no "fundamental" level flight trim problem in roll or yaw. Level flight of a symmetric airplane is pure longitudinal motion. However, no airplane can always be perfectly symmetric. Asymmetric loading, asymmetric thrust, propeller rotation, or simply an asymmetric distribution of bugs on the wings can cause either aerodynamic or inertial asymmetry. Thus, even for level flight, some provision must be made for trimming the airplane in roll and yaw. Furthermore, if equilibrium longitudinal motion is to be statically stable, the airplane must exhibit lateral static stability as well as longitudinal static stability. This means that any small disturbance in roll or yaw must produce an aerodynamic moment that will return the airplane to its original longitudinal equilibrium. We shall now turn our attention to these aspects of static stability and trim.

5.2. Yaw Stability and Trim

Static yaw stability is provided primarily by the vertical tail and is defined as rotational stability about the yaw axis, as shown in the bottom view of Fig. 5.1.1. This is also commonly referred to as *directional stability*. In the early days of aviation, yaw stability was called *weathercock stability*, in reference to the weathercocks that adorned the roof of almost every barn in rural America. A weathercock points into the wind as a result of the same aerodynamic principles that make an airplane stable in yaw. However, since the word *weathercock* has little meaning in the experience of modern-day college students, the more descriptive terminology *yaw stability* is used in this text.

If an airplane is to be statically stable in yaw, then a small disturbance in yaw must produce a yawing moment that will tend to return the airplane to its original equilibrium state. From Fig. 5.1.1, we see that a yaw disturbance resulting in a positive sideslip angle requires a positive yawing moment to restore the disturbance to zero. Conversely, a negative sideslip angle requires a negative restoring moment. Thus, in mathematical terms, static stability in yaw requires that

$$\frac{\partial n}{\partial \beta} > 0$$

In dimensionless form, this gives **the general criterion for static yaw stability**,

$$\frac{\partial C_n}{\partial \beta} \equiv C_{n,\beta} > 0 \tag{5.2.1}$$

The aerodynamic derivative, $C_{n,\beta}$, is the *yaw stability derivative* and is often called the *yaw stiffness*. This is analogous to the pitch stability derivative, $C_{m,\alpha}$. The obvious difference between Eqs. (5.2.1) and (4.2.8) is the sign. This difference in sign is simply a result of the sign convention shown in Fig. 5.1.1.

It is very difficult to specify a general yaw stability criterion in terms of the magnitude of $C_{n,\beta}$. **For typical airplane configurations, good handling qualities are normally found with $C_{n,\beta}$ in the range between about 0.06 and 0.15 per radian, with 0.03 being a reasonable lower limit. These values need to be increased for airplanes with very high wing loading and low span. There is no direct upper limit for the magnitude of $C_{n,\beta}$. Usually, the more static stability an airplane has in yaw, the better it will handle.** This does not mean that there is no limit to the allowable size of the vertical tail. The vertical tail also affects the handling qualities of an airplane through certain dynamic characteristics that will be discussed later in this text. The size of the vertical tail is not usually fixed by consideration of static stability. Fortunately, when the vertical tail is sized based on control and dynamic handling quality requirements, which will be discussed later, sufficient static stability is normally provided.

Static yaw stability is very similar to static pitch stability. When the center of pressure acting normal to the plane of symmetry is aft of the center of gravity, any sideslip angle will produce a pressure imbalance with a resultant force that acts aft of the center of gravity. This causes the airplane to "weathervane" into the relative wind.

An aft vertical tail provides static yaw stability in the same way that an aft horizontal tail provides static pitch stability.

The yaw stability derivative, $C_{n,\beta}$, is estimated in much the same way as the pitch stability derivative, $C_{m,\alpha}$. It is synthesized by combining the contributions made by the various components of the airplane. The major contributions are those made by the fuselage, propeller, and vertical tail. The contributions from the fuselage and propeller are typically destabilizing, but these are small and easily countered by the stabilizing effect of an aft vertical tail. In contrast with pitch stability, an unswept wing has little direct effect on static yaw stability and is usually neglected in preliminary calculations.

Effect of the Vertical Tail

When an airplane is flying with a positive sideslip angle as shown in the bottom view of Fig. 5.1.1, the vertical tail is at an angle of attack to the freestream and develops lift, as is shown in Fig. 5.2.1. The lift developed on the vertical tail as a result of positive sideslip produces a side force from right to left, as also shown in Fig. 5.2.1. Since the vertical tail is aft of the CG, this lift produces a positive yawing moment about the center of gravity. This is a restoring moment, which tends to point the airplane into the relative wind and return the sideslip angle to zero.

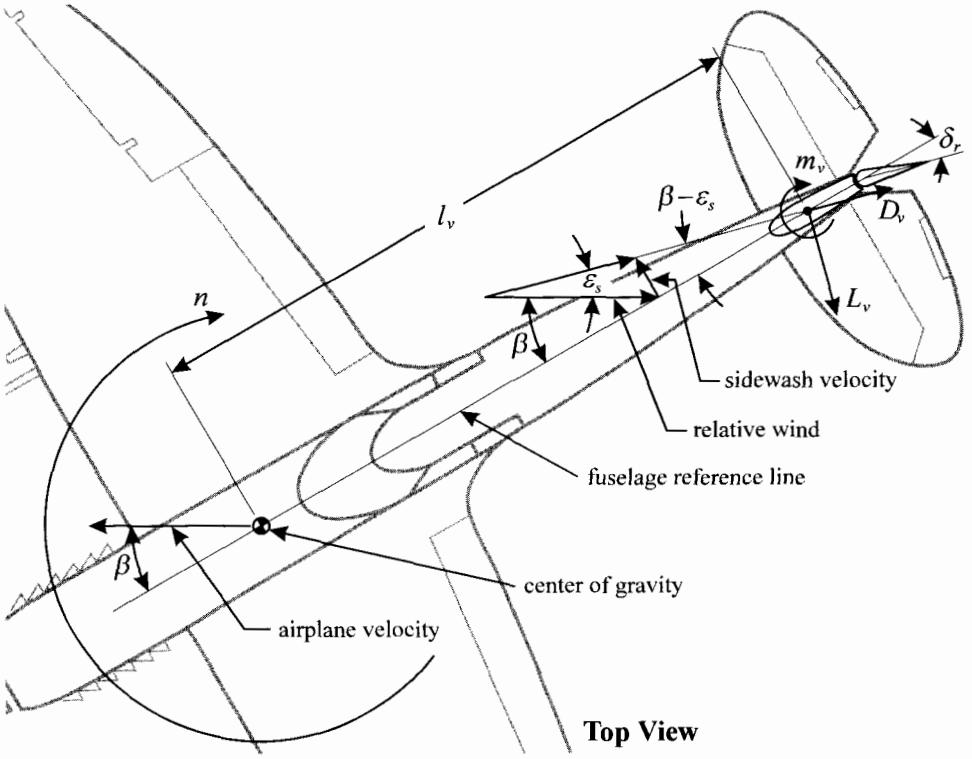


Figure 5.2.1. Effect of sideslip on the aerodynamic yawing moment.

If the vertical tail were isolated in a uniform flow field, the angle of attack for this lifting surface would be equivalent to the sideslip angle, β. However, when installed on an airplane, the airflow relative to the vertical tail is modified in both magnitude and direction. For example, the magnitude of the airflow relative to the vertical tail can be decreased if the surface is in the wake of the wing or the fuselage. This magnitude can be increased if the vertical tail is in the slipstream of a propeller or jet engine. The angle of attack for the vertical tail can be modified by the slipstream of a propeller or by the vorticity shed from the main wing.

As discussed in Chapter 2, the air in the slipstream of a propeller rotates as it moves downstream. Since the vertical tail is usually above the axis of the propeller slipstream, rotation of the slipstream will produce *sidewash* on the vertical tail, as is shown in Fig 5.2.2. The effect of this sidewash on the vertical tail is analogous to the effect of downwash on the horizontal tail. **Sidewash is defined to be positive from left to right** as shown in Fig 5.2.1. Thus, if the propeller is rotating counterclockwise when viewed from the front, the propeller slipstream will generate positive sidewash on a vertical tail mounted above the slipstream axis. This produces a positive *sidewash angle*, ε_s, which reduces the sideslip angle felt by the vertical tail as shown in Fig. 5.2.1. The sidewash angle induced on a centered vertical tail by the propeller of a single engine aircraft is maximum when the sideslip angle is zero and decreases when β becomes either positive or negative. This affects the aircraft trim in yaw but has no effect on yaw stability.

The wingtip vortices can also induce sidewash on the vertical tail when the airplane is flying with a sideslip angle. Since the wingtip vortices trail downstream with the relative wind, when the airplane is in sideslip one vortex is closer to the tail than the other. This is shown in Fig. 5.2.3. If the vertical tail is mounted above the wing, inboard sidewash is induced by each wingtip vortex. When an airplane has zero sideslip angle, the vertical tail is midway between the two wingtip vortices and the sidewash induced by the right wing exactly cancels that induced by the left and the resulting sidewash angle is zero. When the sideslip angle is positive, the vertical tail is closer to the right wingtip vortex than it is to the left, as shown in Fig 5.2.3. Thus, the sidewash moving inboard from the right is greater than that from the left and a negative sidewash angle is induced by the wingtip vortices. Conversely, the sidewash angle induced on a high vertical tail by the wingtip vortices is positive when the sideslip angle is negative. Since ε_s is subtracted from β as shown in Fig. 5.2.1, the wingtip vortices add to the effect of sideslip and are stabilizing, when the vertical tail is above the wing.

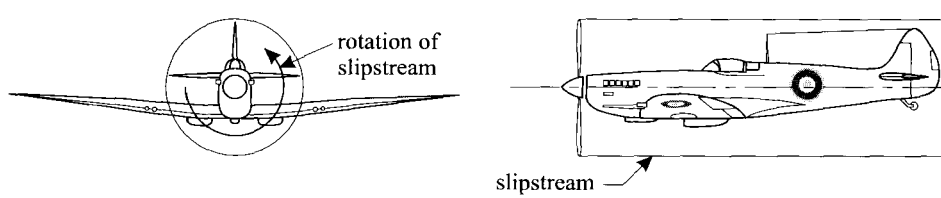


Figure 5.2.2. Sidewash produced on a vertical tail by the propeller slipstream.

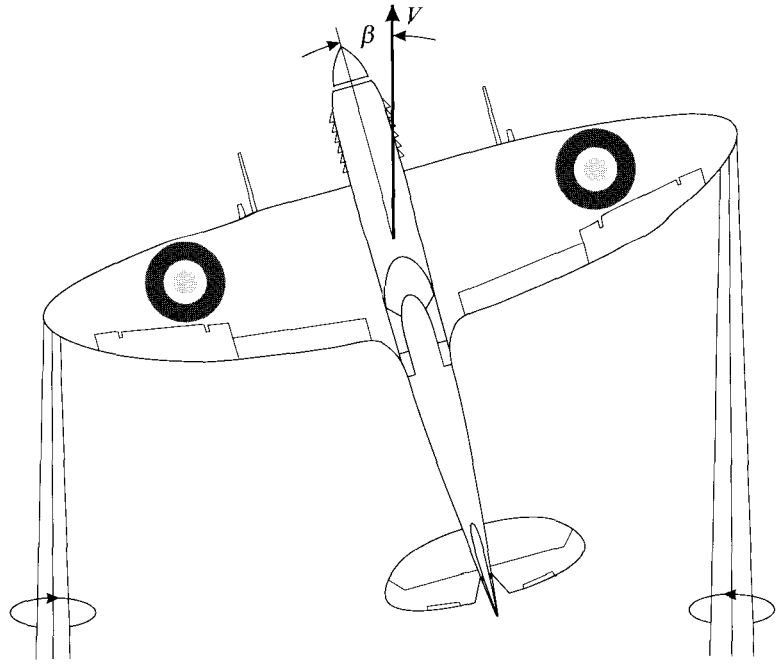


Figure 5.2.3. Sidewash produced on a vertical tail by the wingtip vortices.

Multiple counterrotating propellers produce sidewash on the vertical tail in much the same way as the wingtip vortices. If the engines that are mounted on the right rotate clockwise, when viewed from the front, while the engines mounted on the left rotate counterclockwise, then the propeller slipstream effect is similar to the wingtip vortex effect. That is, the propeller slipstreams have no effect on trim but have a stabilizing effect on an aft vertical tail mounted above the propeller axis. If these propellers were to each rotate in the opposite direction, then there would still be no effect on trim, but the slipstreams would be destabilizing for a high vertical tail.

For small sideslip angles, the sidewash angle on a vertical tail can be considered to be a linear function of β,

$$\varepsilon_s = \varepsilon_{s0} + \varepsilon_{s,\beta}\,\beta \tag{5.2.2}$$

where ε_{s0} is the sidewash angle at zero sideslip and $\varepsilon_{s,\beta}$ is the sidewash gradient,

$$\varepsilon_{s,\beta} \equiv \frac{\partial \varepsilon_s}{\partial \beta} \tag{5.2.3}$$

For small angles of attack and rudder deflection, the lift developed on the vertical tail is linear with both angle of attack and rudder deflection angle, δ_r. By usual convention, **a leftward deflection of the rudder is defined to be positive**, as shown in Fig. 5.2.1.

Thus, positive deflection of an aft rudder produces a rightward increment in the lift developed on the vertical tail and a negative increment in the aerodynamic yawing moment for the airplane.

Using standard sign convention, the contribution of the vertical tail to the yawing moment is

$$(\Delta n)_v = \tfrac{1}{2}\rho V_v^2 S_v\left[l_v C_{L_v,\alpha}(\beta - \varepsilon_s - \varepsilon_r\delta_r) + \bar{c}_v C_{m_v,\delta_r}\,\delta_r\right] \tag{5.2.4}$$

where V_v is the local magnitude of the relative airspeed at the position of vertical tail, $C_{L_v,\alpha}$ is the lift slope for the vertical tail, ε_r is the rudder effectiveness, $\bar{c}_v$ is the mean chord length of the vertical tail, and C_{m_v,δ_r} is the change in the moment coefficient for the vertical tail with respect to rudder deflection. Applying Eq. (5.2.2) and nondimensionalizing Eq. (5.2.4) by utilizing the definition in Eq. (5.1.2), **the contribution of the vertical tail to the yawing moment coefficient** can be estimated from

$$(\Delta C_n)_v = \eta_v \frac{S_v l_v}{S_w b_w}\left[C_{L_v,\alpha}(1-\varepsilon_{s,\beta})_v\beta - C_{L_v,\alpha}\varepsilon_{s0} - \left(\varepsilon_r C_{L_v,\alpha} - \frac{\bar{c}_v}{l_v}C_{m_v,\delta_r}\right)\delta_r\right] \tag{5.2.5}$$

where η_v is the dynamic pressure ratio for the vertical tail, which is analogous to that for the horizontal tail and may be handled in the same way. The ratio $S_v l_v / S_w b_w$ is called the *vertical tail volume ratio*,

$$\mathcal{V}_v \equiv \frac{S_v l_v}{S_w b_w} \tag{5.2.6}$$

and is analogous to the horizontal tail volume ratio.

From Eq. (5.2.5), the contribution of the vertical tail to the yaw stability derivative or yaw stiffness is

$$(\Delta C_{n,\beta})_v = \eta_v \frac{S_v l_v}{S_w b_w} C_{L_v,\alpha}(1-\varepsilon_{s,\beta})_v \tag{5.2.7}$$

As long as the vertical tail is aft of the center of gravity, l_v and this contribution to the yaw stability derivative are both positive. Thus, an aft vertical tail is always stabilizing.

Equation (5.2.5) also provides us with the contribution that the rudder makes to the yaw control derivative,

$$C_{n,\delta_r} \equiv \frac{\partial C_n}{\partial \delta_r} = -\eta_v \frac{S_v l_v}{S_w b_w}\left(\varepsilon_r C_{L_v,\alpha} - \frac{\bar{c}_v}{l_v}C_{m_v,\delta_r}\right) \tag{5.2.8}$$

The aerodynamic derivative C_{m_v,δ_r} is always negative. Thus, the change in the airplane yawing moment coefficient with rudder deflection is always negative for an aft rudder, when leftward deflection of the rudder is considered to be positive.

The sidewash gradient, $\varepsilon_{s,\beta}$, is typically negative and thus increases the stabilizing effect of the vertical tail. The sidewash gradient resulting from multiple propellers is difficult to estimate with any degree of accuracy and is usually neglected in preliminary design. The sidewash gradient produced by the wingtip vortices can be estimated using the same vortex model that was used in Chapter 4 to estimate the downwash gradient for the horizontal tail.

The lift slope for the vertical tail, $C_{L_v,\alpha}$, is not as easy to estimate as one might at first expect. We have previously used the closed-form solution to Prandtl's lifting-line theory to estimate the lift slope for the wing and the horizontal surface. However, the fuselage and the horizontal tail have a significant effect on the apparent aspect ratio of the vertical tail. These surfaces of the airplane act like winglets for the vertical tail and inhibit vortex shedding, thereby increasing the lift produced at a given angle of attack. The lift slope for a vertical tail in combination with a horizontal tail can be accurately estimated using the numerical lifting-line method or from a three-dimensional panel code. However, prior to such calculations, a very rough estimate for this lift slope can be made from the closed-form solution to Prandtl's lifting-line theory by using an effective aspect ratio that is between about 1.4 and 1.6 times the actual geometric aspect ratio. The lift slope for the vertical tail is sensitive to the geometry of the horizontal tail, so this rough estimate should be used with caution.

Effect of the Fuselage and Nacelles

The contribution of the fuselage and nacelles to the static yaw stability of an airplane is very similar to their contribution to pitch stability and is typically destabilizing. In some cases this destabilizing effect can be quite significant. Thus, the fuselage and nacelles should be included in the yaw stability analysis during all phases of the airplane design process.

To accurately estimate the yawing moment produced on the fuselage and nacelles, we must make use of computer simulations and/or wind tunnel tests. However, as a first approximation for preliminary design, the effect of the fuselage and nacelles on yaw stability can be estimated using the method presented in Sec. 4.8. From this approximate experimental correlation, a rough estimate of the fuselage yawing moment coefficient about the airplane center of gravity is given by

$$C_{n_f} \equiv \frac{n_{cg_f}}{\frac{1}{2}\rho V_\infty^2 S_f c_f} = 2\frac{l_f}{c_f}\left[1 - 1.76\left(\frac{d_f}{c_f}\right)^{3/2}\right]\beta \tag{5.2.9}$$

where again S_f is the maximum cross-sectional area of the fuselage, c_f is the chord length of the fuselage, l_f is the distance that the fuselage center of pressure is aft of the airplane center of gravity, and d_f is the diameter of a circle having the same area as the maximum cross-sectional area of the fuselage. The observed difference in sign between Eqs. (5.2.9) and (4.8.1) is simply a function of the sign convention defined in Fig. 5.1.1.

The characteristic area for the complete airplane is the wing area and the characteristic length for yaw is the wingspan. Thus, the contribution of the fuselage to the total airplane yawing moment coefficient can be approximated by multiplying the

result from Eq. (5.2.9) by the product $S_f c_f$ and dividing by the product $S_w b_w$. This gives a result very similar to Eq. (4.8.3),

$$\left(\Delta C_n\right)_f \equiv \frac{n_{cg_f}}{\frac{1}{2}\rho V_\infty^2 S_w b_w} = \frac{S_f c_f}{S_w b_w} C_{n_f} = \left(\Delta C_{n,\beta}\right)_f \beta \tag{5.2.10}$$

where

$$\left(\Delta C_{n,\beta}\right)_f = 2\frac{S_f l_f}{S_w b_w}\left[1 - 1.76\left(\frac{d_f}{c_f}\right)^{3/2}\right] \tag{5.2.11}$$

By comparing Eq. (5.2.11) with Eq. (4.8.6), we can see that this approximation predicts a fuselage contribution to the yaw stability derivative that is related to its contribution to the pitch stability derivative according to

$$\left(\Delta C_{n,\beta}\right)_f \cong -\left(\Delta C_{m,\alpha}\right)_f \frac{\bar{c}_w}{b_w} \tag{5.2.12}$$

The contribution of the nacelles to the yaw stability derivative can be approximated in exactly the same manner. Since the fuselage and nacelles are normally symmetric in the spanwise direction, they do not typically contribute to aircraft trim in yaw.

Because the fuselage and nacelles are not necessarily axisymmetric and the flow induced by the wing is far from being axisymmetric, Eq. (5.2.12) should only be used as a rough first approximation. The aerodynamic forces and moments generated on the fuselage and nacelles are extremely complex and are significantly affected by aerodynamic interactions with the wing and the tail. **It is important to remember that Eq. (5.2.12) gives only a very rough estimate of the contribution to the yaw stability derivative generated by the fuselage and nacelles**. It should only be used as a first approximation for preliminary design. Wind tunnel tests and/or computer simulations should always be used to evaluate this derivative in the later phases of design.

Effect of Rotating Propellers

A propeller can affect both the trim and static stability of an airplane in yaw. As shown in Fig. 5.2.4, a rotating propeller advancing through the air so that the axis of rotation makes some angle with the freestream can produce both a side force, Y_p, and a yawing moment, n_p, in addition to the thrust, T. From the geometry shown in Fig. 5.2.4, the yawing moment that the propeller produces about the airplane's center of gravity is

$$n_{cg_p} = n_p - y_{bp} T - l_p Y_p \tag{5.2.13}$$

where y_{bp} is the spanwise distance from the CG to the propeller axis, measured positive to the right. For consistency, we are defining l_p as the axial distance that the propeller is mounted aft of the CG. For the airplane in Fig. 5.2.4, l_p is negative.

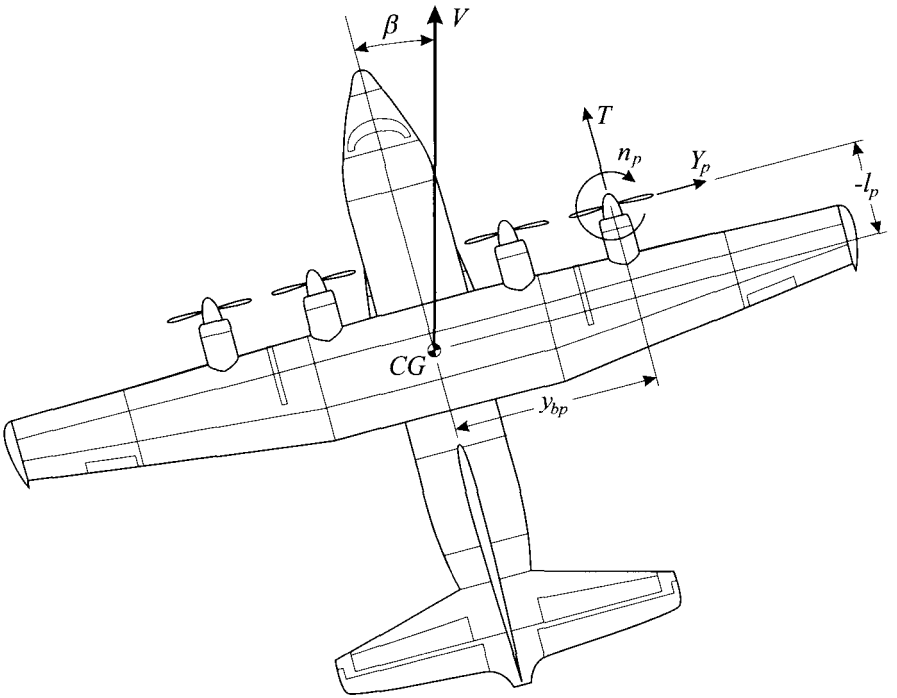


Figure 5.2.4. Side forces and yawing moment generated by a rotating propeller.

The yawing moment computed for each propeller from Eq. (5.2.13) can be added to the yawing moment obtained for all of the other airplane components to determine the yawing moment for the complete airplane. Thus, the contribution of each propeller to the total yawing moment coefficient is found by nondimensionalizing Eq. (5.2.13),

$$(\Delta C_n)_p = \frac{n_{cg_p}}{\frac{1}{2}\rho V_\infty^2 S_w b_w} = \frac{n_p}{\frac{1}{2}\rho V_\infty^2 S_w b_w} - \frac{y_{bp}}{b_w}\frac{T}{\frac{1}{2}\rho V_\infty^2 S_w} - \frac{l_p}{b_w}\frac{Y_p}{\frac{1}{2}\rho V_\infty^2 S_w} \quad (5.2.14)$$

With all engines operational, the total thrust will usually be symmetrically distributed in the spanwise direction and the net contribution of the thrust term in Eq. (5.2.14), for all propellers combined, will typically be zero. However, this term is retained here to account for the possibility of engine failure. For small thrust angles the total equilibrium thrust from all propellers combined is nearly equal to the drag. Thus, the contribution of each propeller can be closely approximated from Eq. (5.2.14) as

$$(\Delta C_n)_p = \frac{n_p}{\frac{1}{2}\rho V_\infty^2 S_w b_w} - \frac{y_{bp}}{b_w} f_T C_D - \frac{l_p}{b_w}\frac{Y_p}{\frac{1}{2}\rho V_\infty^2 S_w} \quad (5.2.15)$$

where f_T is the thrust fraction provided by the propeller.

Following the material presented in Chapter 2, the propeller yawing moment and side force are conventionally expressed in terms of the dimensionless aerodynamic coefficients,

$$C_{n_p} \equiv \frac{n_p}{\rho(\omega/2\pi)^2 d_p^5} \tag{5.2.16}$$

$$C_{Y_p} \equiv \frac{Y_p}{\rho(\omega/2\pi)^2 d_p^4} \tag{5.2.17}$$

where d_p is the propeller diameter and ω is the angular velocity. The yawing moment coefficient is linearly proportional to the propeller angle of attack, α_p,

$$C_{n_p} = C_{n_p,\alpha}\, \alpha_p \tag{5.2.18}$$

and the side force coefficient is linearly proportional to the propeller sideslip angle, β_p,

$$C_{Y_p} = C_{Y_p,\beta}\, \beta_p \tag{5.2.19}$$

The coefficients $C_{n_p,\alpha}$ and $C_{Y_p,\beta}$ depend on propeller geometry and advance ratio, J,

$$J \equiv \frac{2\pi V_\infty}{\omega d_p} \tag{5.2.20}$$

Because the propeller is axisymmetric, the side force is related to the sideslip angle in the same way that the normal force is related to the angle of attack,

$$C_{Y_p,\beta} = -C_{N_p,\alpha} \tag{5.2.21}$$

Here again the negative sign in Eq. (5.2.21) is simply a result of the sign convention shown in Fig. 5.1.1. The reader should examine Fig. 5.1.1 carefully and be sure that the sign in Eq. (5.2.21) can be justified.

Using Eqs. (5.2.16) through (5.2.21) in Eq. (5.2.15), the direct contribution of the propeller to the total airplane yawing moment coefficient is

$$(\Delta C_n)_p = \frac{2d_p^3}{S_w b_w} \frac{C_{n_p,\alpha}}{J^2} \alpha_p - \frac{y_{bp}}{b_w} f_T C_D + \frac{2d_p^2 l_p}{S_w b_w} \frac{C_{N_p,\alpha}}{J^2} \beta_p \tag{5.2.22}$$

The dimensionless yawing moment gradient and the dimensionless normal force gradient, which appear in Eq. (5.2.22), depend on the propeller geometry as well as the advance ratio. For known propeller geometry, these coefficients can be determined as a function of advance ratio using the method presented in Chapter 2. In addition to the direct contribution of the propeller, the interaction of the propeller slipstream with the vertical tail can produce a significant yawing moment, as shown in Fig. 5.2.2.

Both the propeller angle of attack and sideslip angle in Eq. (5.2.22) can be affected by the airflow around the wing. Recall from Eq. (4.9.10) that the angle of attack that the propeller axis makes with the local relative airflow can be written as

$$\alpha_p = \alpha - \varepsilon_{dp} + \alpha_{0p} \tag{5.2.23}$$

where α is the airplane angle of attack relative to the fuselage reference line, ε_{dp} is the local downwash angle at the position of the propeller, and α_{0p} is the angle that the propeller axis makes with the fuselage reference line. Likewise, as was the case for the vertical tail, the propeller sideslip angle depends on the sidewash generated by the wing,

$$\beta_p = \beta - \varepsilon_{sp} \tag{5.2.24}$$

where β is the airplane sideslip angle relative to the fuselage reference line and ε_{sp} is the local sidewash angle at the position of the propeller.

Using Eqs. (5.2.23) and (5.2.24) with Eq. (5.2.22), the direct contribution of the propeller to the total airplane yawing moment coefficient can be written as

$$(\Delta C_n)_p = (\Delta C_{n0})_p + (\Delta C_{n,\alpha})_p \alpha + (\Delta C_{n,\beta})_p \beta \tag{5.2.25}$$

where

$$(\Delta C_{n0})_p = \frac{2 d_p^3}{S_w b_w} \frac{C_{n_p,\alpha}}{J^2} (\alpha_{0p} - \varepsilon_{d0p}) - \frac{y_{bp}}{b_w} f_T C_D \tag{5.2.26}$$

$$(\Delta C_{n,\alpha})_p = \frac{2 d_p^3}{S_w b_w} (1 - \varepsilon_{d,\alpha})_p \frac{C_{n_p,\alpha}}{J^2} \tag{5.2.27}$$

$$(\Delta C_{n,\beta})_p = \frac{2 d_p^2 l_p}{S_w b_w} (1 - \varepsilon_{s,\beta})_p \frac{C_{N_p,\alpha}}{J^2} \tag{5.2.28}$$

ε_{d0p} is the propeller downwash angle with the fuselage reference line at zero angle of attack, $(\varepsilon_{d,\alpha})_p$ is the downwash gradient at the position of the propeller, and $(\varepsilon_{s,\beta})_p$ is the sidewash gradient at the position of the propeller. **For a propeller that is mounted forward of the wing, the sidewash gradient is small and can usually be ignored. However, when the propeller is mounted aft of the wing, the effects of sidewash should be considered.**

Equation (5.2.28) provides the propeller's direct contribution to the total airplane yaw stability derivative. Since the change in the normal force coefficient with angle of attack is positive, if the propeller is forward of the center of gravity, l_p is negative and the propeller contribution to the yaw stability derivative is destabilizing. If the propeller is aft of the center of gravity, l_p is positive and the propeller contribution to the yaw stability derivative is stabilizing.

Notice from Eq. (5.2.25) that the yawing moment contributed by a rotating propeller depends on angle of attack as well as sideslip angle. Thus, rotating propellers can affect trim in yaw as well as yaw stability. The direct contribution of a rotating propeller to the airplane yawing moment coefficient at trim is found from Eq. (5.2.25) by setting the sideslip angle to zero and the angle of attack to the equilibrium angle of attack, α_o. This gives

$$\left(\Delta C_{n_{\text{trim}}}\right)_p = \frac{2d_p^3}{S_w b_w}\frac{C_{n_p,\alpha}}{J^2}[\alpha_{0p} - \varepsilon_{d0p} + (1-\varepsilon_{d,\alpha})_p \alpha_o] - \frac{y_{bp}}{b_w} f_T C_D \quad (5.2.29)$$

The slipstream effects shown in Fig. 5.2.2 can add significantly to the trim requirement specified by Eq. (5.2.29).

The change in propeller yawing moment coefficient with propeller angle of attack is negative for right-hand turning propellers and positive for left-hand turning propellers. Since y_{bp} is positive for propellers mounted to the right of center and negative for propellers mounted to the left of center, **for a multiengine airplane the trim requirement in yaw can be eliminated by using counterrotating propellers**. If the engine locations are symmetric in the spanwise direction and those on the left rotate in one direction while those on the right rotate in the opposite direction, the net propeller trim requirement specified by Eq. (5.2.29) will be zero. **Since the change in propeller normal force coefficient with propeller angle of attack is positive for both right- and left-hand turning propellers, the use of counterrotating propellers does not affect yaw stability.** For a multiengine aircraft, the most significant trim requirement predicted by Eq. (5.2.29) occurs under conditions of engine failure. The need to be able to trim a multiengine aircraft with one or more engines inoperative usually provides the most restrictive constraint on rudder size.

For a single-engine aircraft with the propeller axis in the plane of symmetry, there is a yawing moment generated by the propeller at zero sideslip if the propeller angle of attack is not zero. Some rudder deflection is required to trim the airplane against this yawing moment. For an airplane with low thrust-to-weight ratio, this trim requirement is small. However, for a very high-powered propeller-driven airplane, such as the fighter aircraft of World War II, the rudder deflection needed to trim the airplane against the propeller yawing moment can be quite substantial at high angles of attack.

EXAMPLE 5.2.1. The airplane described in Examples 4.4.1, 4.8.1, and 4.9.1 has a vertical tail area of 11.9 ft^2 and the aerodynamic center of the vertical tail is 14.81 ft aft of the CG. For the operating conditions in Example 4.9.1, estimate the yaw stability derivative for this airplane, including the effects of the fuselage and propeller. Assume that the dynamic pressure ratio for the vertical tail is 1.0, the sidewash gradient is –0.10, and the lift slope for the vertical tail is 3.40.

Solution. From Example 4.9.1 and the additional information presented here,

$$S_w = 180 \text{ ft}^2, \quad b_w = 33 \text{ ft}, \quad \bar{c}_w = 5.455 \text{ ft}, \quad C_{L_w,\alpha} = 4.44, \quad l_w = -0.71 \text{ ft},$$
$$S_h = 36 \text{ ft}^2, \quad C_{L_h,\alpha} = 3.97, \quad l_h = 14.29 \text{ ft}, \quad \eta_h = 1.0, \quad (\varepsilon_{d,\alpha})_h = 0.44,$$

$$(\Delta C_{m,\alpha})_f = 0.1216, \quad d_p = 74 \text{ in}, \quad l_p = -9 \text{ ft}, \quad C_{N_p,\alpha} = 0.04, \quad J = 0.4858,$$
$$S_v = 11.9 \text{ ft}^2, \quad C_{L_v,\alpha} = 3.40, \quad l_v = 14.81 \text{ ft}, \quad \eta_v = 1.0, \quad (\varepsilon_{s,\beta})_v = -0.10$$

From Eq. (5.2.7), the contribution of the vertical tail to the total yaw stability derivative is

$$(\Delta C_{n,\beta})_v = \eta_v \frac{S_v l_v}{S_w b_w} C_{L_v,\alpha}(1-\varepsilon_{s,\beta})_v$$
$$= 1.0\frac{11.9(14.81)}{180(33)}3.40[1-(-0.10)] = 0.1110$$

and from Eq. (5.2.12), the contribution of the fuselage is approximated as

$$(\Delta C_{n,\beta})_f \cong -(\Delta C_{m,\alpha})_f \frac{\bar{c}_w}{b_w} = -0.1216\frac{5.455}{33} = -0.0201$$

Since the propeller is forward of the wing, we can neglect the sidewash gradient, and from Eq. (5.2.28), the propeller contribution to the yaw stability derivative is

$$(\Delta C_{n,\beta})_p = \frac{2d_p^2 l_p}{S_w b_w}(1-\varepsilon_{s,\beta})_p \frac{C_{N_p,\alpha}}{J^2}$$
$$= \frac{2(74/12)^2(-9.0)}{(180)(33)}(1-0.0)\frac{0.04}{0.4858^2} = -0.0195$$

Thus, a reasonable first estimate for the yaw stability derivative of this airplane is

$$C_{n,\beta} \cong (\Delta C_{n,\beta})_v + (\Delta C_{n,\beta})_f + (\Delta C_{n,\beta})_p$$
$$= 0.1110 - 0.0201 - 0.0195 = \underline{0.071}$$

EXAMPLE 5.2.2. The vertical tail of the airplane in Example 5.2.1 has a mean chord of 2.0 ft, the rudder effectiveness is 0.56, and the change in the moment coefficient for the vertical tail with respect to rudder deflection is –0.51. The change in the propeller yawing moment coefficient with respect to propeller angle of attack is –0.013. Assuming that the propeller is mounted with the axis of rotation aligned with the airplane's zero-lift axis, estimate the rudder deflection required to trim the airplane for zero sideslip against the yawing moment produced directly by the propeller in steady level flight at sea level and 80 mph. If no rudder deflection is used, estimate the equilibrium sideslip angle.

Solution. For this airplane we have

$$S_w = 180 \text{ ft}^2, \quad b_w = 33 \text{ ft}, \quad \bar{c}_w = 5.455 \text{ ft}, \quad C_{L_w,\alpha} = 4.44, \quad l_w = -0.71 \text{ ft},$$

$$S_h = 36\,\text{ft}^2,\quad C_{L_h,\alpha} = 3.97,\quad l_h = 14.29\,\text{ft},\quad \eta_h = 1.0,\quad (\varepsilon_{d,\alpha})_h = 0.44,$$
$$d_p = 74/12\,\text{ft},\quad l_p = -9\,\text{ft},\quad (\varepsilon_{d,\alpha})_p = -0.165,\quad C_{n_p,\alpha} = -0.013,\quad J = 0.4858,$$
$$S_v = 11.9\,\text{ft}^2,\quad C_{L_v,\alpha} = 3.40,\quad l_v = 14.81\,\text{ft},\quad \eta_v = 1.0,\quad (\varepsilon_{s,\beta})_v = -0.10,$$
$$\bar{c}_v = 2.0\,\text{ft},\quad \varepsilon_r = 0.56,\quad C_{m_v,\delta_r} = -0.51,\quad V = 80\,\text{mph},\quad W = 2{,}700\,\text{lbf}$$

From Eq. (5.2.8), the yaw control derivative for this airplane is

$$C_{n,\delta_r} = -\eta_v \frac{S_v l_v}{S_w b_w}\left(\varepsilon_r C_{L_v,\alpha} - \frac{\bar{c}_v}{l_v} C_{m_v,\delta_r}\right)$$
$$= -1.0\frac{11.9(14.81)}{180(33)}\left(0.56(3.40) - \frac{2.0}{14.81}(-0.51)\right) = -0.059$$

The rotating propeller produces the only change in the airplane's yawing moment coefficient with respect to angle of attack. From Eq. (5.2.27) we have

$$C_{n,\alpha} = \left(\Delta C_{n,\alpha}\right)_p = \frac{2 d_p^3}{S_w b_w}(1-\varepsilon_{d,\alpha})_p \frac{C_{n_p,\alpha}}{J^2}$$
$$= \frac{2(74/12)^3}{180(33)}[1-(-0.165)]\frac{-0.013}{0.4858^2} = -0.0051$$

The lift slope for the complete airplane can be estimated as

$$C_{L,\alpha} = C_{L_w,\alpha} + \frac{S_h}{S_w}\eta_h C_{L_h,\alpha}(1-\varepsilon_{d,\alpha})_h$$
$$= 4.44 + \frac{36}{180}1.0(3.97)(1-0.44) = 4.88$$

With a level-flight airspeed of 80 mph at sea level, the lift coefficient is

$$C_L = \frac{W}{\frac{1}{2}\rho V^2 S_w} = \frac{2{,}700}{\frac{1}{2}0.0023769(80\times 5{,}280/3{,}600)^2 180} = 0.9168$$

and the angle of attack relative to the zero-lift line is

$$\alpha = \frac{C_L}{C_{L,\alpha}} = \frac{0.9168}{4.88} = 0.1879 = 10.76^\circ$$

Since the propeller rotation axis is aligned with the zero-lift line, a zero yawing moment with zero sideslip requires that

$$C_{n,\alpha}\,\alpha + C_{n,\delta_r}\,\delta_r = 0$$

or

$$\delta_r = -\frac{C_{n,\alpha}}{C_{n,\delta_r}}\alpha = -\frac{-0.0051}{-0.059}10.76^\circ = \underline{-0.93^\circ}$$

In a similar manner, if the rudder deflection is zero, the propeller yawing moment must be balanced with sideslip,

$$C_{n,\alpha}\,\alpha + C_{n,\beta}\,\beta = 0$$

From Example 5.2.1, $C_{n,\beta} = 0.071$ and

$$\beta = -\frac{C_{n,\alpha}}{C_{n,\beta}}\alpha = -\frac{-0.0051}{0.071}10.76^\circ = \underline{0.77^\circ}$$

From Example 5.2.2, we see that negative rudder deflection is needed to trim the airplane for straight and level flight against the yawing moment produced by the conventional right-hand turning propeller. From the sign convention shown in Fig. 5.2.1, we see that negative rudder deflection corresponds to a deflection of the rudder to the right. This is commonly referred to as *right rudder*, not specifically because the rudder is deflected to the right, but because this is the rudder deflection required to yaw the nose of the airplane to the pilot's right.

In Example 5.2.2, we included only the direct yawing moment that was produced by the propeller. The propeller slipstream can also interact with the vertical tail to produce an additional yawing moment. As can be seen in Fig. 5.2.2, the rotation of the slipstream can induce sidewash on the vertical tail. For the conventional right-hand turning propeller shown in this figure, the sidewash on a conventional high vertical tail is from left to right. This changes the angle of attack for the vertical tail and produces a side force to the right. Since the vertical tail is aft of the CG, this produces a moment that tends to yaw the airplane to the left. This adds to the yawing moment produced directly by the propeller and increases the amount of right rudder needed to trim the airplane. In some cases, this slipstream effect can be as large or larger than the direct effect from the propeller itself, so a few degrees of right rudder can be required to trim a single-engine propeller-driven airplane for straight and level flight.

Most single-engine propeller-driven airplanes with a conventional right-hand turning propeller will require some right rudder for trim. If this rudder deflection is not applied, the airplane will yaw to the left. Even more right rudder is required during takeoff, when the engine is at full power and the propeller advance ratio is low. This effect is more pronounced in a tail dragger because during the first phase of the ground roll, the propeller angle of attack is quite high, as seen in Fig. 5.2.5. Once the minimum ground control speed is reached, the pilot can raise the tail, reducing the propeller angle of attack and the required rudder deflection. However, even if the tail is raised enough to reduce the propeller angle of attack to zero, some right rudder is still required to offset the slipstream effect.



Figure 5.2.5. Tail-dragger landing gear typically results in a large propeller angle of attack on takeoff. (Photograph by Barry Santana)

For a tail dragger with very high power-to-weight ratio, such as the P-51 Mustang shown in Fig. 5.2.5 or the Spitfire Mark XVIII shown in Fig. 4.11.2, the yawing moment produced by the propeller can limit the power that can be used on takeoff. Even with full rudder deflection, it is not possible to hold the Spitfire Mark XVIII on the runway if full power is applied before the tail is raised. Most pilots did not apply full power until the spitfire was in the air.

Floatplanes also require a great deal of right rudder during the first phase of the takeoff run, because as full power is applied, the tail is held down with full up elevator to keep spray away from the propeller, as shown in Fig. 5.2.6. This results in a very high propeller angle of attack, which for a conventional right-hand propeller produces a large yawing moment to the left. As the speed increases, the airplane "comes up on the step," as shown in Fig. 5.2.7. This reduces the propeller angle of attack and the required rudder deflection.



Figure 5.2.6. A floatplane requires ample right rudder on takeoff. (Photograph by Lona Santana)



Figure 5.2.7. A floatplane requires less right rudder once it comes up on the step and the propeller angle of attack is reduced. (Photograph by Lona Santana)

For any propeller-driven airplane that does not have balanced counterrotating propellers, the yawing moment produced by the propeller or propellers increases with increasing angle of attack. Thus, the rudder deflection required to trim the airplane against the propeller yawing moment will vary with angle of attack. Since the angle of attack for an airplane in free flight depends on airspeed, rudder deflection at trim is a function of airspeed as well.

Effect of the Wing and Horizontal Tail

As mentioned earlier, an unswept wing has little direct effect on the static yaw stability of an airplane. Generally, the wing's contribution to yaw stability is small and can be neglected in the preliminary design phase. However, if the wing and/or horizontal tail are highly swept, they can contribute to the yaw stability derivative.

When an airplane with swept-back wings yaws to the left with respect to the velocity vector, each section of the right wing is moved farther from the line of flight that passes through the center of gravity. Conversely, each section of the left wing is moved closer to this line of flight. This can be seen in Fig. 5.2.8. If the wing has a quarter-chord sweep angle of Λ, the distance measured parallel to the wing quarter-chord from the CG to the wing section located at the spanwise coordinate, y_b, can be expressed as $y_b/\cos(\Lambda)$. Since drag always acts parallel with the relative wind, the yawing moment arm for the section drag acting on any particular wing section is the perpendicular distance from the line of flight passing through the CG to the given wing section. The yawing moment arm for the drag is then $y_b \cos(\Lambda - \beta)/\cos(\Lambda)$ on an arbitrary section of the right wing and $y_b \cos(\Lambda + \beta)/\cos(\Lambda)$ on an arbitrary section of the left wing. Thus, the wing's contribution to the airplane yawing moment coefficient can be written as

$$(\Delta C_n)_w = \int_{y_b=-b_w/2}^{0} c_w \widetilde{C}_{D_w} \frac{y_b \cos(\Lambda+\beta)}{S_w b_w \cos(\Lambda)} dy_b + \int_{y_b=0}^{b_w/2} c_w \widetilde{C}_{D_w} \frac{y_b \cos(\Lambda-\beta)}{S_w b_w \cos(\Lambda)} dy_b \qquad (5.2.30)$$

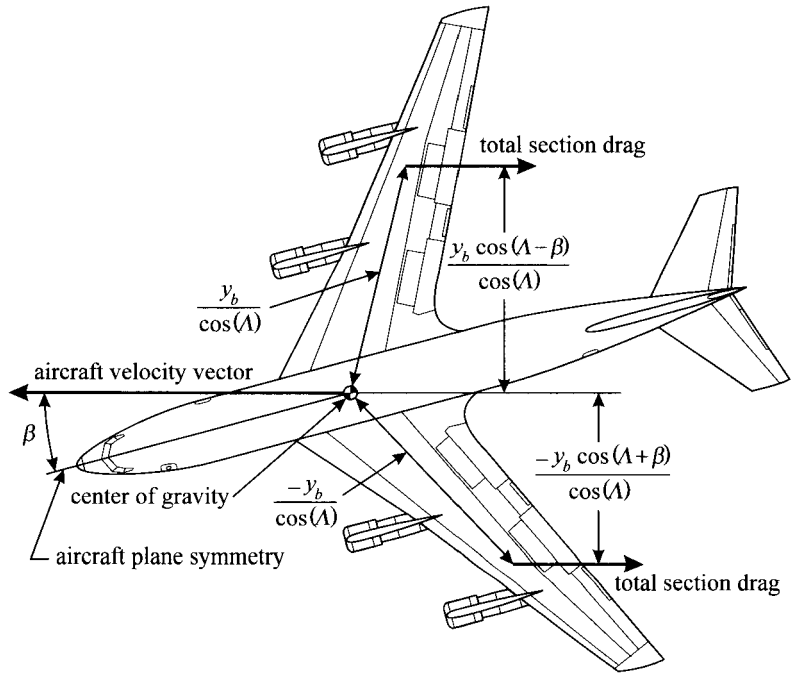


Figure 5.2.8. Wing sweep can affect the static yaw stability of an airplane.

where the section drag coefficient in Eq. (5.2.30) includes both parasitic and induced drag. For small angles of sideslip, we can use the small-angle approximations,

$$\begin{aligned}\cos(\Lambda+\beta) &= \cos\Lambda\cos\beta - \sin\Lambda\sin\beta \cong \cos\Lambda - \beta\sin\Lambda \\ \cos(\Lambda-\beta) &= \cos\Lambda\cos\beta + \sin\Lambda\sin\beta \cong \cos\Lambda + \beta\sin\Lambda\end{aligned}$$

and Eq. (5.2.30) can be closely approximated as

$$(\Delta C_n)_w = \frac{1}{S_w b_w}\int_{y_b=-b_w/2}^{b_w/2} y_b c_w \widetilde{C}_{D_w} dy_b + \frac{\beta\tan\Lambda}{S_w b_w}\int_{y_b=-b_w/2}^{b_w/2} |y_b| c_w \widetilde{C}_{D_w} dy_b \qquad (5.2.31)$$

Typically, both the wing chord and section drag coefficient will vary with y_b.

The contribution of the wing to the aircraft yaw stability derivative is found by differentiating Eq. (5.2.31) with respect to β. At $\beta = 0$, this gives

$$(\Delta C_{n,\beta})_w = \frac{1}{S_w b_w}\int_{y_b=-b_w/2}^{b_w/2} y_b c_w \frac{\partial \widetilde{C}_{D_w}}{\partial\beta} dy_b + \frac{\tan\Lambda}{S_w b_w}\int_{y_b=-b_w/2}^{b_w/2} |y_b| c_w \widetilde{C}_{D_w} dy_b \qquad (5.2.32)$$

The total section drag coefficient and its derivative with sideslip angle are complex functions of the spanwise coordinate, y_b, and depend on the wing planform shape, sweep,

and dihedral, as well as the aerodynamic interaction with the fuselage. Since there is no closed-form solution for the spanwise distribution of induced drag acting on a swept wing, neither of the two integrals on the right-hand side of Eq. (5.2.32) can be evaluated analytically. Computer simulations or wind tunnel tests must be employed to accurately determine the effect of the wing and horizontal tail on the yaw stability derivative. However, by examining Eq. (5.2.32), we can determine the sign of this contribution.

Wing sweep is defined to be positive when the wings are swept back, placing the wingtips aft of the wing root. The second term on the right-hand side of Eq. (5.2.32) will always have the same sign as $\tan\Lambda$. Thus, this term is stabilizing when the wings are swept back and destabilizing when the wings are swept forward.

The sign of the first term on the right-hand side of Eq. (5.2.32) depends on the sign for the change in section drag coefficient with respect to sideslip angle. For small sideslip angles, the section parasitic drag is nearly independent of sideslip angle, so the first term on the right-hand side of Eq. (5.2.32) is dominated by induced drag. Recall that the local lift at any point on a lifting surface is proportional to the cross product of the local velocity and vorticity vectors. The vorticity on the wing is roughly parallel to the wing quarter-chord and the local velocity is roughly parallel to the freestream. From Fig. 5.2.8, we see that as an airplane with positive sweep yaws to the left (positive β), the right wing becomes more perpendicular to the velocity vector and the left wing becomes less perpendicular to the velocity vector. Since the cross product is largest when the two vectors are at 90 degrees to each other, a positive sideslip angle will increase the lift and induced drag on the right wing and reduce the lift and induced drag on the left wing. Thus, for a wing that is swept back, the change in section drag coefficient with respect to sideslip angle is positive on the right wing (positive y_b) and negative on the left wing (negative y_b). So, for a wing with positive sweep, the product of the spanwise coordinate and the change in section drag coefficient with sideslip angle is always positive. For a wing with negative sweep, this product is always negative. As a result, the first term on the right-hand side of Eq. (5.2.32) is also stabilizing when the wings are swept back and destabilizing when the wings are swept forward.

Since both terms on the right-hand side of Eq. (5.2.32) have the same sign as the sweep angle, positive sweep is stabilizing in yaw and negative sweep is destabilizing. For most conventional airplanes with an aft tail, static yaw stability is dominated by the vertical tail. However, for a tailless aircraft, wing sweep is about the only parameter that the designer can vary to provide passive yaw stability. For this reason the wings of a tailless aircraft are almost always swept back. Because of the associated symmetry, sweep in the wing and horizontal tail of a conventional airplane has no effect on the airplane trim in yaw.

Dihedral in the main wing and horizontal tail can also affect the static yaw stability of an airplane. However, these effects are quite complex and intimately coupled with the effect of wing sweep and side flow about the fuselage. Here again, computer simulations or wind tunnel tests must be employed to accurately determine the effect of wing and tail dihedral on the airplane yaw stability derivative. Fortunately, dihedral effects on yaw stability are small and dihedral has no effect on airplane trim in yaw. Dihedral affects roll stability to a much greater extent than it affects yaw stability and will be discussed in greater detail under that heading.

5.3. Estimating the Sidewash Gradient on a Vertical Tail

The sidewash induced on the vertical tail by the wingtip vortices from the main wing can have a significant effect on the static yaw stability of an airplane. For a vertical tail mounted above the main wing, the sidewash gradient is negative and has a stabilizing effect on the airplane. The sidewash gradient produced by the wingtip vortices can be estimated using the same vortex model that was used in Chapter 4 to estimate the downwash gradient for the horizontal tail. Figure 5.3.1 shows this vortex model in relation to a vertical tail mounted above the main wing.

Relative to the aerodynamic coordinate system shown in Fig. 5.3.1, the z-component of velocity induced by this pair of wingtip vortices, at the arbitrary point in space (x,y,z), is readily found from the Biot-Savart law to be

$$V_z = \frac{\Gamma_{wt}}{4\pi}\left\{\frac{y}{y^2+(z+\frac{1}{2}b')^2}\left[1+\frac{x-\frac{1}{2}b'\tan\Lambda}{\sqrt{(x-\frac{1}{2}b'\tan\Lambda)^2+y^2+(z+\frac{1}{2}b')^2}}\right]\right. \\ \left. -\frac{y}{y^2+(z-\frac{1}{2}b')^2}\left[1+\frac{x-\frac{1}{2}b'\tan\Lambda}{\sqrt{(x-\frac{1}{2}b'\tan\Lambda)^2+y^2+(z-\frac{1}{2}b')^2}}\right]\right\} \tag{5.3.1}$$

From the vortex lifting law, the wingtip vortex strength is proportional to the product of the wing lift coefficient and airspeed. The vortex strength, Γ_{wt}, and spacing, b', can be evaluated from Prandtl's lifting-line theory.

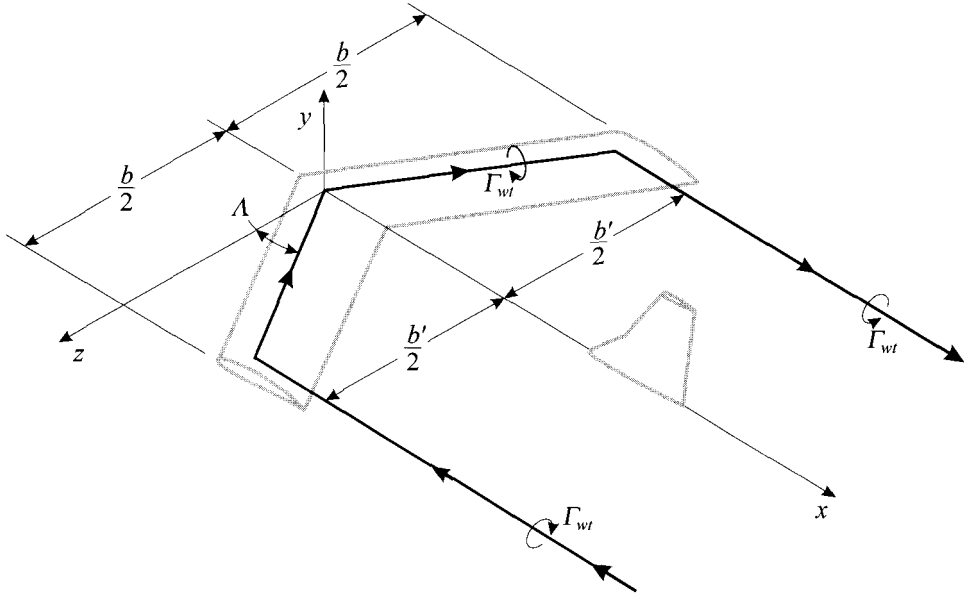


Figure 5.3.1. Vortex model used to estimate the sidewash gradient for the vertical tail.

Since we are using the sign convention that sidewash is positive from left to right, combining Eq. (5.3.1) with Prandtl's lifting-line theory and applying the small-angle approximation, the sidewash angle can be written as

$$\begin{aligned}\varepsilon_s &= -\frac{V_z}{V_\infty} \\ &= \frac{C_{L_w}\kappa_v}{\pi^2 R_{A_w}}\left\{\frac{\bar{y}}{\bar{y}^2+(\bar{z}-\kappa_b)^2}\left[1+\frac{\bar{x}-\kappa_b\tan\Lambda}{\sqrt{(\bar{x}-\kappa_b\tan\Lambda)^2+\bar{y}^2+(\bar{z}-\kappa_b)^2}}\right]\right. \\ &\qquad \left.-\frac{\bar{y}}{\bar{y}^2+(\bar{z}+\kappa_b)^2}\left[1+\frac{\bar{x}-\kappa_b\tan\Lambda}{\sqrt{(\bar{x}-\kappa_b\tan\Lambda)^2+\bar{y}^2+(\bar{z}+\kappa_b)^2}}\right]\right\}\end{aligned} \tag{5.3.2}$$

where C_{L_w} and R_{A_w} are the lift coefficient and aspect ratio for the wing and

$$\bar{x}=\frac{x}{b_w/2}, \quad \bar{y}=\frac{y}{b_w/2}, \quad \bar{z}=\frac{z}{b_w/2}$$

The parameters κ_v and κ_b depend on the planform shape of the wing. The vortex strength factor, κ_v, is a ratio of the wingtip vortex strength to that generated by an elliptic wing having the same lift coefficient and aspect ratio. The vortex span factor, κ_b, is defined as the spacing between the wingtip vortices divided by the wingspan.

For a wing with no sweep or dihedral, both κ_v and κ_b can be determined analytically from the classical series solution to Prandtl's lifting-line equation. For an elliptic wing with no sweep, dihedral, or twist, κ_v is 1.0 and κ_b is $\pi/4$. For an unswept tapered wing with no dihedral or twist, κ_v and κ_b are related to the aspect ratio and taper ratio as shown in Figs. 4.5.2 and 4.5.3. A rough first approximation for swept wings can be made by assuming that κ_v and κ_b are independent of sweep.

Equation (5.3.2) can be directly applied to determine the sidewash angle only when the sideslip angle, β, is zero and the aircraft plane of symmetry is midway between the two trailing vortices. When the airplane has some component of sideslip, the wingtip vortices are displaced relative to the position of the vertical tail, as shown in Fig. 5.3.2. For small sideslip angles, Eq. (5.3.2) gives a very close approximation for the sidewash angle, if the z-coordinate, measured from the aircraft plane of symmetry, is replaced with the z'-coordinate, measured from the centerline midway between the two wingtip vortices, as shown in Fig. 5.3.2. Using the small-angle approximation, the z'-coordinate is related to the z-coordinate according to

$$z'(\beta) = z\cos\beta-(x-\tfrac{1}{2}b'\tan\Lambda)\sin\beta \cong z-(x-\tfrac{1}{2}b'\tan\Lambda)\beta$$

or

$$\bar{z}'(\beta) \cong \bar{z}-(\bar{x}-\kappa_b\tan\Lambda)\beta \tag{5.3.3}$$

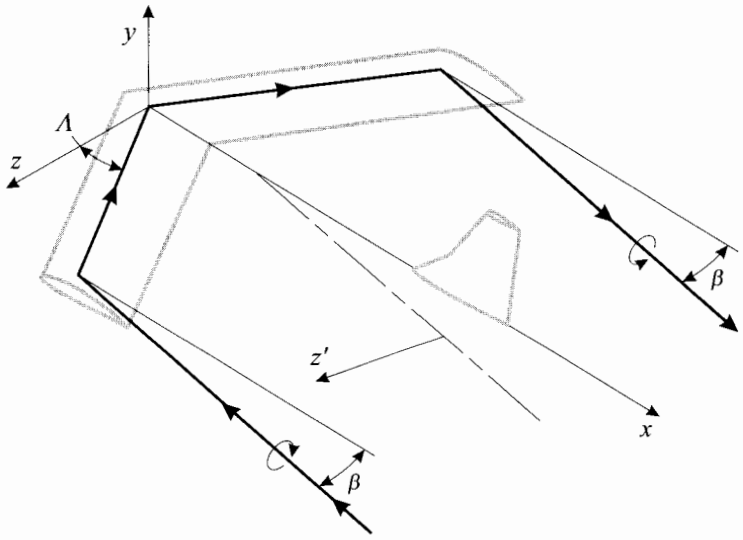


Figure 5.3.2. Effect of sideslip on the position of the wingtip vortices relative to the vertical tail.

Within this small-angle approximation, the sidewash gradient can be written as

$$\frac{\partial \varepsilon_s}{\partial \beta} = \frac{\partial \varepsilon_s}{\partial \bar{z}'} \frac{\partial \bar{z}'}{\partial \beta} \tag{5.3.4}$$

where, from Eq. (5.3.2),

$$\begin{aligned} \frac{\partial \varepsilon_s}{\partial \bar{z}'} = \frac{C_{L_w} \kappa_v}{\pi^2 R_{A_w}} \Bigg\{ & \frac{-2\bar{y}(\bar{z}-\kappa_b)}{[\bar{y}^2+(\bar{z}-\kappa_b)^2]^2} \left[1 + \frac{\bar{x}-\kappa_b \tan \Lambda}{\sqrt{(\bar{x}-\kappa_b \tan \Lambda)^2+\bar{y}^2+(\bar{z}-\kappa_b)^2}} \right] \\ & + \frac{2\bar{y}(\bar{z}+\kappa_b)}{[\bar{y}^2+(\bar{z}+\kappa_b)^2]^2} \left[1 + \frac{\bar{x}-\kappa_b \tan \Lambda}{\sqrt{(\bar{x}-\kappa_b \tan \Lambda)^2+\bar{y}^2+(\bar{z}+\kappa_b)^2}} \right] \\ & - \frac{\bar{y}}{\bar{y}^2+(\bar{z}-\kappa_b)^2} \left[\frac{(\bar{x}-\kappa_b \tan \Lambda)(\bar{z}-\kappa_b)}{[(\bar{x}-\kappa_b \tan \Lambda)^2+\bar{y}^2+(\bar{z}-\kappa_b)^2]^{3/2}} \right] \\ & + \frac{\bar{y}}{\bar{y}^2+(\bar{z}+\kappa_b)^2} \left[\frac{(\bar{x}-\kappa_b \tan \Lambda)(\bar{z}+\kappa_b)}{[(\bar{x}-\kappa_b \tan \Lambda)^2+\bar{y}^2+(\bar{z}+\kappa_b)^2]^{3/2}} \right] \Bigg\} \end{aligned} \tag{5.3.5}$$

and from Eq. (5.3.3),

$$\frac{\partial \bar{z}'}{\partial \beta} = -(\bar{x}-\kappa_b \tan \Lambda) \tag{5.3.6}$$

The sidewash gradient induced at an arbitrary point in space can be estimated by using Eqs. (5.3.5) and (5.3.6) in Eq. (5.3.4). In the plane of symmetry this reduces to

$$\frac{\partial \varepsilon_s}{\partial \beta}(\bar{x},\bar{y},0) = -\frac{\kappa_v \kappa_\beta}{\kappa_b}\frac{C_{L_w}}{R_{A_w}} \tag{5.3.7}$$

where

$$\kappa_\beta(\bar{x},\bar{y},0) = \frac{4\bar{y}(\bar{x}-\kappa_b\tan\Lambda)\kappa_b^2}{\pi^2(\bar{y}^2+\kappa_b^2)^2}\left[1+\frac{\bar{x}-\kappa_b\tan\Lambda}{\sqrt{(\bar{x}-\kappa_b\tan\Lambda)^2+\bar{y}^2+\kappa_b^2}}\right] + \frac{2\bar{y}\kappa_b}{\pi^2(\bar{y}^2+\kappa_b^2)}\left[\frac{(\bar{x}-\kappa_b\tan\Lambda)^2\kappa_b}{[(\bar{x}-\kappa_b\tan\Lambda)^2+\bar{y}^2+\kappa_b^2]^{3/2}}\right] \tag{5.3.8}$$

The tail sidewash factor, κ_β, depends on the planform shape of the wing and the position of the tail relative to the wing. However, the planform shape of the wing affects the value of κ_β only through Λ and κ_b. Thus, κ_β is a unique function of $\bar{x}/\kappa_b - \tan\Lambda$ and $\bar{y}/\kappa_b$, as shown in Fig. 5.3.3.

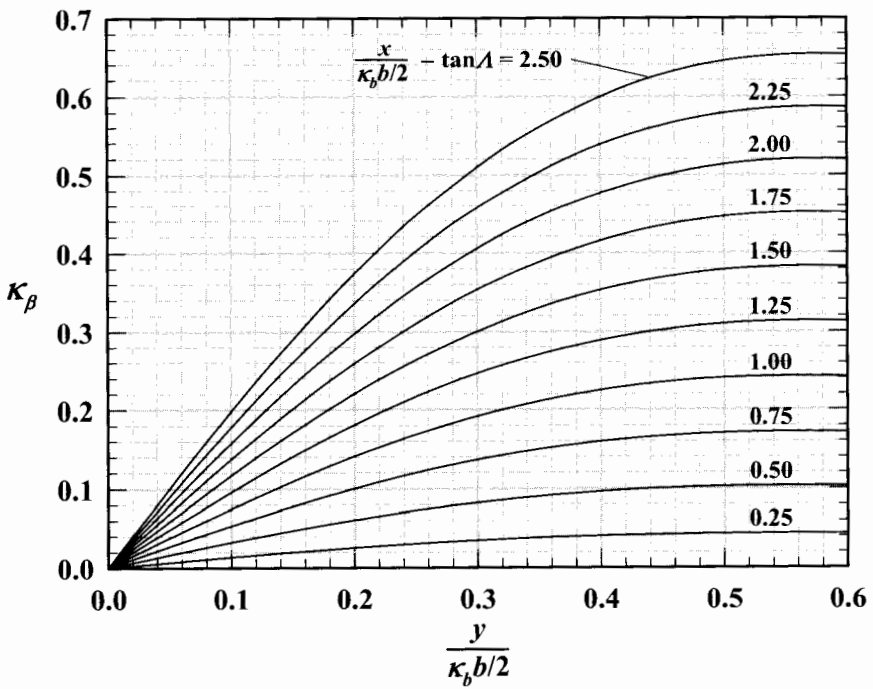


Figure 5.3.3. Effect of tail position on the sidewash gradient in the plane of symmetry.

EXAMPLE 5.3.1. Consider the general aviation aircraft, which was described in Examples 4.3.1 and 4.5.1. If the vertical tail is mounted with the aerodynamic center 5 ft above the wing, using the approximate method presented in this section, estimate the sidewash gradient for an airspeed of 80 mph at sea level.

Solution. For this wing-tail combination we have

$$S_w = 180\,\text{ft}^2, \quad b_w = 33\,\text{ft}, \quad R_{A_w} = 33^2/180 = 6.05, \quad C_{L_w,\alpha} = 4.44, \quad R_{T_w} = 0.40,$$
$$\Lambda = 10°, \quad l_t - l_w = 15\,\text{ft}, \quad \bar{x} = 15/(33/2) = 0.909, \quad \bar{y} = 5/(33/2) = 0.303$$

From Example 4.5.1,

$$\kappa_v = 1.035$$

$$\kappa_b = 0.759$$

From Eq. (5.3.8) or using the results plotted in Fig. 5.3.3, the sidewash factor is found to be

$$\kappa_\beta = 0.230$$

From Example 4.3.1, the lift on the wing for 80 mph at sea level is 2,625.9 lbf and the lift coefficient for the wing is

$$C_{L_w} = \frac{L_w}{\frac{1}{2}\rho V_\infty^2 S_w} = \frac{2{,}625.9}{\frac{1}{2}0.0023769(80\times 5{,}280/3{,}600)^2 180} = 0.8916$$

From Eq. (5.3.7), the sidewash gradient at the position of the vertical tail is

$$\varepsilon_{s,\beta} \equiv \frac{\partial \varepsilon_s}{\partial \beta} = -\frac{\kappa_v \kappa_\beta}{\kappa_b}\frac{C_{L_w}}{R_{A_w}} = -\frac{1.035(0.230)}{0.759}\frac{0.8916}{6.05} = \underline{-0.046}$$

The predicted sidewash gradient on the vertical tail of the airplane in Example 5.3.1 is small. For this airplane with ample wingspan in cruise configuration, the net effect of sidewash is to increase the yaw stability by about 5 percent. However, the reader should recognize that the sidewash gradient goes up very rapidly with decreasing wingspan. Thus, aircraft having wings of smaller span produce much larger sidewash gradients. For example, if the wingspan for the airplane in Example 5.3.1 were cut in half, while the wing area and all other parameters remained the same, the magnitude of the predicted sidewash gradient would be increased by nearly an order of magnitude, to –0.435. In addition, since the sidewash gradient is proportional to the wing lift coefficient, slow flight with high-lift devices deployed can also result in a significant increase in the sidewash gradient induced on the vertical tail.

It is important to remember the orientation of the coordinate system used in the development of Eqs. (5.3.5) and (5.3.8). As shown in Figs. 5.3.1 and 5.3.2, the x-z plane of this coordinate system coincides with the plane of the trailing wingtip vortices and the x-axis is aligned with the equilibrium relative wind. Thus, the y-coordinate is the vertical distance measured above the plane of the trailing wingtip vortices. When computing the downwash from this vortex model according to the relations presented in Sec. 4.5, the y-coordinate was found to have only a second-order effect on downwash. However, as can be seen from Eqs. (5.3.5) and (5.3.8), the y-coordinate has a first-order effect on the sidewash. Thus, the orientation of the x-axis within the aircraft plane of symmetry is critical for predicting the sidewash gradient. This orientation changes with angle of attack as shown in Fig. 5.3.4. The y-coordinate of any point on the aft vertical stabilizer decreases with increasing angle of attack. From Eq. (5.3.5), we have seen that the sidewash on the vertical stabilizer is proportional to the product of the wing lift coefficient and the dimensionless y-coordinate, $\bar{y}$. As angle of attack is increased, the wing lift coefficient increases but $\bar{y}$ decreases. Thus, for a given flap setting, the magnitude of the sidewash gradient does not increase linearly with lift coefficient. In fact, as the angle of attack increases from zero lift, the magnitude of the sidewash gradient will at some point begin to decrease with increasing angle of attack. Ultimately, the sidewash gradient becomes positive and destabilizing, when the angle of attack is large enough to put the vertical stabilizer below the wingtips. Normally, the wing would stall well before this angle of attack was reached. However, this can produce an important destabilizing effect in post-stall maneuvers.

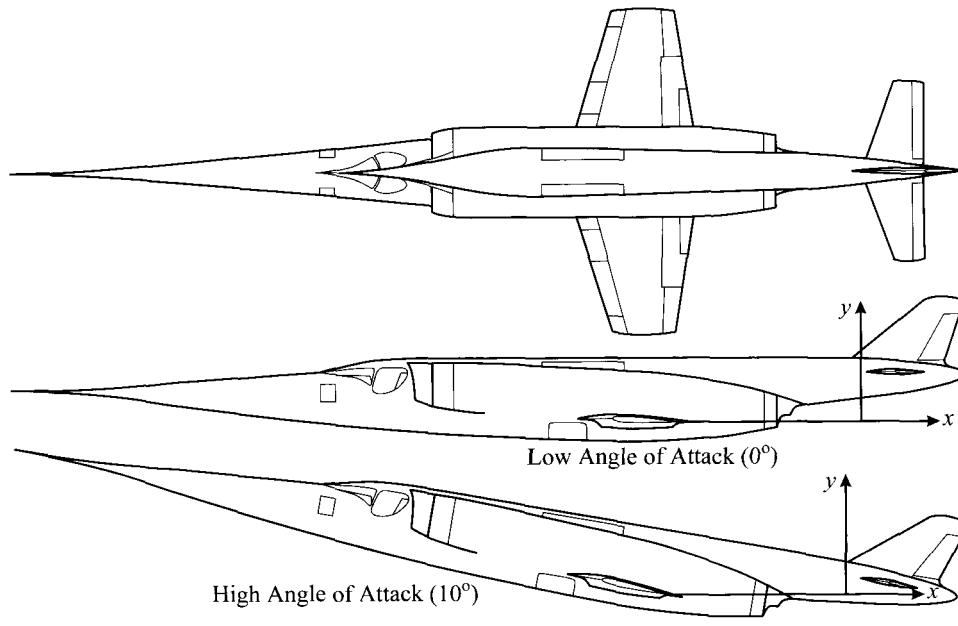


Figure 5.3.4. Effect of aircraft angle of attack on the y-position of the vertical stabilizer.

It is also important to recognize that the sidewash gradient on the vertical stabilizer increases rapidly with its distance aft of the wingtips. From Eq. (5.2.7), we have seen that the yaw stability derivative increases linearly with the product of the area of the vertical stabilizer, S_v, and its distance aft of the center of gravity, l_v. One important consideration in tail design is the trade-off between changing either S_v or l_v to attain the desired level of yaw stability. As the tail is moved aft, the required size of the vertical stabilizer is decreased, which reduces aircraft weight and drag. However, moving the tail aft increases the weight and drag associated with the structure supporting the tail. Thus, there is an optimum in the trade-off between tail area and length. Since the sidewash gradient on a high vertical tail becomes more stabilizing with increasing tail length, sidewash moves this optimum in the direction of smaller tails placed further aft of the CG. As the wingspan is decreased, this effect becomes more important. However, moving the vertical stabilizer farther aft of the wingtips will aggravate the destabilizing effect of sidewash in post-stall maneuvers.

Airplanes are sometimes designed with twin vertical stabilizers symmetrically offset from the midspan. Two examples of aircraft that have used this design feature are the P-38 Lightning and the F-14 Tomcat, both shown in Fig. 5.3.5. One advantage of this tail design is very obvious in this front view of the Lightning. The twin vertical stabilizers are directly aft of the twin counterrotating propellers. This keeps the rudders in the propeller slipstreams and improves rudder control power, especially at low airspeed. A similar but perhaps less obvious advantage is produced by the jet engines of the Tomcat. As shown in Fig. 5.3.6, the entrainment caused by turbulent mixing in the shear layer between the high-speed exhaust jet and the surrounding atmosphere draws increased

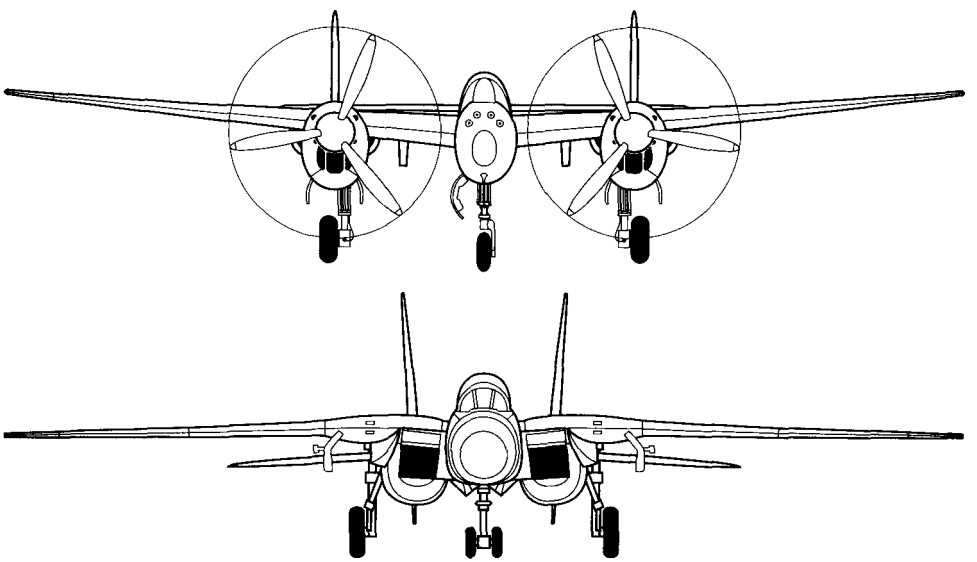


Figure 5.3.5. Use of twin vertical stabilizers above the wing places each stabilizer closer to a wingtip vortex, which increases the sidewash gradient and total yaw stability.

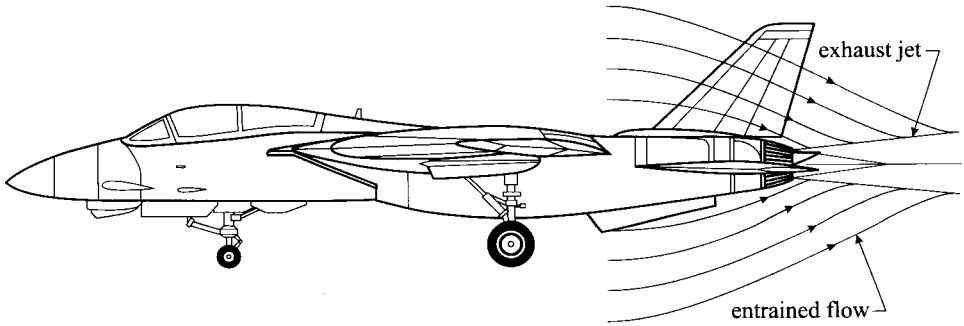


Figure 5.3.6. Increased airflow across the vertical stabilizer caused by exhaust jet entrainment.

airflow over the vertical stabilizers. In the case of the Tomcat, placing the twin vertical stabilizers directly over the exhaust nozzles of the twin turbojet engines maximizes this effect.

Improved rudder control power is not the only advantage of using twin vertical stabilizers. With this tail design, because each of the two vertical stabilizers is closer to one of the wingtip vortices, the sidewash gradient for each stabilizer is greater than that in the aircraft plane of symmetry. For the conventional high tail, this gives the aircraft greater yaw stability than would be attained with a single vertical stabilizer of the same total area, placed the same distance aft of the wing midspan. To estimate the sidewash gradient for this tail design, Eq. (5.3.4) can be used together with Eqs. (5.3.5) and (5.3.6).

5.4. Estimating the Lift Slope for a Vertical Tail

As briefly mentioned in Sec. 5.2, the lift slope for the vertical stabilizer is significantly affected by aerodynamic interactions with the horizontal stabilizer. For either the conventional tail or T-tail configuration, the horizontal stabilizer acts like a very large winglet for the vertical stabilizer. This inhibits vortex shedding and increases the lift slope for the vertical stabilizer over that which would be observed for the same vertical surface isolated in the freestream. Because of the very large number of variations in tail geometry that are possible, it would be extremely difficult to develop a general closed-form expression for estimating the in situ lift slope for the vertical stabilizer as a function of horizontal and vertical tail geometry.

The easiest way to accurately estimate the in situ lift slope for the vertical stabilizer in combination with the horizontal stabilizer is to use the numerical lifting-line method for the actual tail geometry being used. This method gives results that agree almost exactly with results obtained from the more complex vortex panel method. Since fluid viscosity has very little effect on aerodynamic lift in nonseparated flow, these inviscid flow calculations are also in close agreement with experimental data at aerodynamic angles below stall.

To estimate the in situ lift slope for the vertical stabilizer using the numerical lifting-line method, the complete tail geometry is included in the vortex model. The side force coefficient is determined at a small positive angle of sideslip and again at a small

negative angle of sideslip. The in situ lift slope for the vertical stabilizer is estimated as the difference between the two side force coefficients divided by the difference in sideslip angle in radians.

To give the reader a better feeling for the aerodynamic interactions between the horizontal and vertical stabilizers, Fig. 5.4.1 shows the results of numerical lifting-line computations for a specific conventional tail geometry. The vectors displayed along the quarter-chord line show the magnitude and direction for the spanwise lift distribution, and the vectors shown along the trailing edge indicate the magnitude and direction of shed vorticity. In this example, both the horizontal and vertical surfaces have symmetric airfoil sections with no geometric or aerodynamic twist. The quarter-chord sweep for each surface is zero and the horizontal surface has no dihedral. The aerodynamic forces shown in Fig. 5.4.1 were computed for zero angle of attack relative to the chord line of the horizontal surface. All aerodynamic forces shown in this figure are the result of a 4-degree sideslip angle. Notice that the lift on the vertical stabilizer goes to zero at the upper tip, and a strong wingtip vortex is shed in this vicinity. If the vertical stabilizer were isolated in the freestream without the horizontal stabilizer, the lift would also go to zero at the lower extremity, and a similar wingtip vortex would be shed in this region. However, the presence of the horizontal stabilizer inhibits vortex shedding near the base of the vertical stabilizer. The vorticity generated on the vertical stabilizer is spread out over both sides of the horizontal stabilizer. This prevents the lift on the vertical stabilizer from going to zero at the lower extreme and generates additional lift on the horizontal stabilizer. The lift developed on the left semispan of the horizontal stabilizer is upward, while that on the right semispan is downward. Thus, in addition to increasing the side force developed on the vertical stabilizer, the aerodynamic interaction produces a net rolling moment as a result of lift developed on the horizontal stabilizer. Since the vertical stabilizer is usually above the center of gravity, the side force developed on this surface as a result of positive sideslip produces a negative rolling moment. The positive rolling moment produced on the horizontal stabilizer will partially counter this effect.

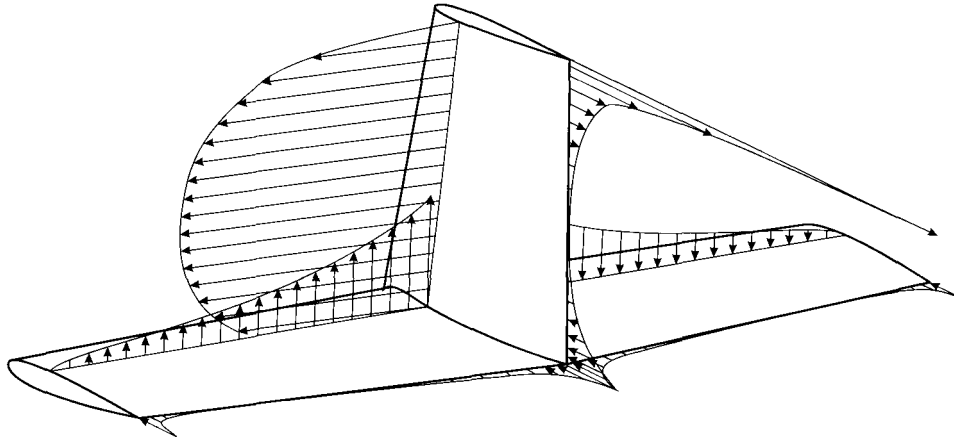


Figure 5.4.1. Aerodynamic interactions between the horizontal and vertical stabilizers in sideslip.

As can be seen from Fig 5.4.1, the aerodynamic forces produced on the tail of an airplane as a result of sideslip are quite complex, even for this very simple tail geometry. Furthermore, the distribution and magnitude of these forces are affected by the geometry of both the horizontal and vertical stabilizers. When one considers all of the many possible variations in tail geometry, it is not practical to present results that show how the lift slope for the vertical stabilizer varies with all attributes of tail geometry. However, aspect ratio plays a major role in the variation of lift slope with tail geometry.

Figure 5.4.2 shows how the effective aspect ratio of the vertical stabilizer varies with the true aspect ratio of both the horizontal and vertical stabilizers for one particular tail configuration. The tail geometry used to generate the data plotted in Fig. 5.4.2 was a conventional tail similar to that shown in Fig. 5.4.1. Both the horizontal and vertical stabilizers had unswept rectangular planforms with the same chord and the horizontal stabilizer had no dihedral. The true aspect ratio of the vertical stabilizer is defined to be the square of the distance from root to tip divided by the planform area. The effective aspect ratio for the vertical stabilizer was defined to be the aspect ratio that when used in the analytical solution to Prandtl's lifting-line equation for the isolated vertical stabilizer, gives the same lift slope as that predicted by the numerical lifting-line solution for the complete tail. Strictly speaking, Fig. 5.4.2 applies only to the particular tail geometry for which it was obtained. However, in preliminary design the exact tail geometry is not typically known, and Fig. 5.4.2 can be used as a guideline.

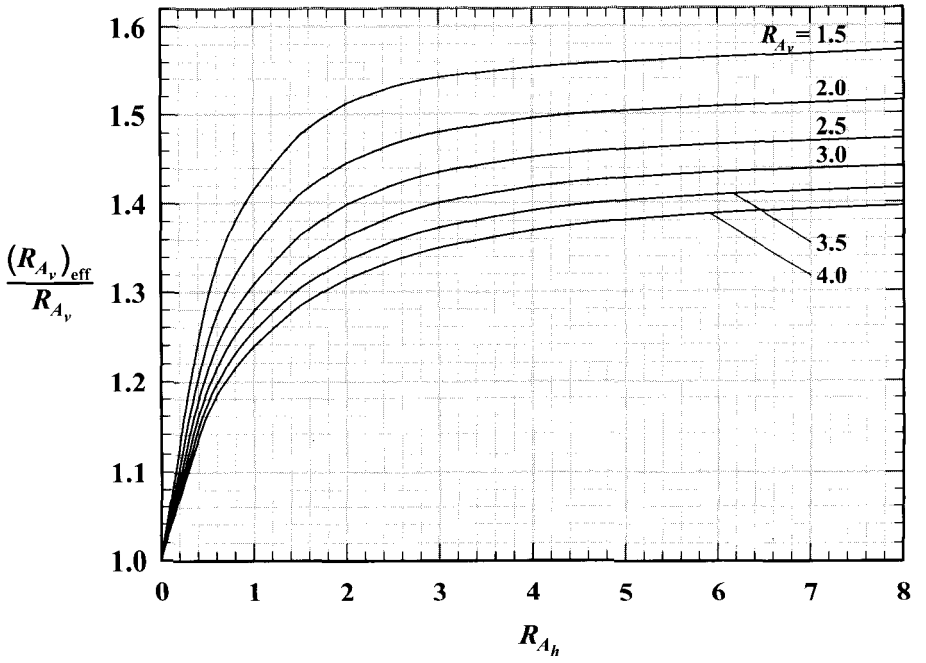


Figure 5.4.2. Effective vertical aspect ratio for a conventional tail with both the horizontal and vertical stabilizers having unswept rectangular planforms.

EXAMPLE 5.4.1. For the preliminary design of an airplane we shall assume that the conventional aft tail is constructed from unswept rectangular surfaces having thin airfoil sections. The size of the tail is not yet known, but the horizontal stabilizer is assumed to have an aspect ratio of 5. Assuming that the vertical stabilizer will have a root-to-tip height of twice the chord, estimate the lift slope for the vertical stabilizer from the results plotted in Fig. 5.4.2.

Solution. For this tail geometry we have

$$R_{A_h} = 5.0, \quad R_{A_v} = 2.0$$

From Fig. 5.4.2,

$$\frac{(R_{A_v})_{\text{eff}}}{R_{A_v}} \cong 1.5$$

and

$$(R_{A_v})_{\text{eff}} = 1.5R_{A_v} = 1.5(2.0) = 3.0$$

Using this aspect ratio and a taper ratio of 1.0 in the series solution to Prandtl's lifting-line equation presented in Chapter 1, the lift slope factor for the vertical stabilizer is found to be

$$\kappa_L \cong 0.04$$

Using this result with the effective aspect ratio of 3.0 and using the theoretical section lift slope for thin airfoils, 2π, the lift slope for the vertical stabilizer is estimated to be

$$C_{L_v,\alpha} = \frac{\widetilde{C}_{L,\alpha}}{[1+\widetilde{C}_{L,\alpha}/\pi(R_{A_v})_{\text{eff}}](1+\kappa_L)} = \frac{2\pi}{[1+2\pi/\pi(3.0)](1+0.04)} = \underline{3.62}$$

If we had ignored the vortex interactions between the horizontal stabilizer and the vertical stabilizer in Example 5.4.1, a smaller lift slope would have been predicted. Using the true aspect ratio of 2.0, the lift slope for the isolated vertical stabilizer is predicted from Prandtl's lifting-line theory to be about 3.02. Hence, lifting-line theory predicts that the presence of the horizontal stabilizer increases the lift slope for this vertical stabilizer by about 20 percent.

The aerodynamic interaction between the vertical stabilizer and fuselage can also increase the lift slope for the vertical stabilizer somewhat. This is typically more significant for the T-tail configuration. The vertical lift slope is usually slightly higher for a T-tail than it is for a conventional tail with the same aspect ratio. This is because the horizontal stabilizer inhibits vortex shedding at the top and the fuselage inhibits vortex shedding at the bottom.

5.5. Roll Stability and Dihedral Effect

An airplane is said to be statically stable in roll if a restoring rolling moment develops as a result of a disturbance in bank angle. At first thought, this may seem quite similar to the definitions of static pitch and yaw stability. Static pitch stability requires that a restoring pitching moment result from a disturbance in angle of attack, and static yaw stability necessitates that a restoring yawing moment develop from a disturbance in sideslip angle. Static roll stability is fundamentally different from static pitch and yaw stability, because the bank angle is fundamentally different from the angle of attack and sideslip angle. As shown in Fig. 5.1.1, the bank angle, ϕ, is defined in terms of the airplane's orientation with respect to the Earth, while the angle of attack, α, and sideslip angle, β, are defined in terms of the airplane's orientation with respect to the relative wind. The bank angle is completely independent of the relative wind.

The aerodynamic forces and moments acting on an airplane depend only on the orientation of the airplane with respect to the relative wind. Since the gravitational force acts through the center of gravity, the only moments produced about the center of gravity are the aerodynamic moments, including thrust. Thus, there can be no moment about the center of gravity that depends directly on the bank angle. As a result, static roll stability is based on an indirect effect of bank angle rather than a direct effect.

A disturbance in pure roll, with no change in angle of attack, sideslip angle, or forward airspeed, produces no direct change in the aerodynamic forces and moments relative to the airplane. As can be seen in Fig. 5.5.1a, a bank angle disturbance with no change in α or β produce a force imbalance in both the normal and spanwise directions. If the airplane was originally trimmed for straight and level flight, the lift is equal to the weight and there is no aerodynamic side force. After the bank angle disturbance, the lift force remains in the plane of symmetry, and the gravitational force acts at an angle, ϕ, to the plane of symmetry. The net upward normal force is now $W(1-\cos\phi)$ and the net side force is $W\sin\phi$. If there is no change in the control inputs, this force imbalance produces changes in both normal velocity and sideslip. The change in normal velocity decreases the angle of attack until the lift balances the normal component of weight and the sideslip will increase until the side force balances the spanwise component of weight.

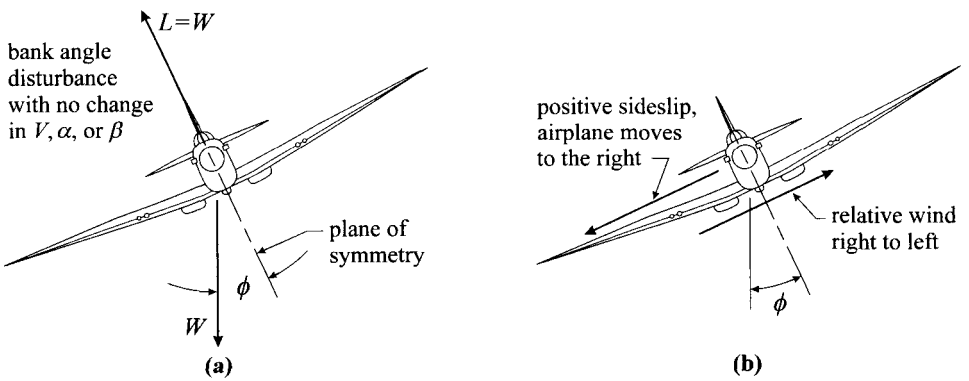


Figure 5.5.1. Force imbalance and resulting sideslip produced by a disturbance in roll.

However, the change in α and β required to restore the force balance can also produce a change in the aerodynamic moments. For a perfectly symmetric airplane, the change in angle of attack does not affect the rolling moment, but the change in sideslip angle can produce a rolling moment that is either positive or negative, depending on the airplane design.

Comparing Fig. 5.5.1b with the sign convention defined in Fig. 5.1.1, we see that a positive disturbance in bank angle results in a positive sideslip velocity component, which was defined to correspond with a positive sideslip angle. Also from the sign convention in Fig. 5.1.1, we see that a negative rolling moment is required to restore a positive disturbance in bank angle. Thus, static roll stability requires that a positive sideslip angle must produce a negative rolling moment,

$$\frac{\partial \ell}{\partial \beta} < 0$$

In dimensionless form, this gives **the general criterion for static roll stability**,

$$\frac{\partial C_\ell}{\partial \beta} \equiv C_{\ell,\beta} < 0 \tag{5.5.1}$$

The aerodynamic derivative, $C_{\ell,\beta}$, is the *roll stability derivative*. If $C_{\ell,\beta}$ is negative, the airplane is said to be statically stable in roll, and if $C_{\ell,\beta}$ is positive, the airplane is statically unstable in roll. When $C_{\ell,\beta}$ is zero, the airplane is neutrally stable in roll.

Roll stability gives an airplane the inherent tendency to fly with the wings level when the airplane is trimmed for zero sideslip. An airplane that is neutrally stable or even unstable in roll can still be flown but requires greater attention by the pilot to keep the wings level. The desired magnitude of roll stability depends significantly on the pilot and aircraft application. Very proficient pilots typically prefer less roll stability than inexperienced pilots do. Airplanes that execute rapid rolling maneuvers, such as fighter aircraft and stunt planes, will be disadvantaged by a high degree of roll stability. Transports and other aircraft that use more gradual rolling maneuvers usually have better handling qualities with somewhat higher levels of roll stability.

For any aircraft and pilot, **too much roll stability will be detrimental.** Most of the reasons for this can be traced to the coupling between roll and yaw. When roll stability is excessive, an airplane becomes very sensitive in roll to the minor changes in sideslip caused by very slight deflections of the rudder. This necessitates very precise coordination between the rudder and ailerons, which can be annoying to a proficient pilot and unacceptable to the less experienced. Excessive roll stability can be particularly problematic in a crosswind landing that requires flying the airplane in sideslip with the wings level. In addition, too much roll stability can result in increased passenger discomfort because the airplane becomes very sensitive in roll to changes in sideslip caused by atmospheric turbulence. The roll stability derivative, $C_{\ell,\beta}$, also affects certain dynamic handling characteristics of an airplane, which will be considered later in this textbook.

Because roll stability affects so many different aspects of an aircraft's handling characteristics, it is difficult to define a general roll stability criterion in terms of $C_{\ell,\beta}$. However, **to give the student a place to start, typical airplane configurations normally display good handling qualities with $C_{\ell,\beta}$ in the range from about 0.00 to –0.10 per radian.** This should not be treated as an absolute rule but simply as a starting point. About the only thing that can be said concerning roll stability in general is that a little roll stability is advantageous, but too much can be worse than none at all.

The roll stability derivative is more difficult to estimate than either the pitch or yaw stability derivative. This is because the roll stability derivative is significantly affected by complex interactions between the fuselage, the wing, and the tail. Furthermore, these interactions can change significantly with power and flap settings. Design changes to vary roll stability are commonly required after wind tunnel testing and sometimes after actual flight testing of the airplane. Nevertheless, the designer must have at least a qualitative understanding of all design considerations that affect roll stability and should be able to predict the effects of the design changes that will be used to make any final adjustments in roll stability.

Effect of Wing Dihedral

The change in rolling moment due to sideslip is heavily influenced by the dihedral angle of the wing, which is shown in Fig. 5.5.2. The dihedral angle is commonly given the symbol Γ and is defined to be positive when the wingtips are above the wing root. Negative dihedral is commonly called *anhedral*. Recall that the symbol Γ is also commonly used to represent circulation and vortex strength. Because the circulation theory of lift can be used to predict certain dihedral effects, this can be confusing if we are not careful. Here an effort will be made to avoid confusion in this regard, but the reader should be forewarned of this potential difficulty.

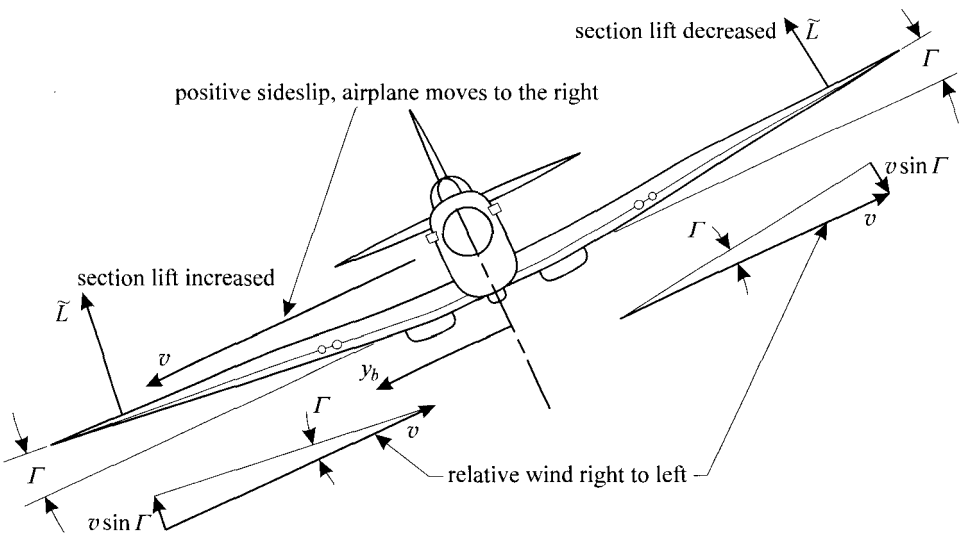


Figure 5.5.2. Efect of sideslip and wing dihedral on local section lift.

Wing dihedral affects the roll stability derivative of an airplane because it causes the lift on the right and left semispans to respond differently to sideslip. As shown in Fig. 5.5.2 for a wing with positive dihedral, sideslip produces an increase in angle of attack on the windward semispan and a decrease in angle of attack on the lee-side semispan. When the sideslip component of relative wind, v, is resolved into components parallel with and normal to each semispan, as shown in Fig. 5.5.2, the upward normal component is $v \sin\Gamma$ on the right-hand semispan and $-v \sin\Gamma$ on the left-hand semispan. For small aerodynamic angles, the sideslip velocity can be closely approximated as the product of the airspeed and sideslip angle, $V\beta$. Likewise, the angle of attack is closely approximated as the upward normal component of relative wind divided by the airspeed. Thus, sideslip produces a change in angle of attack that can be closely approximated for the right and left semispans, respectively, as

$$(\Delta\alpha)_{\text{right}} = \frac{v \sin\Gamma}{V} = \frac{V\beta \sin\Gamma}{V} = \beta \sin\Gamma \tag{5.5.2}$$

$$(\Delta\alpha)_{\text{left}} = \frac{-v \sin\Gamma}{V} = \frac{-V\beta \sin\Gamma}{V} = -\beta \sin\Gamma \tag{5.5.3}$$

The differential in angle of attack between the right and left semispans creates a differential in lift, which in turn produces a rolling moment. From Fig. 5.1.1, we see that lift generated on the left semispan ($y_b < 0$) produces a positive rolling moment, while lift generated on the right semispan ($y_b > 0$) produces a negative rolling moment. Thus, the rolling moment arm for the lift on any wing section is $-y_b$. Using the small-angle approximations given by Eqs. (5.5.2) and (5.5.3), the net rolling moment that results from sideslip combined with wing dihedral can be written as

$$\begin{aligned}(\Delta C_\ell)_{\Gamma w} &= \int_{y_b=-b_w/2}^{0} \widetilde{C}_{L_w,\alpha} \frac{-\beta \sin\Gamma}{S_w b_w}(-y_b)\, c_w\, dy_b + \int_{y_b=0}^{b_w/2} \widetilde{C}_{L_w,\alpha} \frac{\beta \sin\Gamma}{S_w b_w}(-y_b)\, c_w\, dy_b \\ &= -\frac{\beta \sin\Gamma}{S_w b_w} \int_{y_b=-b_w/2}^{b_w/2} \widetilde{C}_{L_w,\alpha} |y_b|\, c_w\, dy_b\end{aligned} \tag{5.5.4}$$

where $\widetilde{C}_{L_w,\alpha}$ is the local *in situ section lift slope*, including the effects of local induced downwash. This should not be confused with the *airfoil section lift slope*, which depends only on airfoil section geometry.

In general, the spanwise variation of local induced downwash is affected by the sideslip. Thus, the derivative of Eq. (5.5.4) with respect to β must be written as

$$\frac{\partial}{\partial\beta}(\Delta C_\ell)_{\Gamma w} = -\frac{\sin\Gamma}{S_w b_w} \int_{y_b=-b_w/2}^{b_w/2} \widetilde{C}_{L_w,\alpha} |y_b|\, c_w\, dy_b - \frac{\beta \sin\Gamma}{S_w b_w} \int_{y_b=-b_w/2}^{b_w/2} \frac{\partial \widetilde{C}_{L_w,\alpha}}{\partial\beta} |y_b|\, c_w\, dy_b$$

However, the roll stability derivative, $C_{\ell,\beta}$, is evaluated at $\beta = 0$, and the contribution of wing dihedral to this aerodynamic derivative can be written

$$\left(\Delta C_{\ell,\beta}\right)_{\Gamma w} = -\frac{\sin\Gamma}{S_w b_w}\left[\int_{y_b=-b_w/2}^{b_w/2} \tilde{C}_{L_w,\alpha}\,|y_b|\,c_w\,dy_b\right]_{\beta=0} \tag{5.5.5}$$

Since the integral in Eq. (5.5.5) is evaluated at $\beta = 0$, both the flow and the wing are symmetric about the midspan. Thus, the integration from $-b_w/2$ to 0 is equivalent to that from 0 to $b_w/2$, and Eq. (5.5.5) can also be written as

$$\left(\Delta C_{\ell,\beta}\right)_{\Gamma w} = -\frac{2\sin\Gamma}{S_w b_w}\left[\int_{y_b=0}^{b_w/2} \tilde{C}_{L_w,\alpha}\,y_b\,c_w\,dy_b\right]_{\beta=0} \tag{5.5.6}$$

For subsonic airspeeds with low Mach number, Prandtl's lifting-line theory can be used to determine the spanwise variation of in situ section lift slope, which is needed to evaluate the integral on the right-hand side of Eq. (5.5.6). For large dihedral angles, it is necessary to use a numerical lifting-line solution, because the classical infinite series solution applies only to wings with no sweep or dihedral. However, for unswept wings in the limit as the dihedral angle approaches zero, the integral in Eq. (5.5.6) can be evaluated from the classical solution to Prandtl's lifting-line equation. For an unswept wing of arbitrary planform, this solution predicts that the change in local section lift coefficient with respect to wing angle of attack is given by

$$\tilde{C}_{L_w,\alpha} = \frac{4b_w}{c_w}\sum_{n=1}^{\infty} a_n \sin(n\theta) \tag{5.5.7}$$

where a_n denotes the coefficients in the infinite series solution to the lifting-line equation, which is described in Sec. 1.8, and θ is the change of variables given by

$$y_b = \tfrac{1}{2} b_w \cos\theta \tag{5.5.8}$$

From Eq. (5.5.8), we have

$$dy_b = -\tfrac{1}{2} b_w \sin\theta\, d\theta \tag{5.5.9}$$

Using Eqs. (5.5.7) through (5.5.9) in Eq. (5.5.6) results in

$$\left(\Delta C_{\ell,\beta}\right)_{\Gamma w} = -\frac{2\sin\Gamma}{S_w b_w}\int_{\theta=\pi/2}^{0}\left(\frac{4b_w}{c_w}\sum_{n=1}^{\infty} a_n \sin(n\theta)\right)\left(\tfrac{1}{2} b_w \cos\theta\right) c_w \left(-\tfrac{1}{2} b_w \sin\theta\, d\theta\right)$$

After using the definition of aspect ratio, $R_{A_w} = b_w^2/S_w$, together with the trigonometric identity, $\sin(2\theta) = 2\sin\theta\cos\theta$, and applying the small-angle approximation, $\sin\Gamma \cong \Gamma$, this reduces to

$$\left(\Delta C_{\ell,\beta}\right)_{\Gamma w} = -R_{A_w}\Gamma\sum_{n=1}^{\infty}a_n\int_{\theta=0}^{\pi/2}\sin(n\theta)\sin(2\theta)\,d\theta \tag{5.5.10}$$

The integral in Eq. (5.5.10) is readily evaluated to yield

$$\int_{\theta=0}^{\pi/2}\sin(n\theta)\sin(2\theta)\,d\theta = \begin{cases}\dfrac{2\sin(n\pi/2)}{4-n^2}, & n\neq 2\\ \dfrac{\pi}{4}, & n=2\end{cases}$$

After applying this result, Eq. (5.5.10) becomes

$$\left(\Delta C_{\ell,\beta}\right)_{\Gamma w} = -R_{A_w}\Gamma\left[\frac{2}{3}a_1+\frac{\pi}{4}a_2+\sum_{n=3}^{\infty}\frac{2\sin(n\pi/2)}{4-n^2}a_n\right] \tag{5.5.11}$$

Also, from the classical solution to Prandtl's lifting-line equation, the lift slope for the complete finite wing is given by

$$C_{L_w,\alpha} = \pi R_{A_w} a_1$$

Thus, Eq. (5.5.11) can be conveniently rearranged as

$$\left(\Delta C_{\ell,\beta}\right)_{\Gamma w} = -\frac{2\Gamma}{3\pi}\kappa_\ell\, C_{L_w,\alpha} \tag{5.5.12}$$

where

$$\kappa_\ell = 1+\frac{3\pi}{8}\frac{a_2}{a_1}+\sum_{n=3}^{\infty}\frac{3\sin(n\pi/2)}{4-n^2}\frac{a_n}{a_1} \tag{5.5.13}$$

For the special case of an elliptic wing with no geometric or aerodynamic twist, all coefficients in the infinite series solution are zero, with the exception of a_1. Hence, the right-hand side of Eq. (5.5.13) is unity for an elliptic wing, and we see that **κ_ℓ is the ratio of the roll stability derivative developed by a wing of arbitrary planform to that developed by an elliptic wing having the same dihedral and lift slope.** Note that since the lift slope for an elliptic wing is greater than that for a wing of any other planform with the same aspect ratio, the two wings that define the ratio for κ_ℓ do not have the same aspect ratio. Figure 5.5.3 shows how κ_ℓ varies with aspect ratio and taper ratio for tapered wings. Since the series solution to Prandtl's lifting-line equation applies to unswept wings with any spanwise variation in section geometry, **the solution can be used for unswept wings of any planform with arbitrary geometric and aerodynamic twist**. From Eqs. (1.8.19) through (1.8.21), it can be shown that wing twist does not affect the change in section lift with respect to wing angle of attack.

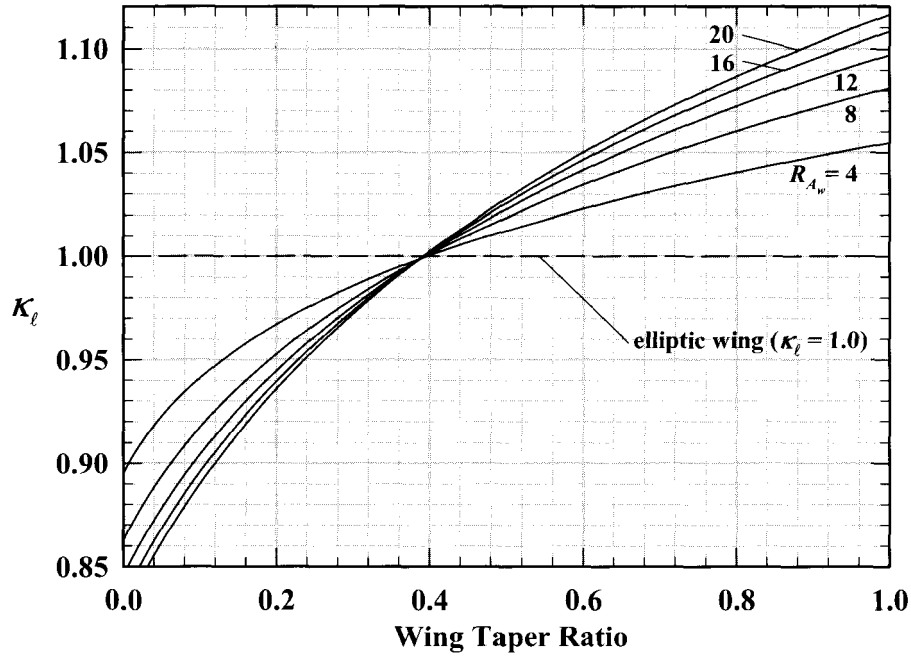


Figure 5.5.3. Dihedral factor for a tapered wing with no geometric or aerodynamic twist.

Strictly speaking, Eqs. (5.5.12) and (5.5.13) apply only at low Mach number to wings with no sweep. However, the contribution of wing dihedral to the roll stability derivative results directly from the lift developed on the wing. Thus, higher subsonic Mach numbers and small sweep angles should affect both lift and wing dihedral contribution to the roll stability derivative in nearly the same proportion. With this line of reasoning, Eqs. (5.5.12) and (5.5.13) could be applied with caution to higher Mach numbers and wings with some sweep, provided that the actual lift slope for the swept wing at the actual flight Mach number is used in Eq. (5.5.12).

One important value in the development that led to Eq. (5.5.12) is the disclosure of the linear relationship between $C_{\ell,\beta}$ and Γ. From Eq. (5.5.6), we see that the linear relation holds for small dihedral angles, regardless of how the in situ section lift slope varies in the spanwise direction. Thus, we should expect the roll stability derivative to change linearly with small dihedral angles for any wing geometry and Mach number.

Effect of Wing Sweep

We now see that wing sweep has an indirect effect on the roll stability derivative, because it affects the lift slope for the wing. This effect is included in our estimate for the contribution of wing dihedral if Eq. (5.5.12) is used. However, wing sweep also has a direct effect on the roll stability derivative, which is not accounted for in Eq. (5.5.12). This direct effect is closely related to the same phenomenon that makes a swept-back wing stabilizing in yaw. This was discussed in Sec. 5.2.

To help the reader better understand the relation between wing sweep and roll stability, we shall again turn to Prandtl's lifting-line theory. In this well-validated model, all of the bound vorticity generated on a lifting wing is represented as a single vortex filament that passes through the aerodynamic centers of the airfoil sections that define the wing (i.e., the wing quarter-chord line for thin airfoil sections in subsonic flow). From the generalized vortex lifting law, for any potential flow containing vortex filaments, a net lift force per unit filament length is exerted by the fluid, which is equal to the fluid density multiplied by the cross product of the local fluid velocity vector and the local circulation vector. Thus, for Prandtl's model of a finite wing, the local lift force per unit length measured along the quarter-chord line is given by

$$\mathbf{f}_L = \rho \mathbf{V} \times \boldsymbol{\Gamma} \tag{5.5.14}$$

where $\mathbf{V}$ and $\boldsymbol{\Gamma}$ are, respectively, the local relative wind vector and the local section circulation vector. **Note that the force per unit length computed from Eq. (5.5.14) is not the section lift, because section lift is defined as the lift force per unit span, not the lift force per unit length along the quarter-chord line.**

The local relative wind is the vector sum of the freestream velocity and the velocity induced by the entire vortex system generated by the wing. The induced velocity is very important in evaluating the induced drag component of the aerodynamic force. However, because the induced velocity is much less than the freestream velocity, for determining the magnitude of lift, the local velocity in Eq. (5.5.14) can be closely approximated with the freestream relative wind.

The magnitude of the cross product of any two vectors is the product of the vector magnitudes multiplied by the sine of the angle from the first vector to the second. With no quarter-chord sweep and no sideslip, the circulation vector aligned with the wing quarter-chord makes an angle of 90 degrees ($\pi/2$ radians) with the relative wind. As can be seen from the geometry in Fig. 5.5.4, positive sweep for a lifting wing decreases this angle on the right semispan and increases it on the left semispan. Positive sideslip, on the other hand, increases this angle on both semispans. Since a distance measured along the quarter-chord line is the spanwise distance divided by the cosine of the quarter-chord sweep angle, from Eq. (5.5.14) and the geometry in Fig. 5.5.4, the magnitudes for section lift on the right and left semispans are, respectively,

$$(\tilde{L})_{\text{right}} \cong \rho V_\infty \Gamma \frac{\sin[(\pi/2) - \Lambda + \beta]}{\cos \Lambda} \tag{5.5.15}$$

and

$$(\tilde{L})_{\text{left}} \cong \rho V_\infty \Gamma \frac{\sin[(\pi/2) + \Lambda + \beta]}{\cos \Lambda} \tag{5.5.16}$$

Once again the reader is cautioned that the symbol Γ is commonly used to represent both circulation and wing dihedral. **In Eqs. (5.5.15) and (5.5.16), Γ denotes wing section circulation, not wing dihedral.**

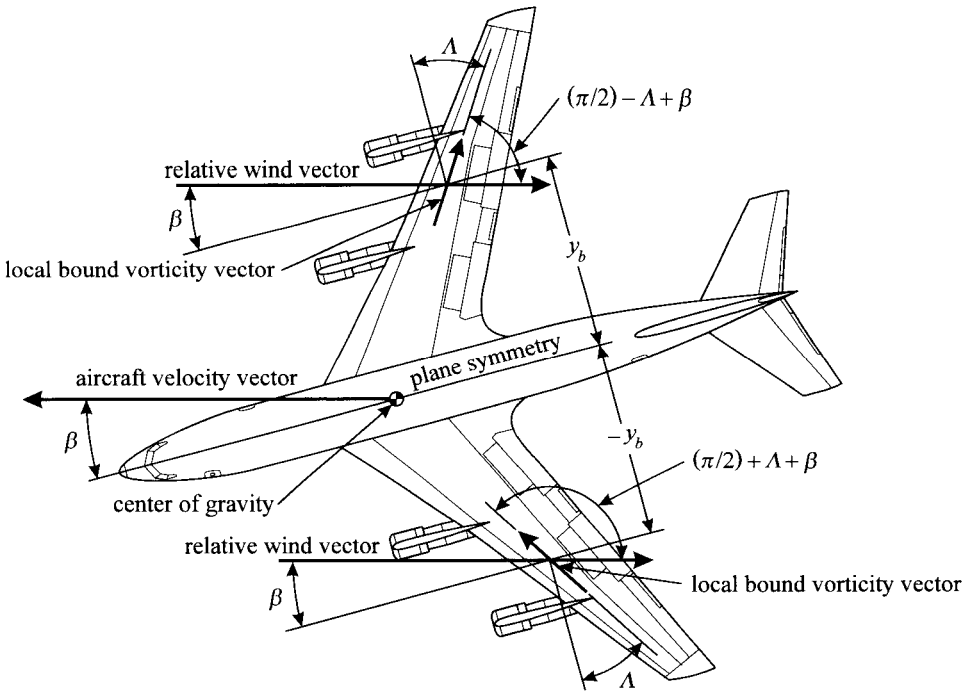


Figure 5.5.4. Effect of wing sweep on the cross product of the relative wind vector with the bound vorticity vector.

Using common trigonometric identities and applying the small-angle approximation for β, it can be shown that

$$\sin[(\pi/2) - \Lambda + \beta] = \cos\Lambda\cos\beta + \sin\Lambda\sin\beta \cong \cos\Lambda + \beta\sin\Lambda \qquad (5.5.17)$$

$$\sin[(\pi/2) + \Lambda + \beta] = \cos\Lambda\cos\beta - \sin\Lambda\sin\beta \cong \cos\Lambda - \beta\sin\Lambda \qquad (5.5.18)$$

From the sign convention shown in Fig. 5.1.1, positive lift on the left semispan ($y_b < 0$) will produce a positive rolling moment, while positive lift on the right semispan ($y_b > 0$) produces a negative rolling moment. Thus the rolling moment arm for section lift is $-y_b$, and after using Eqs. (5.5.17) and (5.5.18) in Eqs. (5.5.15) and (5.5.16), the contribution to the rolling moment that results from wing sweep is

$$(\Delta\ell)_{\Lambda w} = \int_{y_b=-b_w/2}^{0} \rho V_\infty \Gamma(1 - \beta\tan\Lambda)(-y_b)\,dy_b + \int_{y_b=0}^{b_w/2} \rho V_\infty \Gamma(1 + \beta\tan\Lambda)(-y_b)\,dy_b$$

After rearranging and nondimensionalizing this result according to Eq. (5.1.1), the contribution of wing sweep to the rolling moment coefficient is

$$\left(\Delta C_\ell\right)_{\Lambda w} = -\frac{2}{V_\infty S_w b_w}\left[\int_{y_b=-b_w/2}^{b_w/2} \Gamma\, y_b\, dy_b + \beta \tan\Lambda \int_{y_b=-b_w/2}^{b_w/2} \Gamma\, |y_b|\, dy_b\right] \tag{5.5.19}$$

Differentiating Eq. (5.5.19) with respect to β gives

$$\frac{\partial}{\partial\beta}\left(\Delta C_\ell\right)_{\Lambda w}$$

$$= -\frac{2}{V_\infty S_w b_w}\left[\int_{y_b=-b_w/2}^{b_w/2} \frac{\partial\Gamma}{\partial\beta}\, y_b\, dy_b + \tan\Lambda \int_{y_b=-b_w/2}^{b_w/2} \Gamma\, |y_b|\, dy_b + \beta \tan\Lambda \int_{y_b=-b_w/2}^{b_w/2} \frac{\partial\Gamma}{\partial\beta} |y_b|\, dy_b\right]$$

Evaluating this result at $\beta = 0$, the contribution of wing sweep to $C_{\ell,\beta}$ is

$$\left(\Delta C_{\ell,\beta}\right)_{\Lambda w} = -\frac{2}{V_\infty S_w b_w}\left[\int_{y_b=-b_w/2}^{b_w/2} \frac{\partial\Gamma}{\partial\beta}\, y_b\, dy_b + \tan\Lambda \int_{y_b=-b_w/2}^{b_w/2} \Gamma\, |y_b|\, dy_b\right]_{\beta=0} \tag{5.5.20}$$

The wing section circulation, Γ, varies with the spanwise coordinate, y_b, as a result of vorticity shed from the wing, which rolls up to form the wingtip vortices. The variation of Γ with y_b can be determined from the solution to the lifting-line equation. Since no closed-form solution is available for swept wings, a numerical solution must be used and the integration in Eq. (5.5.20) must be carried out numerically. For swept wings, the spanwise variation in Γ changes with angle of attack. Thus, the contribution of wing sweep to the roll stability derivative depends on airspeed.

The sign of the wing sweep contribution to the roll stability derivative is readily ascertained from Eq. (5.5.20). For small sideslip angles, the change in wing section circulation with sideslip angle is small and the second integral in Eq. (5.5.20) dominates the result. For a wing producing positive lift, the circulation is positive, and the bracketed term in Eq. (5.5.20) will have the same sign as $\tan\Lambda$. Thus, **positive sweep (sweep back) is stabilizing in roll and negative sweep (sweep forward) is destabilizing.** This is a direct result of the fact that as an airplane with swept-back wings (positive Λ) yaws to the left (positive β), the vorticity generated on the right wing becomes more perpendicular to the freestream, while that generated on the left wing becomes less perpendicular to the freestream. This change in relative wind, which is shown in Fig. 5.5.4, increases lift on the right, decreases lift on the left, and produces a rolling moment to the left (negative ℓ).

Fuselage Influence

When an airplane experiences sideslip, the cross-flow component of relative wind must flow around the fuselage, as shown in Fig. 5.5.5. This flow field interacts with the wing and can produce a net change in the roll stability derivative. As the airplane slips to the right, the cross-flow above the fuselage center moves up on the right and back down on the left. Below the center of the fuselage, this flow pattern is inverted.

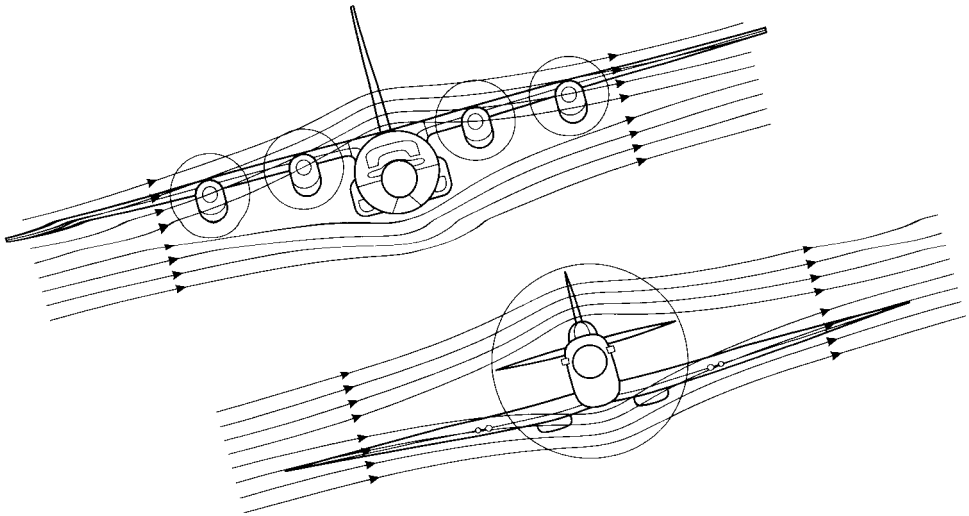


Figure 5.5.5. Effect of the fuselage-wing interaction on the roll stability derivative.

Notice from Fig. 5.5.5 that for a high-wing airplane, the cross-flow around the fuselage creates upwash on the windward semispan and downwash on the lee-side semispan. When the airplane slips to the right, producing a relative wind from right to left (positive β), this increases the angle of attack and lift on the right semispan and decreases the angle of attack and lift on the left, creating a negative and stabilizing contribution to the rolling moment.

For a low-wing airplane, Fig. 5.5.5 shows that flow around the fuselage has the opposite effect on wing lift. When the wing is below the center of the fuselage and the airplane slips to the right, the angle of attack and lift is decreased on the right and increased on the left, as a result of flow around the fuselage. This creates a destabilizing contribution to the rolling moment.

Hence we see that the fuselage contribution to the roll stability derivative of an airplane depends on the vertical position of the wing relative to the fuselage. **A high wing is stabilizing and a low wing is destabilizing.** The interaction between the wing and the fuselage is very complex and depends on the geometry of both the fuselage and the wing. Detailed computer simulations or wind tunnel tests are required to account for this effect accurately. However, **as a very rough initial estimate, a high wing typically has a stabilizing effect equivalent to about 2 to 3 degrees of wing dihedral, and a low wing has a destabilizing effect equivalent to about 3 to 4 degrees of anhedral.** For a mid-wing airplane, the contribution of the fuselage to static roll stability is negligible.

The importance of considering the influence of the fuselage on the roll stability of an airplane becomes very apparent when one examines a variety of airplanes with both high and low wings. The next time that you are near an airport where a large number of general aviation airplanes are tied down, look closely at these airplanes from the front. You will notice that all of the low-wing airplanes have considerably more dihedral than

the high-wing airplanes do. The low wings will typically have 4 degrees of dihedral or more. The high wings, on the other hand, will usually have little or no dihedral. Most of the roll stability for a high-wing airplane is commonly provided by the fuselage-wing interaction. Sometimes a small amount of anhedral is even required in a high wing, to partially counter the stabilizing effect of the fuselage-wing interaction.

Influence of the Tail

As discussed in Sec. 5.2 and shown in Fig.5.2.1, sideslip results in a side force acting on the vertical stabilizer. This side force, applied aft of the CG, generates a stabilizing moment in yaw. When the aerodynamic center of the vertical stabilizer is offset from the axis of roll, as shown in Fig. 5.5.6, this side force can also create a significant rolling moment. When the airplane slips to the right (positive β), the relative wind and side force on the vertical stabilizer are from right to left. If the aerodynamic center of the vertical stabilizer is offset a distance, h_v, above the center of gravity, a negative rolling moment is produced by this side force.

Following a development similar to that used to obtain the yawing moment contribution given by Eq. (5.2.5), the contribution of the vertical tail to the rolling moment coefficient is

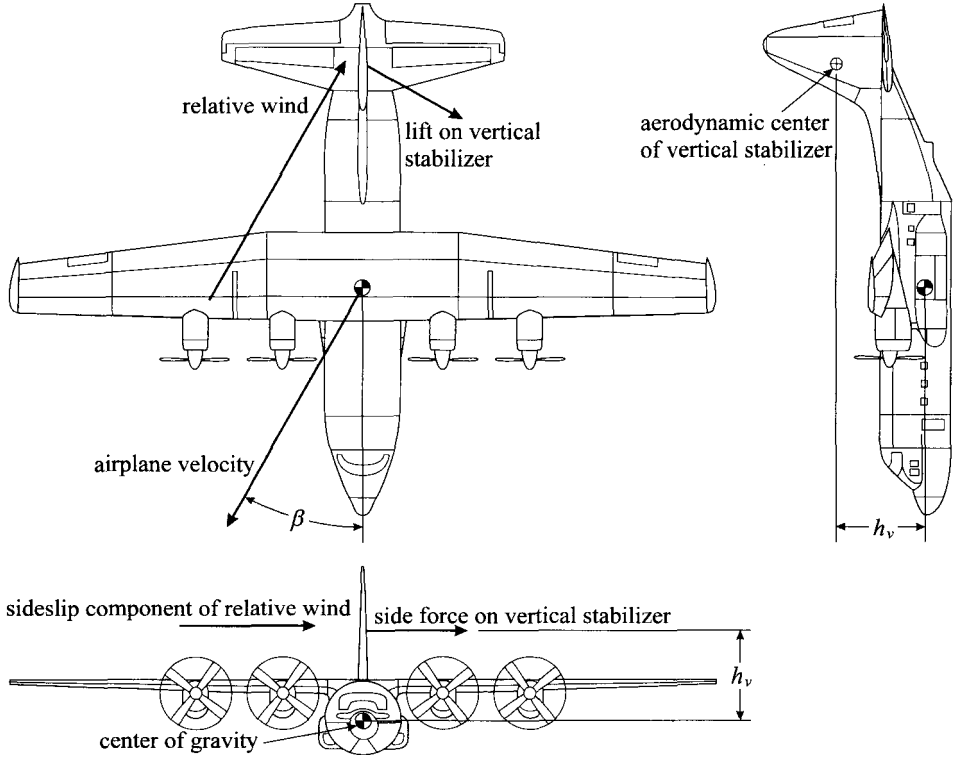


Figure 5.5.6. Effect of the vertical stabilizer on the roll stability derivative.

$$\left(\Delta C_\ell\right)_v = -\eta_v \frac{S_v h_v}{S_w b_w} C_{L_v,\alpha}\left[(1-\varepsilon_{s,\beta})_v \beta - \varepsilon_{s0} - \varepsilon_r \delta_r\right] \tag{5.5.21}$$

and the contribution to the roll stability derivative is

$$\left(\Delta C_{\ell,\beta}\right)_v = -\eta_v \frac{S_v h_v}{S_w b_w}(1-\varepsilon_{s,\beta})_v C_{L_v,\alpha} \tag{5.5.22}$$

From Eq. (5.5.22), we see that when the aerodynamic center of the vertical tail is above the center of gravity ($h_v > 0$), which is typically the case, the vertical tail makes a stabilizing contribution to the roll stability derivative.

Equation (5.5.22) can be used to estimate the direct contribution to the roll stability derivative from lift generated on the vertical tail. However, when lift is generated on the vertical stabilizer, the resulting shed vorticity also produces a rolling moment on the horizontal stabilizer, as shown in Fig 5.4.1. Although the contribution of the horizontal stabilizer to the roll stability derivative has usually been neglected, it can be quite significant. For typical conventional tail geometry, where the horizontal stabilizer is below the vertical stabilizer, the stabilizing contribution that is predicted by Eq. (5.5.22) will be reduced by about 25 to 35 percent as a result of vortex interaction with the horizontal stabilizer. With a T-tail configuration, the horizontal stabilizer mounted above the vertical stabilizer has the opposite effect and will typically increase the roll stability provided by the vertical tail by 25 to 35 percent over that predicted by Eq. (5.5.22). The aerodynamic interaction between the horizontal and vertical stabilizers can be quite accurately determined from a numerical lifting-line solution. As a first approximation for typical tail geometry, a rough estimate for the rolling moment induced on the horizontal stabilizer can be obtained from the relation

$$\left(\Delta C_{\ell,\beta}\right)_h = \pm 0.08\,\eta_v \frac{S_v b_h}{S_w b_w}(1-\varepsilon_{s,\beta})_v C_{L_v,\alpha} \tag{5.5.23}$$

where the positive sign is used when the horizontal stabilizer is mounted below the vertical stabilizer and the negative sign is used for a horizontal stabilizer mounted above the vertical stabilizer. Equation (5.5.23) should be used as a rough estimate only when the exact tail geometry is unknown. A numerical lifting-line solution will give more accurate results if the tail geometry is known.

Effect of Rotating Propellers

As discussed in Sec. 5.2, a rotating propeller can have a significant effect on the trim and static stability of an airplane in yaw. In a similar manner, a propeller will also affect the trim and static stability in roll. One of the largest contributions that a rotating propeller makes to the rolling moment is from the engine torque required to turn the propeller. For a conventional right-hand-turning propeller, the engine must apply a right-hand moment to the propeller. To support this torque, the engine must also exert an equal and opposite moment on the airframe. Thus, a conventional right-hand-turning propeller produces a left-hand rolling moment (negative ℓ).

The rolling moment that results directly from propeller torque is partially countered by the effects of slipstream rotation. The torque applied to the propeller causes the air in the slipstream to rotate in the same direction as the propeller. As shown in Fig. 5.5.7 for a conventional right-hand propeller, slipstream rotation produces sidewash on the vertical stabilizer, downwash on the right semispans of the wing and horizontal stabilizer, and upwash on the left semispans of the wing and horizontal stabilizer. The interactions between the lifting surfaces of the airplane and the rotation of the slipstream produce a rolling moment that is opposite to that produced directly by the propeller (positive ℓ for a right-hand propeller). In some cases, the effects of slipstream rotation will nearly balance the rolling moment produced directly by the propeller. In any case, these moments primarily affect the aircraft trim and have little effect on roll stability.

The axial velocity of the propeller slipstream can also influence the rolling moment acting on an airplane. The slipstream increases the dynamic pressure and lift over the inboard sections of the wing. This does not affect the rolling moment when there is no sideslip. However, as shown in Fig. 5.5.7, sideslip causes the slipstream to impinge on one semispan more than on the other. When the airplane slips to the right (positive β), the slipstream is displaced to the left. This causes the increase in dynamic pressure from the slipstream to affect the left semispan more than the right, which results in more lift produced on the left. The positive increment to the rolling moment produced by this slipstream interaction as a result of positive sideslip is destabilizing. The reduction in roll stability caused by this slipstream effect is appreciably increased with the application of full power at low airspeed, when the ratio of slipstream velocity to forward airspeed is greatest. Flaps and other high-lift devices are normally installed in the inboard sections of the wing where the slipstream influence is high. Thus, slipstream effects are most significant in takeoff and landing configurations with high-lift devices engaged.

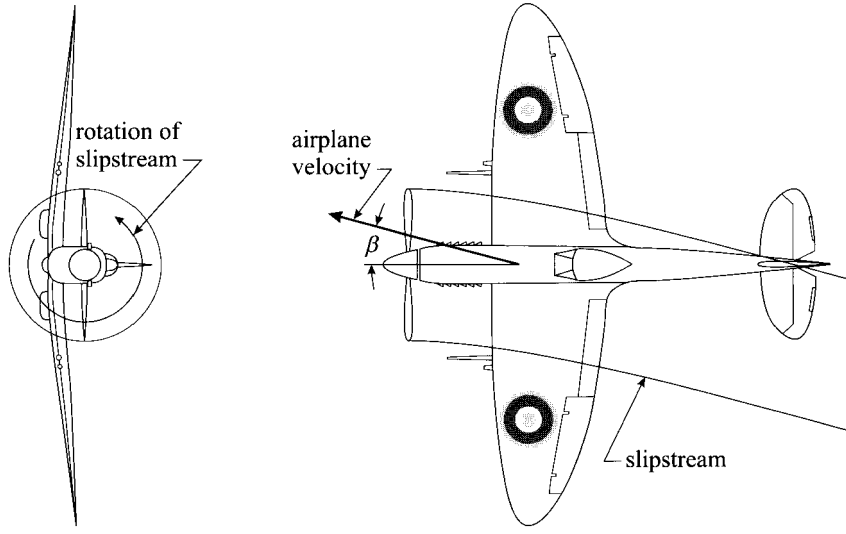


Figure 5.5.7. Effect of the propeller slipstream on an airplane's rolling moment.

The effect of the propeller slipstream on the roll stability derivative is very complex and almost impossible to predict analytically. This effect is usually ignored in the early phases of airplane design.

Summary

We have seen that the roll stability derivative for an airplane is significantly affected by some very complex interactions among the fuselage, wing, vertical stabilizer, horizontal stabilizer, and propulsion system. Furthermore, some of these effects vary with angle of attack as well as flap and power settings. As a result, analytical calculations for the roll stability derivative are not accurate and should be used only as an indication of the expected magnitude of $C_{\ell,\beta}$.

Fortunately, the roll stability derivative is easily adjusted in the later phases of the airplane design process by making small changes to the wing dihedral. The dihedral angle of the wing has such a profound effect on the roll stability derivative that this aerodynamic derivative and its various components are commonly referred to as the *dihedral effect*. For example, the fuselage-wing interaction shown in Fig. 5.5.5 is usually called the *fuselage dihedral effect*.

It is also fortunate that small changes in wing dihedral do not typically have a large effect on other aerodynamic derivatives that also affect the aircraft handling qualities. In a tailless airplane, the roll and yaw stability derivatives are primarily controlled with wing dihedral and sweep. Dihedral has the greatest effect on roll stability, and sweep has the greatest effect on yaw stability. However, the effects of sweep and dihedral are coupled and some iteration is usually required with a tailless aircraft to bring the roll and yaw stability derivatives to the desired magnitude. For an airplane with a conventional aft tail, the roll and yaw stability derivatives are not so closely coupled and a single adjustment of the wing dihedral, after wind tunnel and/or flight tests will usually be sufficient.

EXAMPLE 5.5.1. The airplane described in Examples 5.2.1 and 5.2.2 has a high wing of rectangular planform with no sweep. The tail is of the conventional design, with the horizontal stabilizer mounted below the vertical stabilizer, and the aerodynamic center of the vertical stabilizer is 3.0 ft above the CG. For this airplane in cruise configuration, estimate the wing dihedral required to provide a roll stability derivative of about –0.05.

Solution. For this airplane we have

$$S_w = 180\ \text{ft}^2, \quad b_w = 33\ \text{ft}, \quad C_{L_w,\alpha} = 4.44, \quad R_{A_w} = 6.05, \quad R_{T_w} = 1.0,$$
$$S_v = 11.9\ \text{ft}^2, \quad C_{L_v,\alpha} = 3.40, \quad \eta_v = 1.0, \quad (\varepsilon_{s,\beta})_v = -0.10, \quad h_v = 3.0\ \text{ft},$$
$$S_h = 36\ \text{ft}^2, \quad C_{L_h,\alpha} = 3.97, \quad b_h = 12\ \text{ft}, \quad \eta_h = 1.0, \quad (\varepsilon_{d,\alpha})_h = 0.44$$

From Fig. 5.5.3, for an aspect ratio of about 6.0 and a taper ratio of 1.0, the dihedral factor for the wing is approximately $\kappa_\ell \cong 1.07$, and from Eq. (5.5.12) the wing dihedral effect is given by

$$\left(\Delta C_{\ell,\beta}\right)_{\Gamma w} = -\frac{2\kappa_\ell C_{L_w,\alpha}}{3\pi}\Gamma = -\frac{2(1.07)4.44}{3\pi}\Gamma = -1.01\Gamma$$

where Γ is the dihedral angle in radians. Since this is a high-wing airplane and no other information is available, we shall estimate the fuselage dihedral effect as being equivalent to about +2.5 degrees of wing dihedral,

$$\left(\Delta C_{\ell,\beta}\right)_f = -1.01\,\Gamma = -1.01\left(2.5\frac{\pi}{180}\right) = -0.044$$

From Eq. (5.5.22), the dihedral effect of the vertical stabilizer is

$$\left(\Delta C_{\ell,\beta}\right)_v = -\eta_v \frac{S_v h_v}{S_w b_w}(1-\varepsilon_{s,\beta})_v C_{L_v,\alpha} = -1.0\frac{11.9(3.0)}{180(33)}(1+0.10)3.40$$
$$= -0.022$$

Because this airplane has a conventional tail with the horizontal stabilizer below the vertical stabilizer, the vortex interaction between the lifting surfaces of the tail will produce a destabilizing rolling moment on the horizontal stabilizer. Since the exact geometry of the tail is unknown, we will assume typical conventional tail geometry and apply Eq. (5.5.23),

$$\left(\Delta C_{\ell,\beta}\right)_h = +0.08\eta_v \frac{S_v b_h}{S_w b_w}(1-\varepsilon_{s,\beta})_v C_{L_v,\alpha}$$
$$= +0.08(1.0)\frac{11.9(12.0)}{180(33)}(1+0.10)3.40 = +0.007$$

Because the airplane is in cruise configuration, the effect of power on the roll stability derivative is probably small. Since no other information is available, we will ignore the propeller slipstream effects.

The net roll stability derivative can now be estimated as

$$C_{\ell,\beta} = \left(\Delta C_{\ell,\beta}\right)_{\Gamma w} + \left(\Delta C_{\ell,\beta}\right)_f + \left(\Delta C_{\ell,\beta}\right)_v + \left(\Delta C_{\ell,\beta}\right)_h$$
$$= -1.01\,\Gamma - 0.044 - 0.022 + 0.007 = -0.05$$

Solving this relation for the wing dihedral gives

$$\Gamma = \frac{0.05 - 0.044 - 0.022 + 0.007}{1.01} = -0.009 = \underline{-0.5^\circ}$$

Thus, the tail and the aerodynamic interaction between the fuselage and the wing provide all of the desired dihedral effect. These approximate calculations predict that about ½ degree of wing anhedral is needed.

5.6. Roll Control and Trim Requirements

It is possible to design an airplane that can be flown with only elevator and rudder controls. However, the handling qualities of such an airplane are severely compromised at best. In order to obtain good handling qualities and to trim the airplane in roll over a range of operating conditions, it is necessary to provide the pilot with some means of controlling the aircraft's rolling moment. This is typically accomplished with *ailerons*, which are small trailing-edge flaps located in the outboard sections of the wing. The ailerons are deflected asymmetrically to change the rolling moment. One aileron is deflected downward and the other is deflected upward, as shown in Fig. 5.6.1. This increases lift on the semispan with the downward-deflected aileron and decreases lift on the semispan with the upward-deflected aileron.

The sign convention that is most commonly used for aileron deflection is shown in Fig. 5.6.1. The aileron deflection is assumed positive when the right aileron is deflected downward and the left aileron is deflected upward. With this sign convention, a positive aileron deflection produces a rolling moment to the left (negative ℓ). The two ailerons are not necessarily deflected the same. To help prevent tip stall, the downward-deflected aileron is sometimes deflected less than the upward-deflected aileron. The aileron angle, δ_a, is defined to be the average of the two angular deflections,

$$\delta_a = \frac{(\delta_a)_{\text{right}} + (\delta_a)_{\text{left}}}{2} \tag{5.6.1}$$

At first thought, it may seem quite simple to predict the rolling moment produced by a known deflection of the ailerons from our knowledge of section flap effectiveness. The change in section lift coefficient that results from deflection of a trailing-edge flap was presented in Sec. 1.7 and can be expressed for the ailerons as

$$\left(\Delta \widetilde{C}_{L_w}\right)_{\delta_a} = \pm \widetilde{C}_{L_w,\alpha}\, \widetilde{\varepsilon}_a\, \delta_a \tag{5.6.2}$$

where $\widetilde{\varepsilon}_a$ is the local section flap effectiveness and the positive sign corresponds to the right aileron while the negative sign applies to the left.

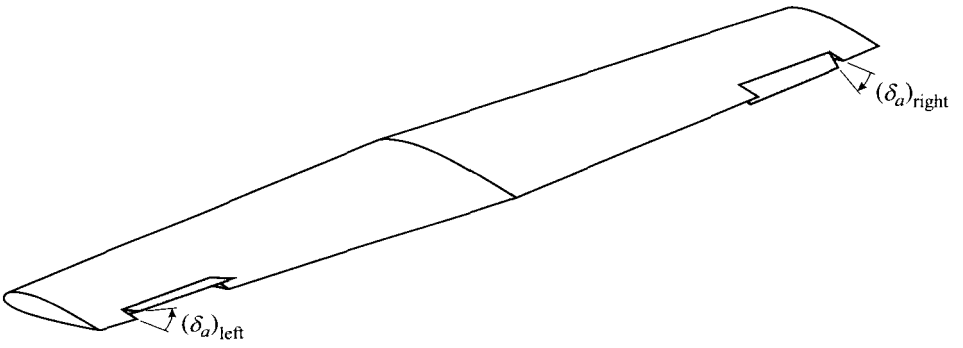


Figure 5.6.1. Ailerons are typically used to control an airplane's rolling moment.

A very simple method that is often recommended for estimating the rolling moment produced by the ailerons is called *strip theory*. This amounts to multiplying the local section lift increment by the local rolling moment arm and integrating over the wing sections containing the ailerons. From Eq. (5.6.2) and the geometry shown in Fig. 5.6.2, the result is

$$(\Delta\ell)_{\delta_a} = \tfrac{1}{2}\rho V_\infty^2 \left[(\delta_a)_{\text{right}} \int_{y_i}^{y_o} (-y_b)\widetilde{C}_{L_w,\alpha}\,\widetilde{\varepsilon}_a\, c_w\, dy_b - (\delta_a)_{\text{left}} \int_{-y_o}^{-y_i} (-y_b)\widetilde{C}_{L_w,\alpha}\,\widetilde{\varepsilon}_a\, c_w\, dy_b \right]$$

After nondimensionalizing and differentiating with respect to the aileron angle, for a symmetric wing with constant section lift slope we have

$$C_{\ell,\delta_a} \equiv \frac{\partial C_\ell}{\partial \delta_a} = \frac{(\Delta\ell)_{\delta_a}}{\tfrac{1}{2}\rho V_\infty^2 S_w b_w \delta_a} = -\frac{(\delta_a)_{\text{right}} + (\delta_a)_{\text{left}}}{S_w b_w \delta_a}\widetilde{C}_{L_w,\alpha} \int_{y_i}^{y_o} y_b\,\widetilde{\varepsilon}_a\, c_w\, dy_b$$

or in view of Eq. (5.6.1),

$$C_{\ell,\delta_a} = -\frac{2\widetilde{C}_{L_w,\alpha}}{S_w b_w} \int_{y_i}^{y_o} y_b\,\widetilde{\varepsilon}_a\, c_w\, dy_b \tag{5.6.3}$$

The variation in local section flap effectiveness with the spanwise coordinate, y_b, depends on the local ratio of flap chord to wing chord. Thus, the integrand in Eq. (5.6.3) is a function of wing and aileron planforms and the integration is easily carried out. Unfortunately, **the physical model of aileron performance on which Eq. (5.6.3) is based has little correspondence with reality**. This model totally ignores the change in vorticity that must accompany any change in lift. As shown in Fig. 5.6.2, the model assumes that the only change in lift produced by a deflection of the ailerons occurs over those wing sections that include the ailerons. This is not realistic. **Equation (5.6.3) gives only a very rough estimate of aileron performance.** However, it has been recommended in the literature and the student should be aware of its shortcomings.

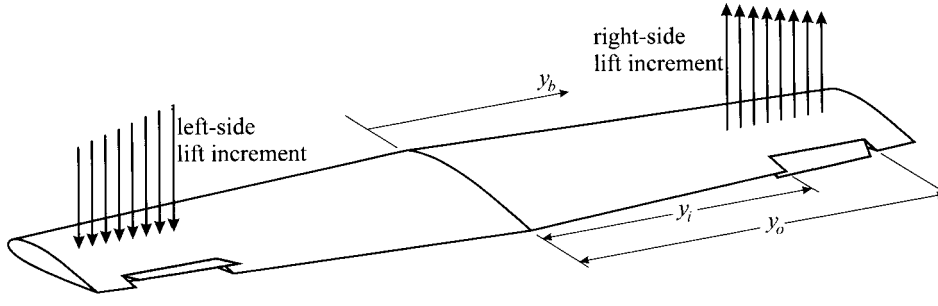


Figure 5.6.2. Lift increment resulting from aileron deflection, as predicted by strip theory.

A more realistic lift distribution is predicted by lifting-line theory. For unswept wings, the series solution presented in Sec. 1.8 can be used to obtain the rolling moment produced directly on the wing by aileron deflection. In general, this can be used as an initial estimate. However, the change in vorticity that results from aileron deflection also produces a significant rolling moment on the tail. To account for the vortex interaction between the wing and the tail, the lifting-line equation can be solved numerically. Results of a numerical lifting-line solution for a particular wing and tail combination are shown in Fig. 5.6.3. In this figure, the vectors displayed along the quarter-chord lines show the magnitude and direction of the local section lift increment, and the lines along the trailing edges indicate the magnitude of the increment in local shed vorticity.

From Fig. 5.6.3, we see that a deflection of the ailerons changes the lift distribution on the entire airplane, not just on those wing sections that contain the ailerons. The changes in lift brought about by the aileron deflection produce a change in the wing vorticity distribution, which in turn modifies the lift distribution on all lifting surfaces. Lift is increased on the entire wing semispan with the downward-deflected aileron and decreased on the entire wing semispan with the upward-deflected aileron. In addition, changes in vorticity shed from the wing modify the distribution of aerodynamic forces acting on the tail. Most notably, a deflection of the ailerons creates sidewash on the vertical stabilizer, which gives rise to a rolling moment that opposes that produced directly by the ailerons.

In addition to producing a rolling moment, aileron deflection gives rise to a change in vorticity that modifies wing downwash and the associated induced drag. The induced drag is increased on the semispan with the downward deflected aileron and decreased on the semispan with the upward-deflected aileron. This produces a yawing moment in the

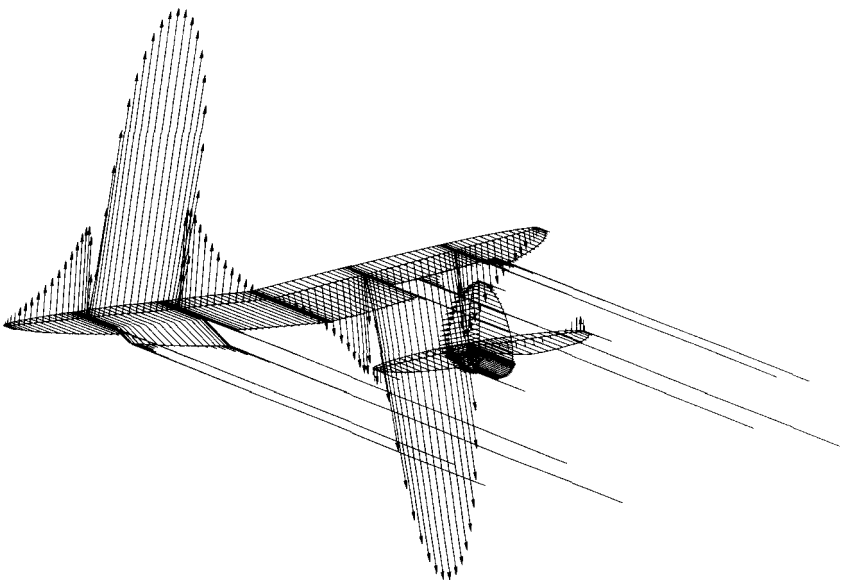


Figure 5.6.3. Lift increment resulting from aileron deflection, as predicted by lifting-line theory.

direction of the downward deflected aileron. For positive aileron deflection (right aileron down), the rolling moment is to the left (negative ℓ), whereas the yawing moment is to the right (positive n). Because the primary reason for applying positive aileron deflection is to initiate a roll to the left, we see that the yawing moment produced by aileron deflection is in the wrong direction. Accordingly, this aileron-induced yawing moment is commonly called *adverse yaw*. In airplanes having wings with very high aspect ratio, aileron adverse yaw can cause significant lateral control problems. Some potential solutions to this problem are discussed in Chapter 6, which treats aircraft controls and maneuverability in greater detail.

Rudder deflection will also generate a moment about the roll axis of most airplanes. The rolling moment contributed directly by the lift developed on the vertical stabilizer can be estimated using Eq. (5.5.21). Differentiating this result with respect to rudder deflection gives

$$\left(\Delta C_{\ell,\delta_r}\right)_v = \eta_v \frac{S_v h_v}{S_w b_w} \varepsilon_r C_{L_v,\alpha} \tag{5.6.4}$$

As discussed previously, the vorticity associated with lift developed on the vertical stabilizer will modify the distribution of lift developed on the horizontal stabilizer as shown in Fig. 5.4.1. The aerodynamic interaction between the horizontal and vertical stabilizers produces a rolling moment, which occurs whether the lift on the vertical stabilizer is the result of sideslip or rudder deflection. For typical tail geometry, the rolling moment predicted by Eq. (5.6.4) will change by 25 to 35 percent as a result of vortex interactions with the horizontal stabilizer. For typical tail geometry, a rough estimate for the rolling moment induced on the horizontal stabilizer as a result of rudder deflection can be obtained from

$$\left(\Delta C_{\ell,\delta_r}\right)_h = \pm 0.08 \eta_v \frac{S_v b_h}{S_w b_w} \varepsilon_r C_{L_v,\alpha} \tag{5.6.5}$$

where **the negative sign is used when the horizontal stabilizer is mounted below the vertical stabilizer, and the positive sign is used for a horizontal stabilizer mounted above the vertical stabilizer.** Equation (5.6.5) should only be used as a rough estimate when the exact tail geometry is unknown. Here again, a numerical lifting-line solution for the specific tail geometry being used will give a more realistic result.

Four lateral control derivatives, C_{ℓ,δ_a}, C_{n,δ_a}, C_{ℓ,δ_r}, and C_{n,δ_r}, have been discussed. While the ailerons are intended to provide the pilot with roll control and the rudder is meant for yaw control, very seldom are these two controls uncoupled. Aileron deflection usually produces a yawing moment, and rudder deflection will typically generate a rolling moment. This means that trim requirements for roll and yaw are coupled as well. For example, as discussed in Sec. 5.2, a conventional right-hand-turning propeller produces a yawing moment to the left, at positive angles of attack. A right-hand propeller also produces a rolling moment to the left. To trim the airplane against the propeller-induced yawing moment, some right rudder is required. For a conventional high tail, right rudder generates a rolling moment to the left, which adds to that produced

by the propeller. Right aileron is needed to compensate for the rolling moment that results from propeller rotation and rudder deflection. However, the adverse yaw associated with right aileron deflection also adds to the right rudder needed to trim the airplane. These lateral trim requirements are best illustrated by example.

EXAMPLE 5.6.1. The P-38 Lightning shown in Fig. 5.3.5 is powered by two 1,425-horsepower Allison V-1710 engines turning 138-inch, three-blade, counter-rotating Curtiss Electric propellers with 2:1 gear reduction. The propeller on the pilot's right has right-hand rotation, and the propeller on the left has left-hand rotation. Each propeller axis is offset from the plane of symmetry by 8 feet and is aligned with the direction of flight at the maximum airspeed of 400 mph at sea level. With the left engine disabled and the prop feathered, the airplane is flying with an airspeed of 240 mph at 25,000 feet. We wish to estimate the rudder and aileron deflection required to trim the airplane for straight and level flight with no sideslip. Use the following for this airplane and operating condition:

$$S_w = 327.5\ \text{ft}^2,\quad b_w = 52\ \text{ft},\quad C_{L,\alpha} = 5.01,\quad V_\infty = 352\ \text{ft/sec},\quad W = 15{,}480\ \text{lbf},$$
$$d_p = 138/12\ \text{ft},\quad h_p = 0.0\ \text{ft},\quad (\omega/2\pi)_p = 1{,}350\ \text{rpm},$$
$$(\varepsilon_{d,\alpha})_p = -0.175,\quad C_{n_p,\alpha} = -0.046,\quad C_D = 0.0466,$$
$$C_{\ell,\delta_a} = -0.131,\quad C_{n,\delta_a} = 0.013,\quad C_{\ell,\delta_r} = 0.006,\quad C_{n,\delta_r} = -0.052$$

Solution. For this estimate we shall neglect compressibility and the effects of slipstream rotation. We will also assume a typical propulsive efficiency for the propeller of 80 percent and will ignore any yawing moment produced by the added drag of the feathered propeller on the left.

The lift coefficient at the maximum airspeed at sea level is

$$(C_L)_{400} = \frac{W}{\frac{1}{2}\rho V_\infty^2 S_w} = \frac{15{,}480}{\frac{1}{2}0.0023769(400\times 5{,}280/3{,}600)^2 327.5} = 0.116$$

and at the actual operating condition, we have

$$(C_L)_{240} = \frac{W}{\frac{1}{2}\rho V_\infty^2 S_w} = \frac{15{,}480}{\frac{1}{2}0.0010663(352)^2 327.5} = 0.716$$

Since the propeller is aligned with the flight direction for 400 mph at sea level, for 240 mph at 25,000 feet the angle between the propeller and the flight velocity is

$$\alpha_{0_p} = \frac{(C_L)_{240} - (C_L)_{400}}{C_{L,\alpha}} = \frac{0.716 - 0.116}{5.01} = 0.1198 = 6.86^\circ$$

The downwash angle in the plane of the propeller is the angle of attack relative to the zero-lift line multiplied by the downwash gradient,

$$\varepsilon_{d0p} = \frac{(C_L)_{240}}{C_{L,\alpha}}(\varepsilon_{d,\alpha})_p = \frac{0.716}{5.01}(-0.175) = -0.0250 = -1.43°$$

The propeller yawing moment is then

$$\begin{aligned} n_p &= \rho(\omega/2\pi)^2 d_p^5 C_{n_p,\alpha}(\alpha_{0p} - \varepsilon_{d0p}) \\ &= 0.0010663(1{,}350/60)^2(138/12)^5(-0.046)[0.1198 - (-0.0250)] \\ &= -723 \text{ ft·lbf} \end{aligned}$$

For steady level flight the thrust is nearly equal to the drag,

$$T = D = \tfrac{1}{2}\rho V_\infty^2 S_w C_D = \tfrac{1}{2}0.0010663(352)^2 327.5(0.0466) = 1{,}008 \text{ lbf}$$

With the left engine disabled, the thrust vector is offset 8 feet to the right of center. Thus, the total contribution that the propeller makes to the airplane yawing moment coefficient is

$$(\Delta C_n)_p = \frac{n_p - y_{bp}T}{\frac{1}{2}\rho V_\infty^2 S_w b_w} = \frac{-723 - 8.0(1{,}008)}{\frac{1}{2}0.0010663(352)^2 327.5(52)} = -0.00781$$

The rolling moment contributed by the right-hand propeller can be estimated from the thrust and airspeed combined with the assumed propulsive efficiency,

$$\ell_p = -\frac{P_b}{\omega_p} = -\frac{(TV_\infty/\eta_p)}{\omega_p} = -\frac{1{,}008(352)/0.80}{2\pi(1{,}350/60)} = -3{,}137 \text{ ft·lbf}$$

This gives the propeller contribution to the airplane rolling moment coefficient,

$$(\Delta C_\ell)_p = \frac{\ell_p}{\frac{1}{2}\rho V_\infty^2 S_w b_w} = \frac{-3{,}137}{\frac{1}{2}0.0010663(352)^2 327.5(52)} = -0.00279$$

To maintain straight and level flight with no sideslip, the moments produced by the propeller must be balanced with rudder and aileron deflection. Since the total rolling and yawing moments must be zero, this requires that

$$\begin{bmatrix} C_{\ell,\delta_a} & C_{\ell,\delta_r} \\ C_{n,\delta_a} & C_{n,\delta_r} \end{bmatrix} \begin{Bmatrix} \delta_a \\ \delta_r \end{Bmatrix} = \begin{Bmatrix} -(\Delta C_\ell)_p \\ -(\Delta C_n)_p \end{Bmatrix}$$

or

$$\begin{bmatrix} -0.131 & 0.006 \\ 0.013 & -0.052 \end{bmatrix} \begin{Bmatrix} \delta_a \\ \delta_r \end{Bmatrix} = \begin{Bmatrix} 0.00279 \\ 0.00781 \end{Bmatrix}$$

This gives

$$\begin{Bmatrix}\delta_a\\ \delta_r\end{Bmatrix} = \begin{Bmatrix}-0.0285\\ -0.1573\end{Bmatrix} = \underline{\begin{Bmatrix}-1.6^\circ\\ -9.0^\circ\end{Bmatrix}}$$

which means that in the absence of slipstream effects, about 9 degrees of right rudder and less than 2 degrees of right aileron are required to trim the airplane for this engine-out flight condition. Slipstream rotation could significantly increase the required rudder deflection while decreasing the required aileron deflection. At lower airspeeds these slipstream effects and the required rudder deflection would be larger.

Since actual wind tunnel data for the P-38 Lightning were not available to the author, the aerodynamic derivatives used in Example 5.6.1 are only approximate and the predicted result is probably not accurate. However, the example does demonstrate what is usually the critical constraint on rudder size for multiengine airplanes. That is the need to provide the yawing moment necessary to trim the airplane for the most critical allowable engine-out flight configuration. The reader will also notice that while some aileron deflection is required for trim, this is quite small. Static trim requirements are not a significant consideration in sizing the ailerons of a conventional airplane. When the ailerons are sized on the basis of dynamic considerations, which will be discussed later, they will be capable of providing any rolling moments needed for static trim.

5.7. Longitudinal-Lateral Coupling

In this chapter and Chapter 4, considerations of aircraft static stability and trim were divided into two distinct categories, those associated with longitudinal motion and those associated with lateral motion. To reiterate, longitudinal motion involves only three degrees of freedom, axial and normal translation in the aircraft plane of symmetry, and rotation in pitch. Lateral motion comprises the remaining three degrees of freedom, sideslip translation combined with rotation in roll and yaw.

The study of most topics within the field of flight mechanics has traditionally been divided along these lines. Longitudinal and lateral motion are usually considered separately and longitudinal-lateral coupling is commonly ignored. In a great many cases, the coupling between the longitudinal and lateral degrees of freedom is very small, and neglecting this coupling is well justified. However, the designer should never lose sight of the fact that longitudinal-lateral coupling can sometimes be very important.

In this chapter we have observed one form of longitudinal-lateral coupling. A rotating propeller produces a yawing moment that varies with angle of attack. This means that lateral trim requirements in yaw can depend on longitudinal trim requirements in pitch. This is only one of many forms of longitudinal-lateral coupling that will be considered as we continue with our study of flight mechanics.

Some forms of longitudinal-lateral coupling were completely unknown prior to the development of high-powered aircraft during and following World War II. On December 10, 1944, a German prototype He-162 jet fighter broke up during a high-speed roll.

Later, a similar incident with the British Fairey Delta aircraft resulted in complete control loss but no severe damage to the aircraft. Despite the fact that both incidents were well documented, the aircraft behavior could not be explained on the basis of flight mechanics knowledge available at that time. In both cases, a form of longitudinal-lateral coupling that was not considered in the aircraft design process was at fault.

In the following chapters we continue to divide our study of flight mechanics along the traditional lines of longitudinal and lateral motion. To begin with, we neglect longitudinal-lateral coupling. This will simplify the initial presentation of fundamental principals and should help the student to grasp the underlying concepts more easily. However, **this approach should not be taken as an indication that longitudinal-lateral coupling is never important.**

Most pilots who have flown an airplane with the tendency to yaw to the left at low airspeeds and high angles of attack are aware of at least some aspects of longitudinal-lateral coupling. On the other hand, the effects of longitudinal-lateral coupling have often been neglected by the designer, sometimes at great cost.

5.8. Control Surface Sign Conventions

A few closing words on sign convention may be in order. The sign convention for aerodynamic angles and moments that is used in this textbook and shown in Fig. 5.1.1 is widely used. If this sign convention is not absolutely universal, it is very close to being so. The same cannot be said for the control surface sign convention used here.

The sign convention that is used in this textbook is based on the right-hand rule for control surface rotations. The elevator sign convention is shown in Fig. 4.3.3, that for the rudder is shown in Fig. 5.2.1, and that for the ailerons is shown in Fig. 5.6.1. Downward deflection of the elevator is assumed positive, deflection of the rudder to the left is assumed positive, and aileron deflection is assumed positive when the right aileron is deflected down and the left aileron is deflected up. When this particular control surface sign convention is combined with the moment sign convention shown in Fig. 5.1.1, the three primary control derivatives (C_{ℓ,δ_a}, C_{m,δ_e}, and C_{n,δ_r}) are all negative. **While the control surface sign convention presented here is probably the most widely used, it is by no means universal.**

A sign convention opposite to that presented in this text is sometimes used for control surface deflections. The argument for using this alternative sign convention is specifically to make the three primary control derivatives positive. For example, since the ailerons are intended to create a rolling moment, it is argued that positive aileron deflection should produce a positive rolling moment. Similar arguments are made for the elevator and rudder. While this argument makes sense, sign conventions are clearly arbitrary and often dictated more by history than by logic.

Any aeronautical engineer will almost assuredly encounter the use of different control surface sign conventions. The author has actually seen different control surface sign conventions used for two different airplanes within the same textbook. With only a little thought, the student should not find this inconsistency too confusing. By simply examining the signs of the primary control derivatives, it is easy to tell what sign convention has been used.

Because there is no universally accepted control surface sign convention, control surface deflections are commonly described as being right or left and up or down. Right aileron is always understood to mean an aileron deflection that will tend to bank the airplane into a right turn. Left aileron will bank the airplane to the left. Similarly, right rudder is always understood to be a rudder deflection that tends to yaw the airplane's nose to the right, and left rudder will yaw the nose to the left. Up elevator will pitch the nose up, and down elevator will pitch the nose down. If you wish to avoid any possibility of confusion, this terminology can be used.

5.9. Problems

5.1. The airplane described in Example 5.2.1 is to be modified to increase the yaw stability derivative to 0.10. As much as possible we would like to leave the other characteristics of the airplane unchanged. What would you suggest as the least expensive design change that would produce the desired result? Your suggestion should be quantitative.

5.2 The vertical stabilizer of the airplane in problem 4.2 is to be sized to give a contribution to the yaw stability derivative of 0.10. Suggest a preliminary design and size for the vertical stabilizer. Use the aircraft dimensions and operating conditions specified in problem 4.1 and clearly state all assumptions.

5.3 During its useful life the British Spitfire underwent many design changes. The first Mark I was powered by a 1,030-horsepower Merlin II engine. Later, a 2,375-horsepower Griffon 67 engine powered the Mark XVIII. Along the way, several changes in the tail were made to accommodate this growth in power. For the Mark XVIII shown in Figs. 4.11.1 and 4.11.2, estimate the vertical tail volume ratio that would be required to give the airplane a yaw stability derivative of 0.10. Use the data given in problems 4.8, 4.10, and 4.11. Assume a lift slope for the vertical stabilizer of 3.50 and clearly state all other assumptions.

5.4 The 2,375-horsepower Griffon engine that powers the Spitfire Mark XVIII turns the 132-inch, five-blade, constant-speed Rotol propeller shown in Fig. 5.9.1. At full power, the propeller turns 1,400 rpm. While taxiing with the tail wheel on the ground, the propeller angle of attack is 11 degrees relative to the freestream. Assume that the pilot uses full power for a takeoff run and raises the tail at an airspeed of 55 mph. At this operating condition, the **magnitude** for the change in the propeller yawing moment coefficient with respect to propeller angle of attack is 0.0785. Estimate the rudder deflection required to trim the airplane for no sideslip at the instant that the tail wheel leaves the ground. Use the data given in problems 4.8, 4.10, and 4.11; neglect the slipstream effects; and assume the following properties for the vertical tail:

$$S_v = 21\,\text{ft}^2, \quad C_{L_v,\alpha} = 3.50, \quad l_v = 18.16\,\text{ft}, \quad \eta_v = 1.0, \quad (\varepsilon_{s,\beta})_v = 0.0,$$
$$\bar{c}_v = 3.8\,\text{ft}, \quad \varepsilon_r = 0.60, \quad C_{m_v,\delta_r} = -0.58$$



Figure 5.9.1. The five-blade, 132-inch, constant-speed Rotol propeller on the Spitfire Mark XVIII. (Photograph by Barry Santana)

Based on the photograph shown in Fig. 5.9.1, is right rudder or left rudder required? Explain how you arrived at your conclusion. Do you expect your estimate for rudder deflection to be low or high? What conclusions can you draw from the result predicted?

5.5 For the wing of the Spitfire Mark XVIII described in problem 4.8, use the method presented in Sec. 5.3 to estimate the sidewash gradient in the aircraft plane of symmetry, 3.0 feet above the plane of the wingtip vortices, and 18.0 feet aft of the wing quarter-chord.

5.6 Repeat the calculations in problem 5.5 for an unswept rectangular wing of the same span and planform area. Explain any difference that you observe.

5.7 One way to increase the yaw stability of an airplane is to lengthen the tail boom. In addition to increasing the moment arm for the vertical stabilizer, this also changes the sidewash gradient. Repeat the calculations in problem 5.5 for an increase of 25 percent in the distance aft of the wing quarter-chord. Explain how this would affect the trade-off between tail boom length and vertical stabilizer area. How would this trade-off change for a rectangular wing? How would this trade-off change if the height of the vertical stabilizer were increased?

5.8 Airplanes are sometimes designed with twin vertical stabilizers symmetrically offset from the midspan, as shown in Fig 5.3.5. The sidewash gradient for such a design is significantly different from that of a single vertical stabilizer placed directly aft of the wing midspan. Repeat the calculations in problem 5.5 for a spanwise position that is 30 percent of the distance between the midspan and the wingtip. How does this affect the total vertical stabilizer area needed to stabilize the airplane, all else being equal?

5.9 Repeat the calculations in problem 5.5 for the case where the wingspan is reduced by 25 percent while the wing area and all other parameters remain unchanged. How would this affect the yaw stability of the airplane if the vertical stabilizer area and tail boom length were unchanged?

5.10 Consider a conventional tail with the horizontal stabilizer below the vertical stabilizer. Both stabilizers are unswept, rectangular, and have the same chord. The horizontal and vertical stabilizers have aspect ratios of 4.0 and 2.0, respectively. Using Fig. 5.4.2, estimate the lift slope for the vertical stabilizer.

5.11 Use a numerical lifting-line solution to estimate the lift slope for the vertical stabilizer in problem 5.10, with and without the horizontal stabilizer present.

5.12 The conventional aft tail described in problem 5.10 is modified to include taper, sweep, and dihedral. The taper ratio for both stabilizers is changed to 0.50. The quarter-chord sweep is changed so that the trailing edges remain unswept. The horizontal stabilizer is given 3.0 degrees of dihedral. The aspect ratio and planform area of each stabilizer remains unchanged. Use a numerical lifting-line solution to estimate the lift slope for the vertical stabilizer, with and without the horizontal stabilizer present.

5.13 Using Eq. (5.3.7) to approximate the sidewash gradient, estimate the total yaw stability derivative for the Spitfire Mark XVIII shown in Fig. 4.11.1 and described in problems 4.8, 4.10, and 4.11. Assume an airspeed of 200 mph at standard sea level, include the effects of the fuselage and propeller, and use the following properties for the vertical stabilizer:

$$S_v = 21\,\text{ft}^2, \quad \bar{c}_v = 3.8\,\text{ft}, \quad C_{L_v,\alpha} = 3.50, \quad l_v = 18.16\,\text{ft}, \quad h_v = 3.0\,\text{ft}, \quad \eta_v = 1.0$$

5.14 As a first approximation for the contribution of a swept wing to the yaw stability derivative of an airplane, we can assume that the wing section drag coefficient is constant. Using this assumption in Eq. (5.2.32), obtain an expression for the contribution of a swept tapered wing to the yaw stability derivative.

5.15 Using the result obtained in problem 5.14, estimate the wing contribution to the yaw stability derivative of the small jet transport described in problem 4.16. Assume a constant section drag coefficient of 0.02.

5.16 Using Eq. (5.3.7) to approximate the sidewash gradient, estimate the total yaw stability derivative for the small jet transport described in problems 4.16, 4.18, 4.19, and 5.15. Assume an airspeed of 400 mph at 30,000 feet, include the effects of the fuselage and thrust deck, and use the following properties for the vertical stabilizer:

$$S_v = 138 \text{ ft}^2, \quad \bar{c}_v = 6.9 \text{ ft}, \quad C_{L_v,\alpha} = 3.40, \quad l_v = 43.2 \text{ ft}, \quad h_v = 7.0 \text{ ft}, \quad \eta_v = 1.0$$

5.17 Using Eq. (5.3.7) to approximate the sidewash gradient, estimate the total yaw stability derivative for the turboprop transport shown in Fig. 4.11.3 and described in problems 4.32, 4.34, and 4.35. Assume an airspeed of 300 mph at standard sea level, include the effects of the fuselage, nacelles, and propeller, and use the following properties for the vertical stabilizer:

$$S_v = 279 \text{ ft}^2, \quad \bar{c}_v = 12.0 \text{ ft}, \quad C_{L_v,\alpha} = 3.50, \quad l_v = 43.3 \text{ ft}, \quad h_v = 15.1 \text{ ft}, \quad \eta_v = 1.0$$

5.18 Using Eq. (5.3.7) to approximate the sidewash gradient, estimate the total roll stability derivative for the Spitfire Mark XVIII shown in Fig. 4.11.1 and described in problems 4.8, 4.10, 4.11, and 5.13. Assume a wing dihedral angle of 4.8 degrees.

5.19 As a first approximation for the contribution of wing sweep to the roll stability derivative of an airplane, we could assume that the wing section circulation does not change with either β or Λ. With this assumption in Eq. (5.5.20), use the classical infinite series solution to Prandtl's lifting-line equation to obtain an expression for the contribution of a swept tapered wing with no dihedral to the roll stability derivative.

5.20 Using the result from problem 5.19, estimate the wing sweep contribution to the roll stability derivative for a 45-degree swept wing having linear taper with a root chord of 20 ft, a tip chord of 8 ft, and a span of 70 ft. The wing has a thin symmetric airfoil, no twist, and is operating at a lift coefficient of 0.50.

5.21 Using a numerical lifting-line solution, estimate the wing sweep contribution to the roll stability derivative for the wing described in problem 5.20. Compare this result with that obtained from the approximate solution in problem 5.20.

5.22 Using the result from problem 5.19, estimate the wing sweep contribution to the roll stability derivative for a 45-degree swept wing having linear taper with a root chord of 14 ft, a tip chord of 14 ft, and a span of 70 ft. The wing has a thin symmetric airfoil, no twist, and is operating at a lift coefficient of 0.50.

5.23 Using a numerical lifting-line solution, estimate the wing sweep contribution to the roll stability derivative for the wing described in problem 5.22. Compare this result with that obtained from the approximate solution in problem 5.22.

5.24 Using Eq. (5.3.7) to approximate the sidewash gradient, estimate the total roll stability derivative for the small jet transport described in problems 4.16, 4.18, 4.19, and 5.16. Assume a T-tail and a low wing with 4.2 degrees of dihedral.

5.25 Using Eq. (5.3.7) to approximate the sidewash gradient, estimate the total roll stability derivative for the turboprop transport shown in Fig. 4.11.3 and described in problems 4.32, 4.34, 4.35, and 5.17. Assume no wing dihedral.

5.26 The XP-38 prototype for the P-38 Lightning had propellers that turned opposite to those of the later production models. Repeat the computations in Example 5.6.1 for the case where the airplane's propellers turn in the opposite direction and all other conditions remain unchanged. Based on a comparison between the results of these two computations and the photograph of the production model that is shown in Fig. 5.9.2, can you suggest any reason why the direction of propeller rotation may have been changed in going from the prototype to the production model?

5.27 The wingtip vortices trailing behind a large airplane can cause loss of control or structural damage to another airplane flying into this wake. Near a busy airport, this can present a serious safety hazard. For this reason, the FAA has developed separation requirements for aircraft of different size. Another situation that presents a similar hazard is formation flying. Pilots engaged in formation flying must take care to avoid flying directly through the core of a wingtip vortex shed from one of the companion aircraft. On the other hand, these wingtip vortices



Figure 5.9.2. A production model P-38 Lightning, showing the right-hand-turning propeller on the pilot's right and the left-hand-turning propeller on the pilot's left.